# Studies in Physical Optics: Coherence Theory and Surface Plasmons

This work is part of the research programme of the "Stichting voor de Technische Wetenschappen (STW)", which is financially supported by the "Nederlandse Organisatie voor Wetenschappelijk Onderzoek (NWO)".

# Studies in Physical Optics: Coherence Theory and Surface Plasmons

Proefschrift

ter verkrijging van de graad van doctor
aan de Technische Universiteit Delft,
op gezag van de Rector Magnificus Prof. ir. K.C.A.M. Luyben,
voorzitter van het College voor Promoties,
in het openbaar te verdedigen op vrijdag 3 mei 2013 om 15:00 uur

door **Shreyas Bhargav RAGHUNATHAN**
Master of Science in Electrical Engineering
geboren te Kolar Gold Fields, Karnataka, India.

Dit proefschrift is goedgekeurd door de promotoren:
Prof. dr. T. D. Visser
Prof. dr. W. M. G. Ubachs

Samenstelling promotiecommissie:

| | |
|---|---|
| Rector Magnificus, | voorzitter |
| Prof. dr. T. D. Visser, | Technische Universiteit Delft, promotor |
| Prof. dr. W. M. G. Ubachs, | Vrije Universiteit Amsterdam, promotor |
| Prof. dr. J. J. Smit, | Technische Universiteit Delft |
| Prof. dr. ir. E. J. G. Peterman, | Vrije Universiteit Amsterdam |
| Dr. B. J. Hoenders, | University of Groningen |
| Prof. dr. A. T. Friberg, | University of Eastern Finland, Finland |
| Dr. ir. M. D. Verweij, | Technische Universiteit Delft |

ISBN: 978-94-6186-146-7



A free electronic version of this thesis can be downloaded from:
http://www.library.tudelft.nl/dissertations

# Contents

# Chapter 1

# Introduction

**When you are looking at something, do you see only light or do you see the object?**

$\cdots$it is one of those dopey philosophical things that an ordinary person has no difficulty with. Even the most profound philosopher, sitting and eating his dinner has many difficulties of making out, that what he looks at is, perhaps only the light from the steak but it still implies the existence of the steak which he can lift with his fork. But the philosophers have been unable to make the analysis of the idea, having fallen by the wayside for hunger.

Richard Feynman in his lecture: “Photons: Corpuscles of light”, Auckland, 1979.

## 1.1 The significance of optics

For centuries scientists and philosophers from Aristotle to Noam Chomsky have attempted to explain and understand the nature of human consciousness and the working of the human mind. John Locke, a seventeenth-century English philosopher, postulated his “Tabula Rasa” theory on the development of human consciousness. According to his ideas individuals are born without any built-in mental content, as a “blank slate”, and knowledge comes from experience and sensory perception. Although his theory and many similar ones have been the subject of a millennia-long debate, it is undeniable that sensory perceptions play an important role in human development. Prime among the senses is vision, i.e. the ability to interpret the surrounding environment, based on the ability to process the information contained in visible light.

One important aspect of visual interpretation is understanding the physical significance of the visual information that reaches the eye. Traditionally, the lack of knowledge of naturally occurring physical phenomena has lead to many superstitions. Solar eclipses, for example, have the distinction of contributing to both the superstitious and scientific theories. Total eclipses have been, for long, interpreted as a bad omen by people unaware of its astronomical explanation. The ancient Chinese believed that solar eclipses were caused by dragons swallowing the sun in its entirety. This lead to their practice of playing drums to scare away the sun-eating dragons. However, Chinese astronomers seemed to understand eclipses as natural phenomena around 720 B.C., with older observations scratched into bones dating back perhaps 3,000 years.

All the Great Apes are known to be self-aware based on the *mirror test*, i.e. they are capable of recognising themselves in the mirror. Since the dawn of civilisation, the self-aware humans have made use of dark stagnant pools of water, or water from vessels as mirrors. Mirrors have been built as early as 6000 B.C. it was not until the time of the Ancient Greeks that the nature of light and reflections was systematically studied and discussed. In the fifth century B.C., Empedocles argued that an interaction between rays from the eyes and rays from a source such as the sun was responsible for human vision. This hypothesis was challenged by Euclid a couple of centuries later, when he postulated that light travelled in a straight line. In his text *Optica* he described the laws of reflection and studied them mathematically.

Mirrors were not the only optical device used in ancients human civilisations. One of the oldest lens artifacts has been dated back to the times of ancient Assyria, where it might have been used as a magnifying glass.

Since the dawn of our civilisation the curiosity in natural optical phenomena has helped us better our understanding in the field of optics. Progressing steadily from rudimentary basics in geometric optics to the more advanced fields of quantum optics and photonics, our curiosities have been fueled by the zeal to understand, record and sometimes recreate a number of naturally occurring phenomena. Considerations like these, have motivated many scientists and myself to take up the study of optics.

## 1.2 Basic concepts

In this subsection we give a brief overview of the different concepts that are discussed in this thesis.

We begin by reviewing some elementary properties of random processes. Let us consider a process that randomly varies in time, denoted by $x(t)$ with $t$ denoting the time. Each measurement of $x(t)$ will yield a different outcome, say ${}^{(1)}x(t), {}^{(2)}x(t), \ldots$ The collection of all possible outcomes of the measurements is known as the *ensemble* of $x(t)$. The ensemble average $\langle x(t)\rangle_e$, or expectation value for a set of $N$ realizations can be defined as

$$\langle x(t)\rangle_e = \lim_{N\to\infty} \frac{1}{N} \sum_{r=1}^{N} {}^{(r)}x(t). \tag{1.1}$$

Let $p_1(x,t)\mathrm{d}x$ denote the probability that $x(t)$ takes on a value in the interval $(x, x+\mathrm{d}x)$ at a time $t$. The ensemble average defined by using the probability density function, $p_1(x,t)$, is given as

$$\langle x(t)\rangle_e = \int x p_1(x,t)\mathrm{d}x, \tag{1.2}$$

where the integration extends over all possible values of $x$. The probability density $p_1(x,t)$, does not describe the random process fully. It is also necessary to consider the possible correlations between $x(t_1)$ and $x(t_2)$. Such correlations are characterized by a *joint probability density* $p_2(x_1, x_2, t_1, t_2)$. The quantity $p_2(x_1, x_2, t_1, t_2)\mathrm{d}x_1\mathrm{d}x_2$ represents the probability that the random variable $x$ will take a value in the range $(x_1, x_1+\mathrm{d}x_1)$ at time $t_1$, and a value in the range $(x_2, x_2+\mathrm{d}x_2)$ at time $t_2$. We can define, in a similar way, an infinite number of probability densities for higher-order correlations that describe the joint probabilities at three or more points in space and time, as

$$p_1(x,t),\ p_2(x_1, x_2, t_1, t_2),\ p_3(x_1, x_2, x_3, t_1, t_2, t_3), \cdots \tag{1.3}$$

The properties described thus far, can also be applied to a complex random process described as $z(t) = x(t) + \mathrm{i}y(t)$ with $x(t)$ and $y(t)$ both real-valued. The statistical properties of such a complex random process can be described by the joint probability density functions similar to Eq. (1.3) as

$$p_1(z,t),\ p_2(z_1,z_2,t_1,t_2),\ p_3(z_1,z_2,z_3,t_1,t_2,t_3),\cdots \tag{1.4}$$

Here, $p_1(z,t)\mathrm{d}x\mathrm{d}y$ represents the probability that $z(t)$ will take on a value within $(x, x+\mathrm{d}x; y, y+\mathrm{d}y)$ at time $t$. The ensemble average of the complex random process $z(t)$ is given by

$$\langle z(t)\rangle_e = \int zp_1(z,t)\ \mathrm{d}x\mathrm{d}y, \tag{1.5}$$

where the integration extends over all values of $z$. The joint probability, $p_2$, allows us to define the ensemble average of the product of $z^*(t_1)z(t_2)$, which is called the *auto-correlation function* $\Gamma(t_1,t_2)$ as

$$\Gamma(t_1,t_2) = \langle z^*(t_1)z(t_2)\rangle_e = \iint z_1^*\ z_2\ p_2(z_1,z_2,t_1,t_2)\ \mathrm{d}x_1\mathrm{d}y_1\mathrm{d}x_2\mathrm{d}y_2, \tag{1.6}$$

where the asterisk denote the complex conjugate.

A random process is called *statistically stationary* when the probability densities $p_1$, $p_2$, $p_3$ and so forth are time-shift invariant, i.e.

$$\langle z^*(t_1)z(t_2)\rangle_e = \langle z^*(t_1+T)z(t_2+T)\rangle_e\,, \tag{1.7}$$

for all values of $T$. A weaker form of stationarity, which is often employed, is known as *wide-sense* stationarity. This requires that the random process' first and the second moments are time-shift invariant. It goes without saying that any strict-sense stationary process is obviously, also wide-sense stationary.

## 1.3 Coherence theory

Optical coherence theory is the study of the statistical properties of light and the influence those statistical properties have on the observable characteristics of optical fields. The theoretical beginnings of coherence theory can be traced back to [Verdet, 1865], who estimated the spatial coherence length of sunlight on the Earth's surface, and [Van Cittert, 1934] and [Zernike, 1938], who calculated the evolution of the spatial coherence of light propagating from an incoherent source.[1]

The modern theory of optical coherence, as championed by Wolf and others, began with the study of the mutual coherence function $\Gamma(\mathbf{r}_1, \mathbf{r}_2, \tau)$ of wide-sense statistically stationary optical fields, defined as

$$\Gamma(\mathbf{r}_1, \mathbf{r}_2, \tau) = \langle U^*(\mathbf{r}_1, t_1) U(\mathbf{r}_2, t_2) \rangle, \tag{1.8}$$

where the time difference $\tau \equiv t_2 - t_1$ and the angled brackets represent time averaging or, equivalently for ergodic fields, ensemble averaging. The field $U(\mathbf{r}, t)$ is typically taken to be scalar, with polarization effects neglected, but the formalism can be readily extended to the fully electromagnetic case, as discussed in detail in [Wolf, 2007]. It was shown by [Wolf, 1955] that the mutual coherence function satisfies a pair of wave equations in free space, namely,

$$\left( \nabla_1^2 - \frac{1}{c^2} \frac{\partial^2}{\partial \tau^2} \right) \Gamma(\mathbf{r}_1, \mathbf{r}_2, \tau) = 0, \tag{1.9}$$

$$\left( \nabla_2^2 - \frac{1}{c^2} \frac{\partial^2}{\partial \tau^2} \right) \Gamma(\mathbf{r}_1, \mathbf{r}_2, \tau) = 0, \tag{1.10}$$

where $\nabla_i^2$ is the Laplacian with respect to the Cartesian coordinates of position vector $\mathbf{r}_i$ and $c$ is the speed of light. From these equations one can see that the statistical properties of light evolve in a well-defined way on propagation, and much of the research in optical coherence theory has involved the study of the consequences of these equations of evolution.

Just as it is possible to study the behaviour of deterministic wave fields in the time domain or the frequency domain, however, it is also possible to study the behaviour of partially coherent wave fields in either time or in frequency. The *cross-spectral density function* $W(\mathbf{r}_1, \mathbf{r}_2, \omega)$ is defined as the temporal Fourier transform of the mutual coherence function with

[1] More details on the history of optical coherence theory can be found in [Born and Wolf, 1999], Section 10.1, and [Wolf, 2001]. Reprints of a number of classic papers can be found in [Mandel and Wolf, 1970].

respect to the time variable $\tau$, i.e.

$$W(\mathbf{r}_1, \mathbf{r}_2, \omega) = \frac{1}{2\pi} \int_{-\infty}^{\infty} \Gamma(\mathbf{r}_1, \mathbf{r}_2, \tau) e^{-\mathrm{i}\omega\tau} \mathrm{d}\tau. \tag{1.11}$$

The cross-spectral density will then satisfy a pair of Helmholtz equations,

$$\left(\nabla_1^2 + k^2\right) W(\mathbf{r}_1, \mathbf{r}_2, \omega) = 0, \tag{1.12}$$

$$\left(\nabla_2^2 + k^2\right) W(\mathbf{r}_1, \mathbf{r}_2, \omega) = 0, \tag{1.13}$$

where $k = \omega/c$ is the wavenumber of light corresponding to frequency $\omega$. This pair of elliptic partial differential equations for the cross-spectral density function is in general easier to solve than the pair of hyperbolic wave equations for the mutual coherence function; the mutual coherence function can, however, be readily determined by an inverse Fourier transform of the cross-spectral density.

The cross-spectral density is commonly written in terms of two other functions, the *spectral density* $S(\mathbf{r}, \omega)$ and the *spectral degree of coherence* $\mu(\mathbf{r}_1, \mathbf{r}_2, \omega)$, as

$$W(\mathbf{r}_1, \mathbf{r}_2, \omega) = \sqrt{S(\mathbf{r}_1, \omega)} \sqrt{S(\mathbf{r}_2, \omega)} \mu(\mathbf{r}_1, \mathbf{r}_2, \omega). \tag{1.14}$$

The spectral density $S(\mathbf{r}, \omega)$ represents the intensity of the wavefield at position $\mathbf{r}$ at frequency $\omega$, and may be written in terms of the cross-spectral density function as

$$S(\mathbf{r}, \omega) \equiv W(\mathbf{r}, \mathbf{r}, \omega). \tag{1.15}$$

The spectral degree of coherence $\mu(\mathbf{r}_1, \mathbf{r}_2, \omega)$ is a measure of the degree of correlation of the field at the two positions $\mathbf{r}_1$ and $\mathbf{r}_2$ and at frequency $\omega$, and may be written in terms of the cross-spectral density function as

$$\mu(\mathbf{r}_1, \mathbf{r}_2, \omega) \equiv \frac{W(\mathbf{r}_1, \mathbf{r}_2, \omega)}{\sqrt{S(\mathbf{r}_1, \omega) S(\mathbf{r}_2, \omega)}}. \tag{1.16}$$

It can be shown that the absolute value of the spectral degree of coherence is restricted to the values

$$0 \leq |\mu(\mathbf{r}_1, \mathbf{r}_2, \omega)| \leq 1, \tag{1.17}$$

where 0 represents a complete lack of coherence, and 1 represents full spatial coherence. The physical significance of $\mu(\mathbf{r}_1, \mathbf{r}_2, \omega)$ is discussed in more detail in [Gbur and Visser, 2010].

An important milestone in the development of coherence theory in the space-frequency domain was the observation by [Wolf, 1982] that the cross-spectral density itself may be represented as a correlation function derived from an ensemble of monochromatic realizations of the field. This can be proven by first noting that the cross-spectral density is Hermitian, i.e.

$$W(\mathbf{r}_2, \mathbf{r}_1, \omega) = W^*(\mathbf{r}_1, \mathbf{r}_2, \omega), \tag{1.18}$$

and that it is non-negative definite, such that

$$\int_D \int_D W(\mathbf{r}_1, \mathbf{r}_2, \omega) f^*(\mathbf{r}_1) f(\mathbf{r}_2)\, \mathrm{d}^2 r_1 \mathrm{d}^2 r_2 \geq 0, \tag{1.19}$$

where $f(\mathbf{r})$ is an arbitrary square-integrable function and, for a secondary source with a field propagating from $z = 0$, the domain of integration $D$ is the source plane. Assuming that the cross-spectral density is also square-integrable over this domain, it represents a *Hilbert-Schmidt kernel*; by *Mercer's theorem*[2], it may be expanded in a series of orthogonal functions of the form

$$W(\mathbf{r}_1, \mathbf{r}_2, \omega) = \sum_n \lambda_n(\omega) \phi_n^*(\mathbf{r}_1, \omega) \phi_n(\mathbf{r}_2, \omega), \tag{1.20}$$

where the eigenvalues $\lambda_n(\omega)$ and the eigenfunctions $\phi_n(\mathbf{r}, \omega)$ satisfy the integral equation

$$\int_D W(\mathbf{r}_1, \mathbf{r}_2, \omega) \phi_n(\mathbf{r}_1, \omega)\, \mathrm{d}^2 r_1 = \lambda_n(\omega) \phi_n(\mathbf{r}_2, \omega). \tag{1.21}$$

The summation in general may be over multiple indices, and may be a finite or infinite sum. The eigenvalues are non-negative and the eigenfunctions are orthogonal and typically taken to be orthonormal. Equation (1.20) represents what is now known as the *coherent mode representation* of the cross-spectral density.

[2] Mercer's theorem and Hilbert-Schmidt kernels are introduced in the theory of integral equations; see, for instance [Moiseiwitsch, 1977].

The coherent mode representation may be used to construct an ensemble of monochromatic wave fields whose second-order average reproduces a given cross-spectral density. To do so, we introduce an ensemble of fields defined by

$$U(\mathbf{r},\omega) = \sum_n a_n(\omega)\phi_n(\mathbf{r},\omega), \tag{1.22}$$

where the coefficients $a_n$ are random variables. We choose these variables such that the average of them over the entire ensemble of fields (denoted by $\langle\cdots\rangle_\omega$) satisfies the condition

$$\langle a_n^*(\omega)a_m(\omega)\rangle_\omega = \lambda_n(\omega)\delta_{nm}. \tag{1.23}$$

It then follows that the cross-spectral density function may be written as

$$W(\mathbf{r}_1,\mathbf{r}_2,\omega) = \langle U^*(\mathbf{r}_1,\omega)U(\mathbf{r}_2,\omega)\rangle_\omega. \tag{1.24}$$

On substitution from Eq. (1.22) into Eq. (1.24), we readily find that Eq. (1.20) is satisfied. Furthermore, on substitution from Eq. (1.24) into Eqs. (1.12) and (1.13), it follows that the individual realizations $U(\mathbf{r},\omega)$ each satisfy the Helmholtz equation and represent valid monochromatic, and therefore coherent, wave fields.

This result, which seems very formal and almost trivial at first glance, is perhaps one of the most useful results in modern coherence theory, because it implies that a valid cross-spectral density can be found by any suitable averaging process over a set of monochromatic realizations. This is used, for instance, in the "beam wander" model discussed in [Gbur and Visser, 2010].

It is to be noted that it is possible to extend the space-frequency theory to higher-order correlation functions, as done by [Wolf, 1986] and [Agarwal and Wolf, 1993]; the formalism becomes significantly more complicated, however.

The theory of optical coherence has developed rapidly with the introduction of the space-frequency representation. Perhaps the most significant result to arise as yet is the theory of *correlation-induced spectral changes*, in which the degree of spatial coherence of a source can affect the properties of the radiated spectral density. The results arising from this theory are too numerous to be included here; a comprehensive review was provided some time ago by [Wolf and James, 1996].

At its heart, the theory of optical coherence may be said to be the *optics of observable quantities*. Whereas traditional optics focuses on the behaviour of wave fields $U(\mathbf{r}, t)$ which are not directly observable, coherence theory describes the behaviour of second-order and higher moments of the wave field such as the mutual coherence function and the cross-spectral density function, which can be measured through interference experiments. An early discussion of this point of view was given by [WOLF, 1954].

## 1.4 Electromagnetic beams

In the previous section, Section 1.3, we have considered scalar fields independent of polarization. The concepts of coherence can be generalised to represents stochastic electromagnetic beams as well. Coherence can be considered as the correlations between two points in space whereas the degree of polarization is the correlation between fluctuations of different components of the electromagnetic beam at a single point in space.

### 1.4.1 General formalism

Let us consider a random electromagnetic beam propagating along the $z-$axis, from the plane $z = 0$ into the half space $z > 0$. The state of coherence and polarization of this beam is characterized by the *electric cross-spectral density matrix*, which is defined as [WOLF, 2007]

$$\mathbf{W}(\mathbf{r}_1, \mathbf{r}_2, \omega) = \begin{pmatrix} W_{xx}(\mathbf{r}_1, \mathbf{r}_2, \omega) & W_{xy}(\mathbf{r}_1, \mathbf{r}_2, \omega) \\ W_{yx}(\mathbf{r}_1, \mathbf{r}_2, \omega) & W_{yy}(\mathbf{r}_1, \mathbf{r}_2, \omega) \end{pmatrix}, \tag{1.25}$$

where

$$W_{ij}(\mathbf{r}_1, \mathbf{r}_2, \omega) = \langle E_i^*(\mathbf{r}_1, \omega) E_j(\mathbf{r}_2, \omega) \rangle, \quad (i, j = x, y). \tag{1.26}$$

Here $E_i(\mathbf{r}, \omega)$ is a Cartesian component of the electric field at a point $\mathbf{r}$ at frequency $\omega$, of a typical realization of the statistical ensemble representing the beam. The *spectral density* $S(\mathbf{r}, \omega)$ of the electromagnetic beam at a point in space, $\mathbf{r}$ is the average electric density at that point. Thus we have

$$S(\mathbf{r}, \omega) = \langle \mathbf{E}^*(\mathbf{r}, \omega) \cdot \mathbf{E}(\mathbf{r}, \omega) \rangle \,, \tag{1.27}$$

$$= \mathrm{Tr}\, \mathbf{W}(\mathbf{r}, \mathbf{r}, \omega), \tag{1.28}$$

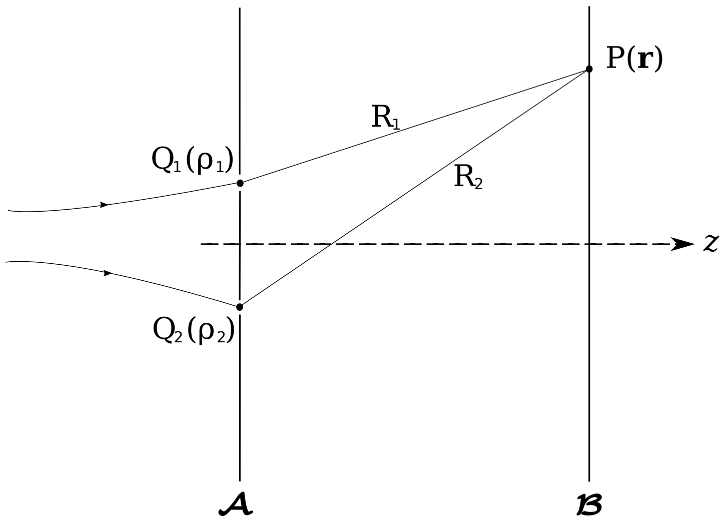


Figure 1.1: Notation pertaining to Young's double slit experiment with a stochastic electromagnetic beam. The two apertures in screen $\mathcal{A}$ are located at $\boldsymbol{\rho}_1$ and $\boldsymbol{\rho}_2$. The observation poitn $P(\mathbf{r})$ is on a second, parallel screen $\mathcal{B}$.

where Tr denotes the trace. Let $\mathbf{E}(\mathbf{r},\omega)$ represent the electrical vector at the point $P(\mathbf{r})$ on the screen as shown in Fig. 1.1. A typical realization for $\mathbf{E}(\mathbf{r},\omega)$ in terms of realisations of $\mathbf{E}(\boldsymbol{\rho}_1,\omega)$ and $\mathbf{E}(\boldsymbol{\rho}_2,\omega)$ of the electric field vector at points $\boldsymbol{\rho}_1$ and $\boldsymbol{\rho}_2$ is given as

$$\mathbf{E}(\mathbf{r},\omega) = K_1\mathbf{E}(\boldsymbol{\rho}_1,\omega)\mathrm{e}^{\mathrm{i}kR_1} + K_2\mathbf{E}(\boldsymbol{\rho}_2,\omega)\mathrm{e}^{\mathrm{i}kR_2}, \tag{1.29}$$

where $R_1$ and $R_2$ are the distances from the points $Q(\boldsymbol{\rho}_1)$ and $Q(\boldsymbol{\rho}_2)$, respectively to the point $P(\mathbf{r})$. The factors $K_1$ and $K_2$ take into account diffraction at the pinholes, which follows from the Huygens-Fresnel principle, see for example Section 8.2 of [Born and Wolf, 1999] and are given as

$$K_j \approx -\frac{\mathrm{i}}{\lambda R_j}\,\mathrm{d}\mathscr{A}_j \quad (j = 1, 2). \tag{1.30}$$

Here $\mathrm{d}\mathscr{A}_1$ and $\mathrm{d}\mathscr{A}_2$ are the areas of the two pinholes. Using Eqs. (1.26), (1.28), and (1.29) we can obtain an expression for the spectral density

$S(\mathbf{r}, \omega)$ as

$$S(\mathbf{r}, \omega) = S^{(1)}(\mathbf{r}, \omega) + S^{(2)}(\mathbf{r}, \omega) + 2\sqrt{S^{(1)}(\mathbf{r}, \omega)}\sqrt{S^{(2)}(\mathbf{r}, \omega)}\, \mathcal{Re}[\eta(\boldsymbol{\rho}_1, \boldsymbol{\rho}_2, \omega)e^{\mathrm{i}k(R_2-R_1)}], \quad (1.31)$$

where $\mathcal{Re}$ denotes the real part. Here $S^{(1)}(\mathbf{r}, \omega)$ is the spectral density at the point $P(\mathbf{r})$ if the pinhole at position $Q_2(\mathbf{r}_2)$ is closed. Thus we have

$$S^{(j)}(\mathbf{r}, \omega) = |K_j|^2 S(\boldsymbol{\rho}_j, \omega), \quad (1.32)$$

where $j = 1$ denotes the pinhole at $Q_1(\boldsymbol{\rho}_1)$ and $j = 2$ corresponds to the pinhole at $Q_2(\boldsymbol{\rho}_2)$. We can see from Eq. (1.31), that the spectrum at the point $P(\mathbf{r})$ at the observation plane $\mathcal{B}$ is the sum of the spectra of the two individual beams from points $Q_1(\boldsymbol{\rho}_1)$, and $Q_2(\boldsymbol{\rho}_2)$ and the interference term with

$$\eta(\boldsymbol{\rho}_1, \boldsymbol{\rho}_2, \omega) = \frac{\mathrm{Tr}\ \mathbf{W}(\boldsymbol{\rho}_1, \boldsymbol{\rho}_2, \omega)}{\sqrt{S(\boldsymbol{\rho}_1, \omega)}\sqrt{S(\boldsymbol{\rho}_2, \omega)}}. \quad (1.33)$$

Here the term $\eta(\boldsymbol{\rho}_1, \boldsymbol{\rho}_2, \omega)$ is analogous to the term $\mu(\rho_1, \rho_2, \omega)$ in Eq. (1.16) and thus is the *complex spectral degree of coherence* of the stochastic electromagnetic field between at points $Q_1(\boldsymbol{\rho}_1)$ and $Q_2(\boldsymbol{\rho}_2)$.

It is crucial to note that the spectral degree of coherence for electromagnetic beams, $\eta(\boldsymbol{\rho}_1, \boldsymbol{\rho}_2, \omega)$ depends only on the diagonal elements of the correlation matrix $\mathbf{W}$, i.e. $W_{xx}$ and $W_{yy}$. The spectral degree of coherence between two points of the electromagnetic beam is defined as the capability of the field at these points to produce interference fringes, analogous to the scalar case. However, according to the Fresnel-Argo laws, two orthogonal linearly polarized waves do not interfere. The fact that orthogonal components of the random electric field do not interfere with each other does not imply that these components are uncorrelated.

Despite the fact that the off-diagonal elements of the cross-spectral density $\mathbf{W}$ do not contribute to the correlation properties of the beam, they play a role in determining the degree of polarization at any point in the beam. The electromagnetic beam can be decomposed into two parts, one of which is completely polarized and the other completely unpolarized (see Section 8.2.3, [Wolf, 2007]). The spectral degree of polarization

$\mathcal{P}(\mathbf{r},\omega)$ of the stochastic electromagnetic beam at a point is the ratio of the intensity of the completely polarized beam to its total intensity, which can be shown to be

$$\mathcal{P}(\mathbf{r},\omega) = \sqrt{1 - \frac{4\,\mathrm{Det}\,\mathbf{W}(\mathbf{r},\mathbf{r},\omega)}{[\mathrm{Tr}\,\mathbf{W}(\mathbf{r},\mathbf{r},\omega)]^2}}. \tag{1.34}$$

Here Det denotes the determinant.

### 1.4.2 Quasi-Homogeneous beams

A secondary planar source producing an electromagnetic beam is characterized by a cross-spectral density matrix of the form

$$W_{ij}^{(0)}(\boldsymbol{\rho}_1', \boldsymbol{\rho}_2', \omega) = \sqrt{S_i^{(0)}(\boldsymbol{\rho}_1', \omega)}\sqrt{S_j^{(0)}(\boldsymbol{\rho}_2', \omega)}\mu_{ij}^{(0)}(\boldsymbol{\rho}_1', \boldsymbol{\rho}_2', \omega), \quad (i = x, y), \tag{1.35}$$

where $S_i^{(0)}(\boldsymbol{\rho}_1', \omega) = W_{ii}^{(0)}(\boldsymbol{\rho}_1', \boldsymbol{\rho}_1', \omega)$, denotes the spectral density of the $i^{\mathrm{th}}$ component of the electric field and $\mu_{ij}^{(0)}(\boldsymbol{\rho}_1', \boldsymbol{\rho}_2', \omega)$ is the correlation between $E_i$ at $\boldsymbol{\rho}_1'$ and $E_j$ at $\boldsymbol{\rho}_2'$ and the superscript (0) indicates the source plane. A secondary planar source is said to be a *Schell-model* source, when its correlation function $\mu_{ij}(\boldsymbol{\rho}_1', \boldsymbol{\rho}_2')$ depends only on the difference $\boldsymbol{\rho}_2' - \boldsymbol{\rho}_1'$, i.e.

$$\mu_{ij}^{(0)}(\boldsymbol{\rho}_1', \boldsymbol{\rho}_2', \omega) = \mu_{ij}^{(0)}(\boldsymbol{\rho}_2' - \boldsymbol{\rho}_1', \omega). \tag{1.36}$$

It is quite often the case that the spectral degree of coherence $\mu_{ij}^{(0)}(\boldsymbol{\rho}_2' - \boldsymbol{\rho}_1', \omega)$ of light in the source plane varies rapidly with the argument $\boldsymbol{\rho}_2' - \boldsymbol{\rho}_1'$, in comparison to the variation of the spectral density $S_i^{(0)}(\boldsymbol{\rho}', \omega)$ with its argument $\boldsymbol{\rho}'$ for all the frequency components present. Such planar secondary sources are said to be *quasi-homogeneous*. Since then both $S_x^{(0)}(\boldsymbol{\rho}, \omega)$ and $S_y^{(0)}(\boldsymbol{\rho}, \omega)$ are 'slow' functions compared to $\mu_{xx}^{(0)}(\boldsymbol{\rho}_2' - \boldsymbol{\rho}_1', \omega)$ and $\mu_{yy}^{(0)}(\boldsymbol{\rho}_2' - \boldsymbol{\rho}_1', \omega)$, respectively, we can write

$$W_{xx}^{(0)}(\boldsymbol{\rho}_1', \boldsymbol{\rho}_2') \approx S_x^{(0)}\left(\frac{\boldsymbol{\rho}_1' + \boldsymbol{\rho}_2'}{2}\right)\,\mu_{xx}^{(0)}(\boldsymbol{\rho}_2' - \boldsymbol{\rho}_1'), \tag{1.37}$$

$$W_{yy}^{(0)}(\boldsymbol{\rho}_1', \boldsymbol{\rho}_2') \approx S_y^{(0)}\left(\frac{\boldsymbol{\rho}_1' + \boldsymbol{\rho}_2'}{2}\right)\,\mu_{yy}^{(0)}(\boldsymbol{\rho}_2' - \boldsymbol{\rho}_1'), \tag{1.38}$$

where for brevity the $\omega$-dependence of the various quantities has been omitted. If we now introduce sum and difference variables defined as

$$\boldsymbol{\rho}^{(+)} = \frac{\boldsymbol{\rho}'_1 + \boldsymbol{\rho}'_2}{2},$$
$$\boldsymbol{\rho}^{(-)} = \boldsymbol{\rho}'_2 - \boldsymbol{\rho}'_1, \tag{1.39}$$

then the diagonal elements of the cross-spectral density matrix factorize into a product of two functions of independent variables, namely

$$W^{(0)}_{xx}(\boldsymbol{\rho}'_1, \boldsymbol{\rho}'_2) \approx S^{(0)}_x[\boldsymbol{\rho}^{(+)}]\, \mu^{(0)}_{xx}[\boldsymbol{\rho}^{(-)}], \tag{1.40}$$
$$W^{(0)}_{yy}(\boldsymbol{\rho}'_1, \boldsymbol{\rho}'_2) \approx S^{(0)}_y[\boldsymbol{\rho}^{(+)}]\, \mu^{(0)}_{yy}[\boldsymbol{\rho}^{(-)}]. \tag{1.41}$$

This factorization has profound implications, as will be discussed in Chapter 3 of this thesis.

### 1.4.3 Phase singularities in electromagnetic beams

All wave fields are characterized by a local amplitude and phase. At points where the amplitude vanishes the phase is "singular" or undefined. Phase singularities have been observed in tides [Berry, 1981], in the quantum mechanical wavefunction [Hirschfelder *et al.*, 1974a; Hirschfelder *et al.*, 1974b], and in optics in the energy flow of a convergent beam in the focal plane [Boivin *et al.*, 1967]. A systematic study of optical phase singularities started with the seminal paper by [Nye and Berry, 1974] which spawned a new branch of optics, called *Singular Optics* [Nye, 1999; Soskin *et al.*, 1997; Allen *et al.*, 2003]. The subject of singular optics is the structure of wave fields in the vicinity of optical vortices and polarization singularities.

Unlike the above-mentioned wave fields, the spectral degree of coherence is a function of two points. The spectral degree of coherence of partially coherent fields emerging from two pinholes in Young's double slit experiment has been shown to exhibit singular behaviour [Schouten *et al.*, 2003a]. These *correlation singularities* occur at pairs of points at which the fields are completely uncorrelated. The phase of the spectral degree of coherence around these singular pairs of points typically exhibits a vortex-like behavior [Gbur and Visser, 2003b]. These and subsequent studies on correlation singularities were dealing with scalar fields.

In Chapters 4 and 5 the concept of a correlation singularity is extended to electromagnetic beams.

As described in the previous sections, the state of coherence of an electromagnetic beam is characterized by its cross-spectral density matrix defined by, Eq. (1.35). The degree of coherence between two points in the electromagnetic beam is described by the spectral degree of coherence, namely

$$\eta(\boldsymbol{\rho}_1, \boldsymbol{\rho}_2, \omega) = \frac{\mathrm{Tr}\,\mathbf{W}(\boldsymbol{\rho}_1, \boldsymbol{\rho}_2, \omega)}{\sqrt{S(\boldsymbol{\rho}_1, \omega)}\sqrt{S(\boldsymbol{\rho}_2, \omega)}}, \tag{1.42}$$

which is complex-valued. Let us represent the numerator of $\eta(\boldsymbol{\rho}_1, \boldsymbol{\rho}_2, \omega)$ as a product of an amplitude function $A(\boldsymbol{\rho}_1, \boldsymbol{\rho}_2, z)$ and a phase function $\phi(\boldsymbol{\rho}_1, \boldsymbol{\rho}_2, z)$ as

$$W_{xx}(\boldsymbol{\rho}_1, \boldsymbol{\rho}_2, z) + W_{yy}(\boldsymbol{\rho}_1, \boldsymbol{\rho}_2, z) = A(\boldsymbol{\rho}_1, \boldsymbol{\rho}_2, z) e^{\mathrm{i}\phi(\boldsymbol{\rho}_1, \boldsymbol{\rho}_2, z)}. \tag{1.43}$$

A correlation singularity arises at pairs of points in the vector field where the amplitude function $A(\boldsymbol{\rho}_1, \boldsymbol{\rho}_2, z) = 0$ and hence the phase $\phi(\boldsymbol{\rho}_1, \boldsymbol{\rho}_2, z)$ is undefined. In three-dimensional space the locus of these singular points is typically a curve. A two-dimensional cross-section which includes the singular point would show that equiphase lines usually display a vortex-like behavior around the singularity. So if we consider $C$ to be a closed curve traversed in the counter-clockwise direction around a single correlation singularity, with the phase $\phi$, the *topological charge* $s$ of the singularity is defined as

$$s \equiv \frac{1}{2\pi} \oint_C \mathrm{d}\phi = \frac{1}{2\pi} \oint_C \nabla\phi \cdot \mathrm{d}\mathbf{r}, \quad s = 0, \pm 1, \pm 2, \cdots . \tag{1.44}$$

Since the phase is single-valued, $s$ has an integer value and is independent of the choice of the curve $C$. The topological charge is conserved for smooth changes in the field. The only way for a singularity with a non-zero charge, to disappear is by annihilating with another singularity of opposite charge.

Another typical topological feature in the context of correlation singularities are *stationary points.* These are points of the field, where the phase is well-defined, yet the gradient of the phase vanishes. These points represent a minimum, or a maximum or a saddle point.

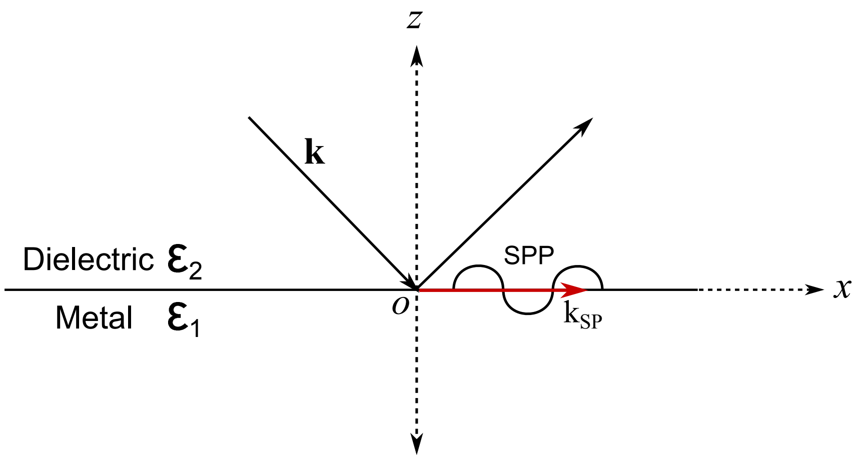


Figure 1.2: The interface between a metal of permittivity $\varepsilon_1$ and a dielectric of permittivity $\varepsilon_2$.

Similar to the topological charge $s$, one can also define a topological charge of the singularities of the vector field $\nabla\phi$, which is called the *topological index*. This index $t$, for a positive and negative vortex is unity, while a saddle point (which has no topological charge) has an index $t = -1$ and a maximum or a minimum has an index $t = 1$. Just like the topological charge, the topological index is also a conserved quantity.

The fact that topological charge and topological index are both conserved, imposes constraints of the creation and annihilation of these topological features. For example, the creation of phase singularities usually happens in pairs with one having a topological charge $s = -1$ and a topological index $t = 1$, while the other has a charge of $s = 1$ and index $t = 1$. Conservation of topological index dictates that this process can be accompanied by the creation of two phase saddles with $s = 0$, $t = -1$. Several other topological reaction are described in Chapter 5.

## 1.5 Surface plasmons

The interaction of metals with incident electromagnetic radiation is governed, largely, by the amount of free electrons in the metal. The Drude model assumes that the metal is made up of positively charged ions and "free" electrons that are detached from their respective atoms. This model ignores any long-range interaction between the ions and the electrons and assumes that electrons do not interact with each other. At optical frequencies, the metal's "free electron gas" can sustain surface-charge density oscillations called Surface Plasmon Polaritons (SPP). These oscillations are essentially electromagnetic waves trapped on the metal surface. They can give rise to a strongly enhanced electromagnetic field localized at the interface between a metal and a dielectric.

Now let us consider an interface between a metal and a dielectric as shown in Fig 1.2. Let $\varepsilon_1$ denote the permittivity of the metal and $\varepsilon_2$ denote the permittivity of the dielectric. By solving Maxwell's equation under appropriate boundary conditions for an incident field that is TM-polarized, we can obtain for the frequency-dependent surface plasmon wave-number $k_{\mathrm{SP}}$ the expression [Raether, 1988; Novotny and Hecht, 2006]

$$k_{\mathrm{SP}}^2 = \frac{\varepsilon_1 \varepsilon_2}{\varepsilon_1 + \varepsilon_2} k_0^2, \tag{1.45}$$

where $k_0$ is the free-space wavenumber $\omega/c$. The normal component of the wave-vector is given as

$$k_{j,z}^2 = \frac{\varepsilon_j^2}{\varepsilon_1 + \varepsilon_2} k_0^2. \tag{1.46}$$

A sustained surface plasmon oscillations requires $k_{\mathrm{SP}}^2$ to be positive. This is possible, if $\varepsilon_1 + \varepsilon_2 > 0$ and if both $\varepsilon_1$ and $\varepsilon_2$ are positive or if $\varepsilon_1 + \varepsilon_2 < 0$ and $\varepsilon_1 < 0$. For the oscillation to be localized to the interface, the normal components of the wave-vector $k_{1,z}$ and $k_{2,z}$ must be imaginary, giving rise to an exponentially decaying solution. This can be achieved if $\varepsilon_1 + \varepsilon_2 < 0$ in Eq. (1.46). Thus the conditions for sustained surface plasmon oscillations are

$$\varepsilon_1 \varepsilon_2 < 0, \tag{1.47}$$

$$\varepsilon_1 + \varepsilon_2 < 0. \tag{1.48}$$

These conditions are satisfied for noble metals like gold or silver at optical frequencies [Johnson and Christy, 1972] at the interface with an dielectric like air or glass.

### 1.5.1 Propagation lengths of surface plasmons

Let us next write the complex-valued permittivity of the metal as

$$\varepsilon_1 = \varepsilon_1' + \mathrm{i}\varepsilon_1'', \tag{1.49}$$

where $\varepsilon_1'$ and $\varepsilon_1''$ are both real. The imaginary part of $\varepsilon_1$ is associated with ohmic losses in the metal. We assume that the dielectric medium is lossless and hence the permittivity $\varepsilon_2$ is real-valued. Applying Eq. (1.49) in Eq. (1.45) we find an expression for $k_{\mathrm{SP}} = k_{\mathrm{SP}}' + \mathrm{i}k_{\mathrm{SP}}''$ (Section 2.1, [Raether, 1988]), under the assumption $|\varepsilon_1''| \ll |\varepsilon_1'|$ as

$$k_{\mathrm{SP}}' = k_0 \left(\frac{\varepsilon_1'\varepsilon_2}{\varepsilon_1' + \varepsilon_2}\right)^{1/2}, \tag{1.50}$$

$$k_{\mathrm{SP}}'' = k_0 \left(\frac{\varepsilon_1'\varepsilon_2}{\varepsilon_1' + \varepsilon_2}\right)^{3/2} \frac{\varepsilon_1''}{2\varepsilon_1'^2}. \tag{1.51}$$

The imaginary part of the wavenumber $k_{\mathrm{SP}}''$ is responsible for the decay of the SPPs on a smooth surface. The length, after which the intensity of the SPPs reduces to $1/e$ is around 10 $\mu$m for gold at a wavelength of 633 nm.

Similarly we can obtain an expression for the value of the skin depths $\hat{z}_i$ in the two media, namely

$$\hat{z}_2 = \frac{\lambda}{2\pi} \left(\frac{\varepsilon_1' + \varepsilon_2}{\varepsilon_2^2}\right)^{1/2}, \tag{1.52}$$

$$\hat{z}_1 = \frac{\lambda}{2\pi} \left(\frac{\varepsilon_1' + \varepsilon_2}{\varepsilon_1'^2}\right)^{1/2}. \tag{1.53}$$

For gold at 633 nm, the typical skin depth of the metal is around 28 nm and that of air is 328 nm.

Thus three decay lengths are associated with the SPPs on an interface, given as

1. a relatively large propagation length of SPPs on the surface dictated by the ohmic losses in the metal,

2. a much smaller exponential decay length in the dielectric material, typically of the order of the free-space wavelength, and

3. a very small exponential decay length within the metal, typical an order of magnitude smaller than the free-space wavelength.

### 1.5.2 Excitation of surface plasmons

The SPP dispersion curves show that $k_{\mathrm{SP}}$ is larger than $k_0$ and hence the momentum of a surface plasmon, $\hbar k_{\mathrm{SP}}$, is greater than that of a free-space photon $\hbar k_0$ at the same wavelength. The use of photons to excite SPPs, thus runs into trouble owing to this momentum mismatch. Different techniques have been designed to provide this "missing" momentum and excite SPPs on a surface. The more popular ones are the Otto and Kretschmann configurations, where the missing momentum is provided by coupling an evanacent wave to the interface [Novotny and Hecht, 2006].

Another method makes use of periodic surface corrugations, or a grating on the metal surface to excite the surface plasmons [Raether, 1988]. The surface wavevector component of an electromagnetic field illuminating such a diffraction grating can be momentum-matched with the SPPs, and thus is capable of exciting them. Similarly, non-radiative SPPs propagating on a smooth surface can be decoupled into photons when they are scattered by surface corrugations or diffraction gratings.

This property of surface corrugations is used in Chapter 6 for the design of our SPP-switching device. The device consists of a subwavelength slit etched on a thin gold film. The slit is flanked on both sides by a series of periodic grooves, positioned at a distance of 4 $\mu$m (which is smaller than the propagation length) from the slit to convert the SPPs to a freely propagating field. The intensity of this field is measured in the far zone.

## 1.6 The structure of this thesis

In this thesis, the concepts of coherence theory that we have just described are applied to a variety of problems. In Chapter 2, the influence of the state of coherence on the intensity distribution near focus is studied. Usually, a decrease of spatial coherence of the field leads to an intensity distribution that is "smoothed out" compared to its fully coherent counterpart. It is shown, experimentally, that for a special class of fields, namely those that are Bessel-correlated, the intensity at the geometric focus is a minimum rather than a maximum, i.e. such fields produce a hollow sphere of light when focused. Furthermore, by using a variable aperture, the focal intensity can be changed in a continuous way from a minimum to a maximum. Having the ability to tailor the focal intensity distribution allows one, for example, to switch from trapping high-index particles to trapping low-index particles.

In Chapters 3-5, we generalize the concepts of scalar theory of coherence to electromagnetic beams. We begin, in Chapter 3, by deriving expressions for the far-field properties of an electromagnetic beam generated by a planar quasi-homogeneous source. We derive two reciprocity relations, the first of which relates the spectral density of the beam in the far-zone to the Fourier transform of the correlation coefficients in the source plane. The second one relates the spectral degree of coherence in the far zone to the Fourier transforms of both the spectral density and of the correlation coefficients of the source field. Using these two reciprocity relations, we demonstrate that the spectral density, the the state of coherence and the state of polarization of these beams may change significantly on propagation.

The propagation-induced changes in the correlation properties of an electromagnetic Gaussian Schell-model beam are studied in Chapter 4. An expression for the spectral density matrix is derived and it is shown that coherence vortices, singularities of the correlation function, generally occur in these beams. These correlation singularities are three-dimensional in nature and their locus forms a closed string.

In Chapter 5, the three-dimensional structure of the correlation function of Chapter 4 is analyzed by considering its surfaces of equal phase. It is shown that in different cross-sections, the phase structures go through a rich set of topological reactions, including the creation and annihilation of singularities, dipoles, maxima, minima and phase saddles.

In Chapters 6 and 7 we describe an experiment to control the excitation of guided modes in a sub-wavelength slit that sustains two TM-modes. By varying the relative phase of three incident beams, the phase difference of the two modes can be changed in a continuous manner. In Chapter 6 this is used for the first demonstration of a dynamic surface plasmon switch. In Chapter 7 the same technique is employed to steer the radiation of the slit in a preferred direction.

# Chapter 2

# Creating an Intensity Minimum at the Focus of a Laser Beam using Spatial Coherence

This chapter is based on the following publication:

- S. B. Raghunathan, T. van Dijk, E. J. G. Peterman, and T. D. Visser "*Experimental demonstration of an intensity minimum at the focus of a laser beam created by spatial coherence: Application to optical trapping of dielectric particles*", Opt. Lett. **35**, pp. 4166 – 4168 (2011).

**Abstract**
In trying to manipulate the intensity distribution of a focused field, one typically uses amplitude or phase masks. Here we explore a novel approach, namely varying the state of spatial coherence of the incident field. We experimentally demonstrate that focusing of a Bessel-correlated beam produces an intensity minimum at the geometric focus, rather than a maximum. By varying the spatial coherence width of the field, which can be achieved by merely changing the size of an iris, it is possible to change this minimum into a maximum, in a continuous manner. This method can be used, for example, in novel optical trapping schemes, to selectively manipulate particles with either a low or a high index of refraction.

## 2.1 Introduction

The intensity distribution of a wave field in the focal region of a lens is a classical subject of physical optics [Stamnes, 1986]. One can manipulate this distribution by employing phase or amplitude masks. Recent theoretical studies showed that the state of spatial coherence of the field can also be used for this goal [Lu *et al.*, 1995; Wang *et al.*, 1997; Friberg *et al.*, 2001; Fischer and Visser, 2004; Wang and Lu, 2006; Pu *et al.*, 2006; Rao and Pu, 2007]. It was found, for example, that partially coherent, Gaussian-correlated beams produce a focal intensity distribution that is more spread out than that of a fully coherent beam [Visser *et al.*, 2002]. Two studies of Bessel-correlated fields yielded the surprising prediction that it is possible to change the maximum of intensity at the geometric focus into a minimum, in a continuous manner [Gbur and Visser, 2003a; Van Dijk *et al.*, 2008]. In this Chapter we discuss an experimental setup with which these predictions have been verified. Having the ability to tailor the focal intensity distribution allows one, for example, to switch from trapping high-index particles to trapping low-index particles [Gahagan and Swartzlander, 1999].

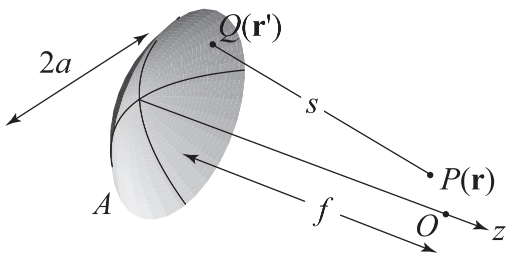


Figure 2.1: Illustration of the focusing configuration.

## 2.2 Theory

Let us first consider a converging, monochromatic field of frequency $\omega$ emerging from a circular aperture of radius $a$ in a plane opaque screen. The origin $O$ of a right-handed Cartesian coordinate system is taken at the geometric focus (see Fig. 2.1). The field at a point $Q(\mathbf{r}')$ on the

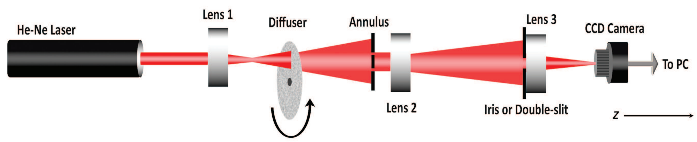


Figure 2.2: Schematic of the setup.

wavefront $A$ is denoted by $U^{(0)}(\mathbf{r}',\omega)$, where $\mathbf{r}'$ is a position vector. The field at a point $P(\mathbf{r})$ in the focal region is, according to the Huygens-Fresnel principle ([Born and Wolf, 1999], Chapter 8), given by the expression

$$U(\mathbf{r},\omega) = -\frac{\mathrm{i}}{\lambda}\int_A U^{(0)}(\mathbf{r}',\omega)\frac{e^{\mathrm{i}ks}}{s}\,\mathrm{d}^2r', \tag{2.1}$$

where $s = |\mathbf{r}-\mathbf{r}'|$ denotes the distance $QP$ and $\lambda$ is the wavelength of the field. (A periodic time-dependent factor $\exp(-\mathrm{i}\omega t)$ is suppressed.)

For a partially coherent wave field one must, apart from the field, also consider the cross-spectral density function of the field at two points $Q(\mathbf{r}'_1)$ and $Q(\mathbf{r}'_2)$, namely [Wolf, 2007]

$$W^{(0)}(\mathbf{r}'_1,\mathbf{r}'_2,\omega) = \left\langle U^*(\mathbf{r}'_1,\omega)U(\mathbf{r}'_2,\omega)\right\rangle, \tag{2.2}$$

where the angular brackets denote the average taken over a statistical ensemble of realizations. From equations (2.1) and (2.2) it follows that the cross-spectral density function in the focal region satisfies the formula

$$W(\mathbf{r}_1,\mathbf{r}_2,\omega) = \frac{1}{\lambda^2}\iint_A W^{(0)}(\mathbf{r}'_1,\mathbf{r}'_2,\omega)\frac{e^{\mathrm{i}k(s_2-s_1)}}{s_1s_2}\,\mathrm{d}^2r'_1\mathrm{d}^2r'_2, \tag{2.3}$$

where $s_1 = |\mathbf{r}_1-\mathbf{r}'_1|$, and $s_2 = |\mathbf{r}_2-\mathbf{r}'_2|$. The spectral density (or intensity at frequency $\omega$) at an observation point $P(\mathbf{r})$ is given by the 'diagonal elements' of the cross-spectral density function, i.e. $S(\mathbf{r},\omega) = W(\mathbf{r},\mathbf{r},\omega)$. A normalized measure of the field correlation is provided by the spectral

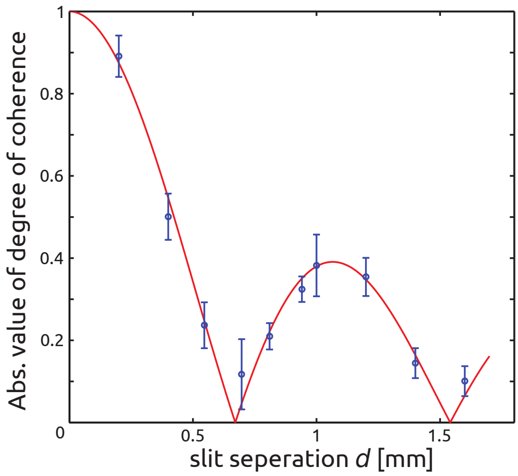


Figure 2.3: Modulus of the degree of spatial coherence of the field as a function of the slit separation $d$. The solid line indicates the theoretical prediction, the circles indicate experimental values with error bars.

degree of coherence, which is defined as [Mandel and Wolf, 1995]

$$\mu^{(0)}(\mathbf{r}_1, \mathbf{r}_2, \omega) = \frac{W^{(0)}(\mathbf{r}_1, \mathbf{r}_2, \omega)}{\sqrt{S^{(0)}(\mathbf{r}_1, \omega) S^{(0)}(\mathbf{r}_2, \omega)}}. \tag{2.4}$$

In our experiment the cross-spectral density of the field in the entrance pupil of the lens is of the form

$$W^{(0)}(\mathbf{r}_1, \mathbf{r}_2, \omega) = S^{(0)}(\omega) J_0(\beta |\mathbf{r}_2 - \mathbf{r}_1|). \tag{2.5}$$

Here $S^{(0)}$ is the spectrum of the incident field, taken to be independent of position, and $J_0$ denotes the Bessel function of the first kind and zeroth order. The parameter $\beta$ is, roughly speaking, the inverse of the coherence length. The numerical evaluation of Eq. (2.3) is discussed in [Gbur and Visser, 2003a] and [Van Dijk *et al.*, 2008].

Several tools, e.g. a programmable Spatial Light Modulator, can be used to obtain a $J_0$-correlated field. We have chose to create such a field using the van Cittert-Zernike theorem [Wolf, 2007]. According to that

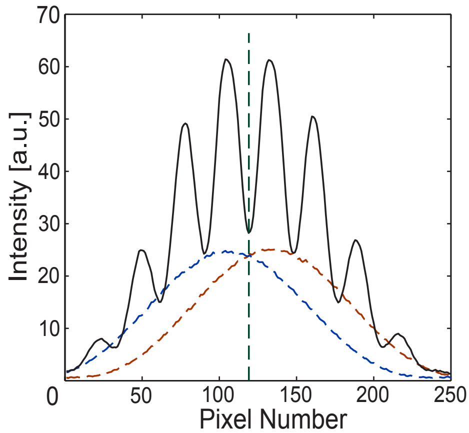


Figure 2.4: Illustration of negative correlation of the field at the two slits. At the center of the fringe pattern (vertical dashed line) an intensity minimum is observed. The dashed lines represent measurements with one slit covered.

theorem, the degree of coherence between two points in the far-zone of a completely incoherent source can be expressed in terms of the Fourier transform of the intensity distribution across the source. Thus, for a incoherent annular source, the degree of coherence follows a $J_0$-distribution in the far zone.

## 2.3 Experimental verification

The experimental setup is shown in Fig. 2.2. The output of a 15 mW Helium-Neon laser, operating at 632.8 nm, is focused by Lens 1 onto a rotating optical diffuser. As was verified, this renders the field practically incoherent. The incoherent beam illuminates a thin annulus of inner radius 1.2 mm and outer radius 1.5 mm. The annulus is positioned in the back focal plane of a 3.7 m lens (Lens 2), which produces a $J_0$-correlated field in its focal plane. This field is incident on an iris of radius 2.5 mm and focused by a lens of focal length 10.6 cm (Lens 3). The focused image is captured using a CCD camera connected to a PC via a frame grabber.

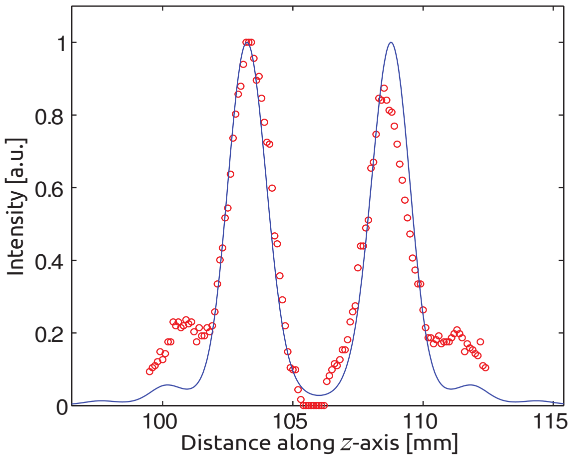


Figure 2.5: Intensity along the $z$-axis. The solid line represents the theoretical prediction, the circles correspond to experimental measurements.

This provides a transverse image of the focused field. The CCD camera is mounted on top of a translator, capable of taking steps of 0.01 mm along the $z$-axis.

### 2.3.1 Producing and measuring a Bessel-correlated field

The state of coherence of the far-zone field produced by the annulus was tested by replacing the iris by a series of identical double slits of width 0.172 mm and with varying slit spacing $d$. These pairs of slits were placed at the focus of Lens 2 and the resulting interference pattern was recorded. When the intensity at both slits is equal, the fringe visibility corresponds to the absolute value of the degree of coherence $\mu_{12}(\omega)$ of the field at the two slits [Mandel and Wolf, 1995]. Fig. 2.3 shows very good agreement between the measured values of the modulus of the degree of coherence and the theoretical predictions. For a slit spacing between 0.7 and 1.5 mm the fields at the two slits are anti-correlated, i.e. $\mu_{12}(\omega) < 0$. This was verified using a slit pair with separation distance $d = 0.8$ mm. The recorded interference pattern is shown in Fig. 2.4. The blue and the red lines represent measurements with one of the slits covered, and the black lines shown the

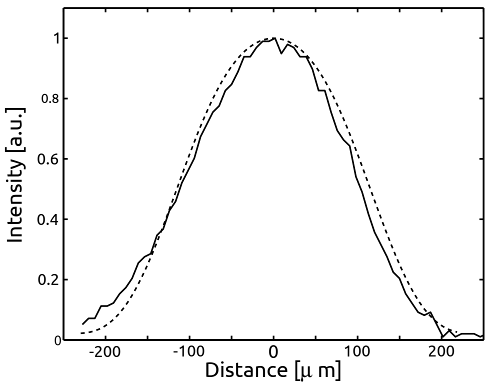


Figure 2.6: Intensity distribution in the focal plane for an iris of radius 0.25mm

double-slit interference pattern. At the center of the fringe pattern (indicated by the vertical dotted line), a minimum rather than a maximum is observed, confirming the predicted anti-correlation. Having thus established that the field that has indeed the desired Bessel-correlation, the slits were replaced by an iris and Lens 3 (with $a = 2.5$ mm and $f = 10.6$ cm), in order to study the focal intensity distribution.

### 2.3.2 Focusing the Bessel-correlated field

Intensity measurements in the $xy$-plane were made with steps of 0.1 mm along the $z$-axis. The results are shown in Fig. 2.5 where the horizontal axis represents the distance of the CCD camera from Lens 3. The solid blue curve represents the theoretical prediction, while the red circles are the experimental results. Instead of a maximum, an intensity minimum is observed at the geometric focus (around 106 mm) between two intensity peaks. It is seen that the experimental results closely follow the theoretical predictions.

To observe the rotationally symmetric intensity profile in the focal plane a set of three irises was used. The usage of irises with different radii (0.25 mm, 0.75 mm, and 1.2 mm) changes the spatial coherence width of the field. It is seen from Fig. 2.3 that for the smallest iris all points of

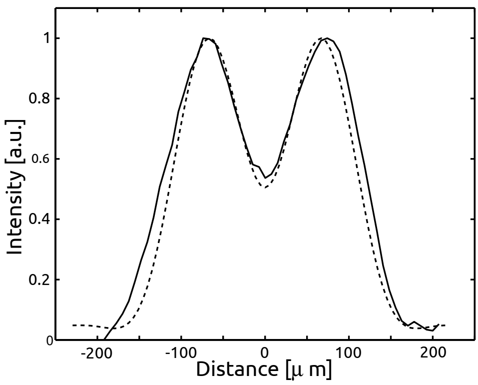


Figure 2.7: Intensity distribution in the focal plane for an iris of radius 0.75mm

the incident field are positively correlated. For the two larger ones both positive and negative field correlations occur. This enables us to observe the transition of the focal plane intensity from a maximum to a minimum. In order to maintain a Fresnel number larger than 20 in every case (to avoid the focal shift phenomenon [Stamnes, 1986; Wolf and Li, 1981]), Lens 3 was replaced by a lens with $f = 1$ cm. This results in a reduced separation between the maxima in the transverse direction of the order of 2 $\mu$m. Since the size of a pixel on the CCD camera is 8.6 $\mu$m, a simple magnification system was placed between Lens 3 and the camera.

The results of varying the radius of the iris is shown in Figs. 2.6, 2.7, and 2.8. In Fig. 2.6 the magnified intensity profile in the focal plane is shown for the case of an iris with a radius of 0.25 mm. The intensity reaches its maximum at the geometric focus (at distance 0 $\mu$m). Fig. 2.7 depicts the gradual transition to a intensity minimum when the iris radius is increased to 0.75 mm. In Fig. 2.8 this radius is further increased to 1.2 mm, and the intensity minimum at focus has become a near zero.

## 2.4 Conclusion

In conclusion, we have shown that the focusing of a $J_0$-correlated field produces an intensity minimum at the geometric focus. The observed in-

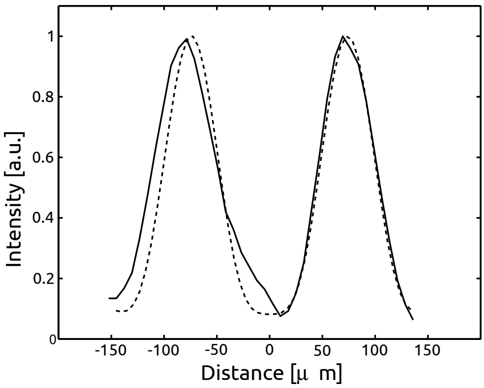


Figure 2.8: Intensity distribution in the focal plane for an iris of radius 1.2mm

tensity profiles along the $z$-axis and in the focal plane agree well with the theoretical predictions. The intensity minimum at the geometric focus can be manipulated by changing the spatial coherence width of the incident field. This is done by simply varying the aperture radius of the focusing system, and this enables us to change the intensity minimum of the focused field to a maximum, in a continuous manner. We have thus shown that, next to phase and amplitude control, there exists a fundamentally different mechanism to shape the intensity distribution in the focal region, namely the manipulation of the state of coherence of the incident field. This approach may prove to be of value in optical tweezers and in optical trapping, where it can be used to selectively manipulate particles with either a high or a low index of refraction. nmm

# Chapter 3

# Far-zone Properties of Electromagnetic Beams Generated by Quasi-homogeneous Sources

This chapter is based on the following publication:

- S. B. Raghunathan, T. D. Visser, and E. Wolf "*Far-zone properties of electromagnetic beams generated by quasi-homogeneous sources*", Opt. Commun. **295**, pp. 11-16(2013).

**Abstract**
We derive so-called reciprocity relations for the far-zone properties of electromagnetic beams generated by a broad class of partially coherent sources, namely those of the quasi-homogeneous type. We use these results to study the intensity distribution, the state of coherence and the polarization properties of such beams.

## 3.1 Introduction

The fully coherent, monochromatic beams that are often encountered in the literature are idealizations. In practice, optical fields are partially coherent. This may be due to several causes. The source may emit several modes, or it may be fluctuating due to mechanical vibrations or quantum noise. In addition, if the field propagates through a random medium such as the atmosphere, its coherence will degrade. Partially coherent beams have several interesting properties. For example, they may have the same directionality as nearly coherent laser beams, but they do not give rise to unwanted speckle [Mandel and Wolf, 1995, Sec. 5.4.2]. Equally important, the state of coherence of a field can be controlled to optimize it for certain uses such as propagation through atmospheric turbulence [Gbur and Wolf, 2002], optical coherence tomography [Brezinski, 2006], and the trapping of low index particles [Raghunathan *et al.*, 2010]. Reviews of partially coherent fields are given in [Mandel and Wolf, 1995], [Wolf, 2007] and [Gbur and Visser, 2010].

The majority of studies dealing with partially coherent electromagnetic beams, is concerned with beams that are generated by Gaussian Schell model (GSM) sources, see, for example [James, 1994; Korotkova *et al.*, 2004; Korotkova *et al.*, 2008]. Another important class of partially coherent sources, which partially overlaps with those of the GSM type, is formed by so-called *quasi-homogeneous planar sources* [Mandel and Wolf, 1995, Sec. 5.3.2]. Such sources are characterized, at each frequency $\omega$, by a) a spectral degree of coherence that is homogeneous, meaning that it only depends on the distance between two source points $\boldsymbol{\rho}'_1$ and $\boldsymbol{\rho}'_2$, i.e., $\mu^{(0)}(\boldsymbol{\rho}'_1, \boldsymbol{\rho}'_2, \omega) = \mu^{(0)}(\boldsymbol{\rho}'_2 - \boldsymbol{\rho}'_1, \omega)$, and b) by a spectral density $S^{(0)}(\boldsymbol{\rho}', \omega)$ that varies much slower with $\boldsymbol{\rho}'$ than $|\mu^{(0)}(\boldsymbol{\rho}'_2 - \boldsymbol{\rho}'_1, \omega)|$ varies with $\boldsymbol{\rho}'_2 - \boldsymbol{\rho}'_1$. The properties of such sources and the fields they generate have been extensively studied. In particular, *reciprocity relations*, equations that express far-zone properties of the field in terms of Fourier transforms of properties of the source, were derived [Carter and Wolf, 1977; Collett and Wolf, 1980; Wolf and Carter, 1984; Carter and Wolf, 1985; Kim and Wolf, 1987; Foley and Wolf, 1995; T. D. Visser and Wolf, 2006]. All these studies, however, were limited to scalar fields. In this article we extend the concept of quasi-homogeneity to sources that generate *electromagnetic* beams, and derive new reciprocity relations for the spectral density and degree of coherence of the beams in the far zone. These results are then used to study changes in the spectrum, the state of coherence, and the state of polarization that such beams undergo on propagation.

## 3.2 Partially coherent electromagnetic beams

The state of coherence and polarization of a random electromagnetic beam that propagates along the $z$-axis may be characterized, in the space-frequency domain, by a $2 \times 2$ *electric cross-spectral density matrix* [Wolf, 2007]

$$\mathbf{W}(\mathbf{r}_1, \mathbf{r}_2, \omega) = \begin{pmatrix} W_{xx}(\mathbf{r}_1, \mathbf{r}_2, \omega) & W_{xy}(\mathbf{r}_1, \mathbf{r}_2, \omega) \\ W_{yx}(\mathbf{r}_1, \mathbf{r}_2, \omega) & W_{yy}(\mathbf{r}_1, \mathbf{r}_2, \omega) \end{pmatrix}, \tag{3.1}$$

where

$$W_{ij}(\mathbf{r}_1, \mathbf{r}_2, \omega) = \langle E_i^*(\mathbf{r}_1, \omega) E_j(\mathbf{r}_2, \omega) \rangle, \quad (i, j = x, y). \tag{3.2}$$

Here $E_i(\mathbf{r}, \omega)$ is a Cartesian component of the electric field at a point $\mathbf{r}$ at frequency $\omega$, of a typical realization of the statistical ensemble representing the beam. The angled brackets indicate an ensemble average. From this matrix several quantities can be derived.

The *spectral density* of the field is given by the expression

$$S(\mathbf{r}, \omega) = \mathrm{Tr}\, \mathbf{W}(\mathbf{r}, \mathbf{r}, \omega), \tag{3.3}$$

where Tr denotes the trace.

The *spectral degree of coherence* of the field at two points $\mathbf{r}_1$ and $\mathbf{r}_2$ is defined as

$$\eta(\mathbf{r}_1, \mathbf{r}_2, \omega) = \frac{\mathrm{Tr}\, \mathbf{W}(\mathbf{r}_1, \mathbf{r}_2, \omega)}{[\mathrm{Tr}\, \mathbf{W}(\mathbf{r}_1, \mathbf{r}_1, \omega)\, \mathrm{Tr}\, \mathbf{W}(\mathbf{r}_2, \mathbf{r}_2, \omega)]^{1/2}}. \tag{3.4}$$

It can be shown the modulus of the spectral degree of coherence is bounded, viz.,

$$0 \leq |\eta(\mathbf{r}_1, \mathbf{r}_2, \omega)| \leq 1. \tag{3.5}$$

The upper bound represents full coherence, whereas the lower bound indicates a complete lack of coherence.

The *degree of polarization*, the ratio of the intensity of the polarized portion of the beam and its total intensity, can be shown to be

$$P(\mathbf{r},\omega) = \sqrt{1 - \frac{4\,\mathrm{Det}\,\mathbf{W}(\mathbf{r},\mathbf{r},\omega)}{[\mathrm{Tr}\,\mathbf{W}(\mathbf{r},\mathbf{r},\omega)]^2}}, \tag{3.6}$$

where Det denotes the determinant.

We will make use of definitions (3.3), (3.4) and (3.6) to study the far-zone behavior of beams generated by quasi-homogeneous sources.

## 3.3 Quasi-homogeneous electromagnetic sources

Let us consider a planar, secondary, planar source that produces an electromagnetic beam which propagates along the $z$-direction (see Fig. 3.1). Such a source may be characterized by an electric cross-spectral density matrix $\mathbf{W}^{(0)}$, whose diagonal elements can be expressed as [Wolf, 2007, Sec. 9.4.2]

$$W_{xx}^{(0)}(\boldsymbol{\rho}'_1,\boldsymbol{\rho}'_2,\omega) = \sqrt{S_x^{(0)}(\boldsymbol{\rho}'_1,\omega)\; S_x^{(0)}(\boldsymbol{\rho}'_2,\omega)}\; \mu_{xx}^{(0)}(\boldsymbol{\rho}'_1,\boldsymbol{\rho}'_2,\omega), \tag{3.7}$$

$$W_{yy}^{(0)}(\boldsymbol{\rho}'_1,\boldsymbol{\rho}'_2,\omega) = \sqrt{S_y^{(0)}(\boldsymbol{\rho}'_1,\omega)\; S_y^{(0)}(\boldsymbol{\rho}'_2,\omega)}\; \mu_{yy}^{(0)}(\boldsymbol{\rho}'_1,\boldsymbol{\rho}'_2,\omega). \tag{3.8}$$

Here $S_i^{(0)}(\boldsymbol{\rho}',\omega)$ is the spectral density associated with a Cartesian component $E_i$ ($i = x, y$) of the electric field vector, and $\mu_{ii}^{(0)}$ is the correlation coefficient of $E_i$ at points $\boldsymbol{\rho}'_1$ and $\boldsymbol{\rho}'_2$. The superscript (0) refers to quantities in the source plane, taken to be at $z = 0$.

If the source is of the *Schell-model* type, the correlation coefficients $\mu_{ii}(\boldsymbol{\rho}'_1,\boldsymbol{\rho}'_2,\omega)$ depend only on the difference $\boldsymbol{\rho}'_2 - \boldsymbol{\rho}'_1$, i.e.,

$$\mu_{ii}(\boldsymbol{\rho}'_1,\boldsymbol{\rho}'_2,\omega) = \mu_{ii}(\boldsymbol{\rho}'_2 - \boldsymbol{\rho}'_1,\omega). \tag{3.9}$$

Furthermore, a source is said to be *quasi-homogeneous* if the modulus of the correlation coefficient $\mu_{ii}^{(0)}(\boldsymbol{\rho}'_2 - \boldsymbol{\rho}'_1,\omega)$ varies much more rapidly with its argument $\boldsymbol{\rho}'_2 - \boldsymbol{\rho}'_1$, than the spectral density $S_i^{(0)}(\boldsymbol{\rho},\omega)$ varies with $\boldsymbol{\rho}$.

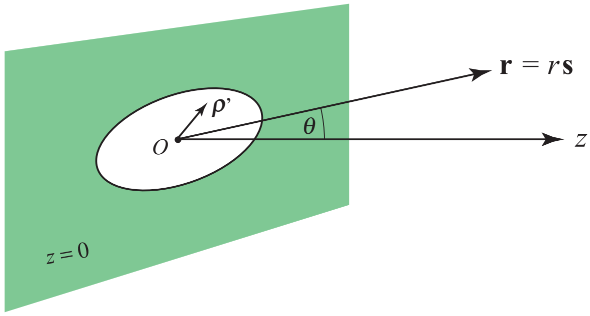


Figure 3.1: Illustrating the notation. The vector $\boldsymbol{\rho}' = (x, y)$ indicates a transverse position in the source plane $z = 0$. The line from the origin $O$ to an observation point $\mathbf{r} = r\mathbf{s}$, with $|\mathbf{s}| = 1$, makes an angle $\theta$ with the positive $z$-axis.

Since then both $S_x^{(0)}(\boldsymbol{\rho}, \omega)$ and $S_y^{(0)}(\boldsymbol{\rho}, \omega)$ are 'slow' functions compared to $\mu_{xx}^{(0)}(\boldsymbol{\rho}_2' - \boldsymbol{\rho}_1', \omega)$ and $\mu_{yy}^{(0)}(\boldsymbol{\rho}_2' - \boldsymbol{\rho}_1', \omega)$, respectively, we can write

$$W_{xx}^{(0)}(\boldsymbol{\rho}_1', \boldsymbol{\rho}_2') \approx S_x^{(0)}\left(\frac{\boldsymbol{\rho}_1' + \boldsymbol{\rho}_2'}{2}\right) \mu_{xx}^{(0)}(\boldsymbol{\rho}_2' - \boldsymbol{\rho}_1'), \tag{3.10}$$

$$W_{yy}^{(0)}(\boldsymbol{\rho}_1', \boldsymbol{\rho}_2') \approx S_y^{(0)}\left(\frac{\boldsymbol{\rho}_1' + \boldsymbol{\rho}_2'}{2}\right) \mu_{yy}^{(0)}(\boldsymbol{\rho}_2' - \boldsymbol{\rho}_1'), \tag{3.11}$$

where for brevity we have omitted the $\omega$-dependence of the various quantities. [1]

Next we make the change of variables

$$\boldsymbol{\rho}^{(+)} = \frac{\boldsymbol{\rho}_1' + \boldsymbol{\rho}_2'}{2}, \tag{3.12}$$

$$\boldsymbol{\rho}^{(-)} = \boldsymbol{\rho}_2' - \boldsymbol{\rho}_1'. \tag{3.13}$$

The Jacobian of this transformation is unity, and the inverse transforma-

[1] Although in the derivation of the reciprocity relations of Section 3.4 the off-diagonal elements are not used, it is to be noted that because of the non-negative definiteness of the cross-spectral density matrix these elements are not independent from the diagonal elements.

tion is given by the expressions

$$\begin{aligned} \boldsymbol{\rho}'_1 &= \boldsymbol{\rho}^{(+)} - \boldsymbol{\rho}^{(-)}/2, & (3.14) \\ \boldsymbol{\rho}'_2 &= \boldsymbol{\rho}^{(+)} + \boldsymbol{\rho}^{(-)}/2. & (3.15) \end{aligned}$$

For the purpose of later analysis we now derive an expression for the four-dimensional, spatial Fourier transformation of $W_{ij}^{(0)}(\boldsymbol{\rho}'_1, \boldsymbol{\rho}'_2)$, defined as

$$\tilde{W}_{ij}^{(0)}(\mathbf{f}_1, \mathbf{f}_2) = \left(\frac{1}{2\pi}\right)^2 \iint_{z=0} W_{ij}^{(0)}(\boldsymbol{\rho}'_1, \boldsymbol{\rho}'_2)\, e^{-\mathrm{i}[\mathbf{f}_1 \cdot \boldsymbol{\rho}'_1 + \mathbf{f}_2 \cdot \boldsymbol{\rho}'_2]}\, \mathrm{d}^2\rho'_1 \mathrm{d}^2\rho'_2. \tag{3.16}$$

It is readily seen that $\tilde{W}_{ii}^{(0)}(\mathbf{f}_1, \mathbf{f}_2)$ factorizes into the product of two two-dimensional Fourier transforms, viz.

$$\tilde{W}_{ii}^{(0)}(\mathbf{f}_1, \mathbf{f}_2) = \tilde{S}_i^{(0)}(\mathbf{f}_1 + \mathbf{f}_2)\, \tilde{\mu}_{ii}^{(0)}\left(\frac{\mathbf{f}_2 - \mathbf{f}_1}{2}\right), \tag{3.17}$$

where

$$\tilde{S}_i^{(0)}(\mathbf{f}) = \frac{1}{(2\pi)^2} \int_{z=0} S_i^{(0)}(\boldsymbol{\rho}') e^{-\mathrm{i}\mathbf{f}\cdot\boldsymbol{\rho}'}\, \mathrm{d}^2\rho', \tag{3.18}$$

and

$$\tilde{\mu}_{ii}^{(0)}(\mathbf{f}) = \frac{1}{(2\pi)^2} \int_{z=0} \mu_{ii}^{(0)}(\boldsymbol{\rho}') e^{-\mathrm{i}\mathbf{f}\cdot\boldsymbol{\rho}'}\, \mathrm{d}^2\rho'. \tag{3.19}$$

We notice that the fact that $\mu_{ii}^{(0)}(\boldsymbol{\rho}') = \mu_{ii}^{(0)*}(-\boldsymbol{\rho}')$, implies that $\tilde{\mu}_{ii}^{(0)}(\mathbf{f})$ is real-valued. In the next section we will make use of Eqs. (3.17)–(3.19).

## 3.4 Two reciprocity relations

The elements of the cross-spectral density matrix in the far-zone, which we denote by the superscript $(\infty)$, are related those in the source plane by the formula

$$W_{ij}^{(\infty)}(r_1\mathbf{s}_1, r_2\mathbf{s}_2) = (2\pi k)^2 \cos\theta_1 \cos\theta_2 \frac{e^{\mathrm{i}k(r_2 - r_1)}}{r_1 r_2} \tilde{W}_{ij}^{(0)}(-k\mathbf{s}_{1_\perp}, k\mathbf{s}_{2_\perp}), \tag{3.20}$$

where $\mathbf{s}_{i_\perp}$ is the two-dimensional projection, considered as a vector, of $\mathbf{s}_i$ onto the $xy$-plane. Equation (3.20) is a straightforward generalization of a similar expression for scalar fields [MANDEL AND WOLF, 1995, Sec. 5.3.1]. A derivation is presented in Appendix A.

On substituting from Eq. (3.17) into Eq. (3.20) we obtain the expressions

$$\begin{aligned} W_{xx}^{(\infty)}(r_1\mathbf{s}_1, r_2\mathbf{s}_2) &= (2\pi k)^2 \cos\theta_1 \cos\theta_2 \, \frac{e^{\mathrm{i}k(r_2-r_1)}}{r_1 r_2} \\ &\quad \times \tilde{S}_x^{(0)}[k(\mathbf{s}_{2_\perp} - \mathbf{s}_{1_\perp})]\, \tilde{\mu}_{xx}^{(0)}[k(\mathbf{s}_{1_\perp} + \mathbf{s}_{2_\perp})/2], \end{aligned} \tag{3.21}$$

$$\begin{aligned} W_{yy}^{(\infty)}(r_1\mathbf{s}_1, r_2\mathbf{s}_2) &= (2\pi k)^2 \cos\theta_1 \cos\theta_2 \, \frac{e^{\mathrm{i}k(r_2-r_1)}}{r_1 r_2} \\ &\quad \times \tilde{S}_y^{(0)}[k(\mathbf{s}_{2_\perp} - \mathbf{s}_{1_\perp})]\, \tilde{\mu}_{yy}^{(0)}[k(\mathbf{s}_{1_\perp} + \mathbf{s}_{2_\perp})/2]. \end{aligned} \tag{3.22}$$

On making use of Eqs. (3.21) and (3.22) in expression (3.3), we find for the far-zone spectral density that

$$S^{(\infty)}(r\mathbf{s}) = \left(\frac{2\pi k \cos\theta}{r}\right)^2 \left[\tilde{S}_x^{(0)}(0)\tilde{\mu}_{xx}^{(0)}(k\mathbf{s}_\perp) + \tilde{S}_y^{(0)}(0)\tilde{\mu}_{yy}^{(0)}(k\mathbf{s}_\perp)\right]. \tag{3.23}$$

Equation (3.23) is a *reciprocity relation* that shows that the far-zone spectral density of an electromagnetic beam which is generated by a planar, secondary, quasi-homogeneous source, is a linear function of the two Fourier transforms of the correlation coefficients of the electric field components. This relation takes on a particularly simple form for an on-axis observation point [i.e., $\mathbf{s} = (0, 0, 1)$], viz.,

$$S^{(\infty)}(0,0,z) = \left(\frac{2\pi k}{z}\right)^2 \left[\tilde{S}_x^{(0)}(0)\tilde{\mu}_{xx}^{(0)}(0) + \tilde{S}_y^{(0)}(0)\tilde{\mu}_{yy}^{(0)}(0)\right]. \tag{3.24}$$

Next we derive a reciprocity relation for the spectral degree of coherence. On substituting from Eqs. (3.21) and (3.22) into expression (3.4) we

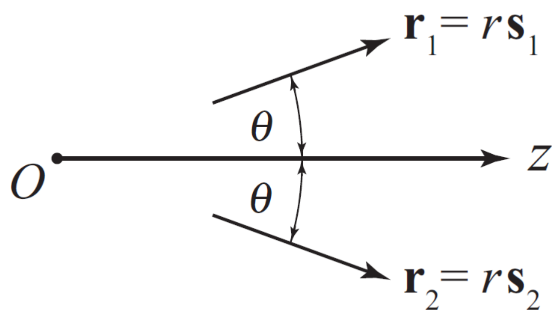


Figure 3.2: Two symmetrically located observation points, with $\mathbf{s}_{1_\perp} = -\mathbf{s}_{2_\perp}$.

find that

$$\begin{aligned}
\eta^{(\infty)}(r_1\mathbf{s}_1, r_2\mathbf{s}_2) \;=\; & \Big\{ \tilde{S}_x^{(0)}[k(\mathbf{s}_{2_\perp} - \mathbf{s}_{1_\perp})]\tilde{\mu}_{xx}^{(0)}\left[\frac{k}{2}(\mathbf{s}_{1_\perp} + \mathbf{s}_{2_\perp})\right] \\
& + \tilde{S}_y^{(0)}[k(\mathbf{s}_{2_\perp} - \mathbf{s}_{1_\perp})]\tilde{\mu}_{yy}^{(0)}\left[\frac{k}{2}(\mathbf{s}_{1_\perp} + \mathbf{s}_{2_\perp})\right]\Big\} e^{\mathrm{i}k(r_2 - r_1)} \\
& \times \left[\tilde{S}_x^{(0)}(0)\tilde{\mu}_{xx}^{(0)}(k\mathbf{s}_{1_\perp}) + \tilde{S}_y^{(0)}(0)\tilde{\mu}_{yy}^{(0)}(k\mathbf{s}_{1_\perp})\right]^{-1/2} \\
& \times \left[\tilde{S}_x^{(0)}(0)\tilde{\mu}_{xx}^{(0)}(k\mathbf{s}_{2_\perp}) + \tilde{S}_y^{(0)}(0)\tilde{\mu}_{yy}^{(0)}(k\mathbf{s}_{2_\perp})\right]^{-1/2} \qquad (3.25)
\end{aligned}$$

Since $\mu_{ii}^{(0)}$ is a "fast" function of its argument, its Fourier transform $\tilde{\mu}_{ii}^{(0)}$ is a "slow" function. Hence

$$\tilde{\mu}_{xx}^{(0)}(k\mathbf{s}_{1_\perp}) \approx \tilde{\mu}_{xx}^{(0)}(k\mathbf{s}_{2_\perp}) \approx \tilde{\mu}_{xx}^{(0)}\left[k(\mathbf{s}_{1_\perp} + \mathbf{s}_{2_\perp})/2\right], \qquad (3.26)$$

$$\tilde{\mu}_{yy}^{(0)}(k\mathbf{s}_{1_\perp}) \approx \tilde{\mu}_{yy}^{(0)}(k\mathbf{s}_{2_\perp}) \approx \tilde{\mu}_{yy}^{(0)}\left[k(\mathbf{s}_{1_\perp} + \mathbf{s}_{2_\perp})/2\right]. \qquad (3.27)$$

On making use of these approximations in Eq. (3.25) we obtain the formula

$$\begin{aligned}\eta^{(\infty)}(r_1\mathbf{s}_1, r_2\mathbf{s}_2) = \quad & \Big\{\tilde{S}_x^{(0)}[k(\mathbf{s}_{2_\perp} - \mathbf{s}_{1_\perp})]\tilde{\mu}_{xx}^{(0)}\left[\tfrac{k}{2}(\mathbf{s}_{1_\perp} + \mathbf{s}_{2_\perp})\right] \\ & + \tilde{S}_y^{(0)}[k(\mathbf{s}_{2_\perp} - \mathbf{s}_{1_\perp})]\tilde{\mu}_{yy}^{(0)}\left[\tfrac{k}{2}(\mathbf{s}_{1_\perp} + \mathbf{s}_{2_\perp})\right]\Big\} \\ & \times \Big[\tilde{S}_x^{(0)}(0)\tilde{\mu}_{xx}^{(0)}[k(\mathbf{s}_{1_\perp} + \mathbf{s}_{2_\perp})/2] \\ & + \tilde{S}_y^{(0)}(0)\tilde{\mu}_{yy}^{(0)}[k(\mathbf{s}_{1_\perp} + \mathbf{s}_{2_\perp})/2]\Big]^{-1} \times e^{ik(r_2 - r_1)}. \end{aligned} \tag{3.28}$$

Equation (3.28) is a second reciprocity relation. It asserts that the far-field spectral degree of coherence of an electromagnetic beam which is generated by a planar, secondary, quasi-homogeneous source, is a related to the Fourier transforms of both the spectral densities and of the correlation coefficients of the field in the source plane. If we choose two observation points that are located opposite each other with respect to the $z$-axis (i.e., $r_1 = r_2 = r$; $\mathbf{s}_{1_\perp} = -\mathbf{s}_{2_\perp}$), as is illustrated in Fig. 3.2, this relation simplifies to the form

$$\begin{aligned}\eta^{(\infty)}(r\mathbf{s}_1, r\mathbf{s}_2) &= \left[\tilde{S}_x^{(0)}(2k\mathbf{s}_{2_\perp})\tilde{\mu}_{xx}^{(0)}(0) + \tilde{S}_y^{(0)}(2k\mathbf{s}_{2_\perp})\tilde{\mu}_{yy}^{(0)}(0)\right] \\ & \times \left[\tilde{S}_x^{(0)}(0)\tilde{\mu}_{xx}^{(0)}(0) + \tilde{S}_y^{(0)}(0)\tilde{\mu}_{yy}^{(0)}(0)\right]^{-1}. \end{aligned} \tag{3.29}$$

We notice that the two reciprocity relations (3.23) and (3.28) are generalizations of well-known results for scalar fields, derived by Carter and Wolf [Carter and Wolf, 1977].

## 3.5 Off-diagonal matrix elements

In order to study the degree of polarization [see Eq. (3.6)], we must also consider the off-diagonal elements of the cross-spectral density matrix. The first matrix element in the source plane reads

$$W_{xy}^{(0)}(\boldsymbol{\rho}'_1, \boldsymbol{\rho}'_2) = \sqrt{S_x^{(0)}(\boldsymbol{\rho}'_1)\, S_y^{(0)}(\boldsymbol{\rho}'_2)}\, \mu_{xy}^{(0)}(\boldsymbol{\rho}'_2 - \boldsymbol{\rho}'_1). \tag{3.30}$$

In writing Eq. (3.30) the homogeneity of the source has been used. Next we assume that both $S_x^{(0)}(\boldsymbol{\rho}'_1)$ and $S_y^{(0)}(\boldsymbol{\rho}'_2)$ vary much slower with their argument than $\mu_{xy}^{(0)}(\boldsymbol{\rho}_2' - \boldsymbol{\rho}_1')$ varies with $\boldsymbol{\rho}_2' - \boldsymbol{\rho}_1'$. We then have to a good approximation that

$$S_x^{(0)}(\boldsymbol{\rho}_1') \approx S_x^{(0)}(\boldsymbol{\rho}_2') \approx S_x^{(0)}\left(\frac{\boldsymbol{\rho}_1' + \boldsymbol{\rho}_2'}{2}\right), \tag{3.31}$$

$$S_y^{(0)}(\boldsymbol{\rho}_2') \approx S_y^{(0)}(\boldsymbol{\rho}_1') \approx S_y^{(0)}\left(\frac{\boldsymbol{\rho}_1' + \boldsymbol{\rho}_2'}{2}\right). \tag{3.32}$$

In such a case we may introduce a new function

$$S_{xy}^{(0)}\left(\frac{\boldsymbol{\rho}_1' + \boldsymbol{\rho}_2'}{2}\right) \equiv \sqrt{S_x^{(0)}\left(\frac{\boldsymbol{\rho}_1' + \boldsymbol{\rho}_2'}{2}\right)}\sqrt{S_y^{(0)}\left(\frac{\boldsymbol{\rho}_1' + \boldsymbol{\rho}_2'}{2}\right)}, \tag{3.33}$$

$$\approx \sqrt{S_x^{(0)}(\boldsymbol{\rho}_1')}\sqrt{S_y^{(0)}(\boldsymbol{\rho}_2')}. \tag{3.34}$$

In terms of $S_{xy}^{(0)}$ the matrix element of Eq. (3.30) may be expressed in the form

$$W_{xy}^{(0)}(\boldsymbol{\rho}_1', \boldsymbol{\rho}_2') = S_{xy}^{(0)}[\boldsymbol{\rho}^{(+)}]\, \mu_{xy}^{(0)}[\boldsymbol{\rho}^{(-)}], \tag{3.35}$$

where the sum and difference variables defined by Eqs. (3.12) and (3.13) have been used. In strict analogy with the derivation of Eq. (3.17) we find that the Fourier transform of this matrix element equals

$$\tilde{W}_{xy}^{(0)}(\mathbf{f}_1, \mathbf{f}_2) = \tilde{S}_{xy}^{(0)}(\mathbf{f}_1 + \mathbf{f}_2)\, \tilde{\mu}_{xy}^{(0)}\left(\frac{\mathbf{f}_2 - \mathbf{f}_1}{2}\right). \tag{3.36}$$

On substituting from Eq. (3.36) into Eq. (3.20) we obtain the formula

$$\begin{aligned} W_{xy}^{(\infty)}(r_1\mathbf{s}_1, r_2\mathbf{s}_2) &= (2\pi k)^2 \cos\theta_1 \cos\theta_2\, \tilde{S}_{xy}^{(0)}[k(\mathbf{s}_{2_\perp} - \mathbf{s}_{1_\perp})] \\ &\quad \times \tilde{\mu}_{xy}^{(0)}[k(\mathbf{s}_{1_\perp} + \mathbf{s}_{2_\perp})/2]\frac{e^{\mathrm{i}k(r_2 - r_1)}}{r_1 r_2}. \end{aligned} \tag{3.37}$$

The remaining matrix element is given by the expression

$$W_{yx}^{(0)}(\boldsymbol{\rho}_1', \boldsymbol{\rho}_2') = \sqrt{S_y^{(0)}(\boldsymbol{\rho}_1')\, S_x^{(0)}(\boldsymbol{\rho}_2')}\, \mu_{yx}^{(0)}(\boldsymbol{\rho}_2' - \boldsymbol{\rho}_1'). \tag{3.38}$$

It follows from the definition of the cross-spectral density matrix that

$$W_{yx}^{(0)}(\boldsymbol{\rho}_1', \boldsymbol{\rho}_2') = \left[W_{xy}^{(0)}(\boldsymbol{\rho}_2', \boldsymbol{\rho}_1')\right]^*, \tag{3.39}$$

$$= S_{xy}^{(0)}[\boldsymbol{\rho}^{(+)}]\mu_{xy}^{(0)*}[-\boldsymbol{\rho}^{(-)}]. \tag{3.40}$$

Since

$$\frac{1}{(2\pi)^2}\int \mu_{xy}^{(0)*}[-\boldsymbol{\rho}^{(-)}]e^{-\mathrm{i}\mathbf{f}\cdot\boldsymbol{\rho}^{(-)}}\,\mathrm{d}^2\rho^{(-)} = [\tilde{\mu}_{xy}^{(0)}(\mathbf{f})]^*, \tag{3.41}$$

we find that

$$\begin{aligned} W_{yx}^{(\infty)}(r_1\mathbf{s}_1, r_2\mathbf{s}_2) &= (2\pi k)^2 \cos\theta_1\cos\theta_2\,\tilde{S}_{xy}^{(0)}[k(\mathbf{s}_{2_\perp} - \mathbf{s}_{1_\perp})] \\ &\quad \times\tilde{\mu}_{xy}^{(0)*}[k(\mathbf{s}_{1_\perp} + \mathbf{s}_{2_\perp})/2]\frac{e^{\mathrm{i}k(r_2-r_1)}}{r_1 r_2}. \end{aligned} \tag{3.42}$$

All four elements of the cross-spectral density matrix of the far-zone beam have now been established. On substituting from Eqs. (3.21), (3.22), (3.37), and (3.42) into Eq. (3.6) we find for the degree of polarization of the beam on-axis in the far zone the expression

$$\begin{aligned} P^{(\infty)}(0,0,z) &= \left\{\left[\tilde{S}_x^{(0)}(0)\tilde{\mu}_{xx}^{(0)}(0) - \tilde{S}_y^{(0)}(0)\tilde{\mu}_{yy}^{(0)}(0)\right]^2\right. \\ &\quad \left. +4\left[\tilde{S}_{xy}^{(0)}(0)|\tilde{\mu}_{xy}^{(0)}(0)|\right]^2\right\}^{1/2} \\ &\quad \times\left|\tilde{S}_x^{(0)}(0)\tilde{\mu}_{xx}^{(0)}(0) + \tilde{S}_y^{(0)}(0)\tilde{\mu}_{yy}^{(0)}(0)\right|^{-1}. \end{aligned} \tag{3.43}$$

It is seen from Eq. (3.43) that in this case the degree of coherence does *not* depend on the specific forms of the spectral densities or the correlation coefficients, but rather on their Fourier transform at frequency zero, i.e., on their spatial integrals.

## 3.6 Examples

In this section we will make use of the two reciprocity relations [Eqs. (3.24) and (3.29)], and Eq. (3.43) to illustrate changes in the spectrum, the degree of coherence, and the degree of polarization that occur on propagation to the far zone.

### 3.6.1 The far-field spectrum

Coherence-induced spectral changes have been examined for several years now. A review of this subject was given by Wolf and James [Wolf and

James, 1996]. As mentioned before, in contrast to the present work, almost all these studies deal with scalar fields. To see how the vectorial nature of the beam influences the far-zone spectrum, we repeat Eq. (3.24),

$$S^{(\infty)}(0,0,z;\omega) = \left(\frac{2\pi k}{z}\right)^2 \left[\tilde{S}_x^{(0)}(0;\omega)\tilde{\mu}_{xx}^{(0)}(0;\omega) + \tilde{S}_y^{(0)}(0;\omega)\tilde{\mu}_{yy}^{(0)}(0;\omega)\right], \tag{3.44}$$

where we have for clarity again displayed the frequency-dependence of the various quantities.

Let us now investigate the incoherent superposition of two laser beams, with constant intensity $A$ and an identical Gaussian spectrum, with central frequency $\omega_0$. One beam is $x$-polarized and has a radius $a$, whereas the other beam is $y$-polarized and has a radius $b$. In that case the two spectral densities are given by the expressions

$$S_x^{(0)}(\boldsymbol{\rho};\omega) = \begin{cases} Ae^{-(\omega-\omega_0)^2/\Delta^2} & \text{if } |\boldsymbol{\rho}| \leq a, \\ 0 & \text{if } |\boldsymbol{\rho}| > a, \end{cases} \tag{3.45}$$

$$S_y^{(0)}(\boldsymbol{\rho};\omega) = \begin{cases} Ae^{-(\omega-\omega_0)^2/\Delta^2} & \text{if } |\boldsymbol{\rho}| \leq b, \\ 0 & \text{if } |\boldsymbol{\rho}| > b, \end{cases} \tag{3.46}$$

with $\Delta$ the effective width of the two spectra. The two-dimensional spatial Fourier transforms now equal

$$\tilde{S}_x^{(0)}(\mathbf{f};\omega) = \frac{a^2 A}{2\pi} e^{-(\omega-\omega_0)^2/\Delta^2} \frac{J_1(fa)}{fa}, \tag{3.47}$$

$$\tilde{S}_y^{(0)}(\mathbf{f};\omega) = \frac{b^2 A}{2\pi} e^{-(\omega-\omega_0)^2/\Delta^2} \frac{J_1(fb)}{fb}, \tag{3.48}$$

where $J_1$ denotes the first order Bessel function of the first kind, and $f = |\mathbf{f}|$. Hence we find that

$$\tilde{S}_x^{(0)}(0;\omega) = \frac{a^2 A}{4\pi} e^{-(\omega-\omega_0)^2/\Delta^2}, \tag{3.49}$$

$$\tilde{S}_y^{(0)}(0;\omega) = \frac{b^2 A}{4\pi} e^{-(\omega-\omega_0)^2/\Delta^2}. \tag{3.50}$$

In addition, we assume that the correlation coefficients $\mu_{xx}^{(0)}$ and $\mu_{yy}^{(0)}$ are both Gaussians, but with different spatial and spectral widths, i.e.

$$\mu_{xx}^{(0)}(\boldsymbol{\rho}';\omega) = e^{-\boldsymbol{\rho}'/2\delta_{xx}^2} e^{-(\omega-\omega_0)^2/\Delta_{xx}^2}, \tag{3.51}$$

$$\mu_{yy}^{(0)}(\boldsymbol{\rho}';\omega) = e^{-\boldsymbol{\rho}'/2\delta_{yy}^2} e^{-(\omega-\omega_0)^2/\Delta_{yy}^2}. \tag{3.52}$$

It then follows that

$$\tilde{\mu}_{xx}^{(0)}(0;\omega) = \frac{\delta_{xx}^2}{2\pi} e^{-(\omega-\omega_0)^2/\Delta_{xx}^2}, \tag{3.53}$$

$$\tilde{\mu}_{yy}^{(0)}(0;\omega) = \frac{\delta_{yy}^2}{2\pi} e^{-(\omega-\omega_0)^2/\Delta_{yy}^2}. \tag{3.54}$$

On substituting from Eqs. (3.49), (3.50), (3.53) and (3.54) into Eq. (3.44), we obtain for the on-axis spectral density in the far zone the formula

$$\begin{aligned} S^{(\infty)}(0,0,z;\omega) &= \frac{A}{2}\left(\frac{k}{z}\right)^2 e^{-(\omega-\omega_0)^2/\Delta^2} \\ &\times \left\{ a^2\delta_{xx}^2 e^{-(\omega-\omega_0)^2/\Delta_{xx}^2} + b^2\delta_{yy}^2 e^{-(\omega-\omega_0)^2/\Delta_{yy}^2} \right\}. \end{aligned} \tag{3.55}$$

Using the fact that the on-axis spectral density in the source plane is given by the expression

$$S^{(0)}(0,0,0;\omega) = S_x^{(0)}(0,0,0;\omega) + S_y^{(0)}(0,0,0;\omega), \tag{3.56}$$

$$= 2Ae^{-(\omega-\omega_0)^2/\Delta^2}, \tag{3.57}$$

we can write the on-axis far-zone spectral density in the form

$$S^{(\infty)}(0,0,z;\omega) = M(\omega)\, S^{(0)}(0,0,0;\omega), \tag{3.58}$$

where the *spectral modifier function* $M$ is defined as

$$M(\omega) = \frac{1}{4}\left(\frac{\omega}{zc}\right)^2 \left\{ a^2\delta_{xx}^2 e^{-(\omega-\omega_0)^2/\Delta_{xx}^2} + b^2\delta_{yy}^2 e^{-(\omega-\omega_0)^2/\Delta_{yy}^2} \right\}. \tag{3.59}$$

Eq. (3.58) shows that the on-axis spectrum in the far-zone equals the on-axis spectrum in the source plane modified by the function $M(\omega)$. We

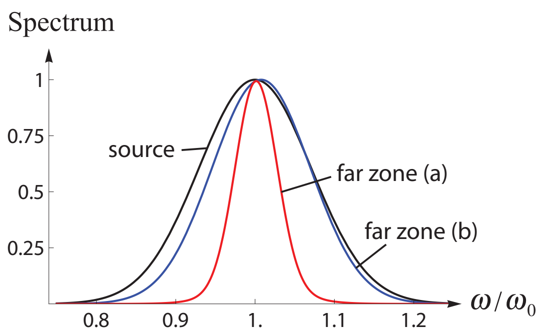


Figure 3.3: The on-axis spectrum in the source plane (black curve), and two on-axis spectra in the far zone. All spectra are normalized to unity. In this example $a = 1$, $b = 2a$, $\delta_{xx} = 1$, $\delta_{yy} = 2$, $\Delta = \omega_0/10$, $\Delta_{xx} = 0.1$ and $\Delta_{yy} = 0.04$ [far-zone spectrum (a)] or 0.2 [far-zone spectrum (b)].

note that the spectral modifier function contains several parameters: the beam sizes $a$ and $b$, the coherence lengths $\delta_{xx}$ and $\delta_{yy}$ and the spectral widths $\Delta_{xx}$ and $\Delta_{yy}$. Each of these parameters can give rise to changes of the spectrum on propagation. An example of the far-zone spectrum is shown in Fig. 3.3. It is seen the far-zone spectrum can be significantly narrower than that in the source plane (case a). Also, the maximum of the far-zone spectrum can be moved to higher frequencies (case b).

### 3.6.2 The far-field spectral degree of coherence

Let us next consider a source with two equal diagonal correlation coefficients, i.e. $\mu_{xx}^{(0)}(\boldsymbol{\rho}) = \mu_{yy}^{(0)}(\boldsymbol{\rho})$. It is also assumed that the two spectral densities are Gaussian functions with equal maxima, but with different widths, viz.

$$S_x^{(0)}(\boldsymbol{\rho}') = Ae^{-\rho'^2/2\sigma_x^2}, \tag{3.60}$$

$$S_y^{(0)}(\boldsymbol{\rho}') = Ae^{-\rho'^2/2\sigma_y^2}. \tag{3.61}$$

We have from Eq. (3.29) that in this the spectral degree of coherence of the field at two far field points is given by the formula

$$\eta^{(\infty)}(r\mathbf{s}_1, r\mathbf{s}_2) = \frac{\sigma_x^2 e^{-2(k\sigma_x \sin\theta)^2} + \sigma_y^2 e^{-2(k\sigma_y \sin\theta)^2}}{\sigma_x^2 + \sigma_y^2}, \quad (\mathbf{s}_{1\perp} = -\mathbf{s}_{2\perp}). \tag{3.62}$$

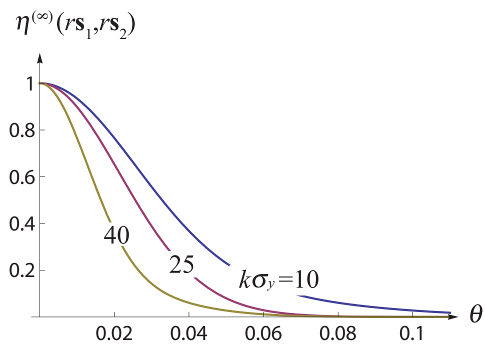


Figure 3.4: The spectral degree of coherence of a beam generated by a quasi-homogeneous source in the far field. The two symmetrically located observation points each make an angle $\theta$ with the beam axis (see Fig. 3.2). The normalized widths of the two spectral densities are $k\sigma_x = 20$ and $k\sigma_y = 10, 25, 40$.

An example of the angular dependence of $\eta^{(\infty)}(r\mathbf{s}_1, r\mathbf{s}_2)$ is shown in Fig. 3.4 for various values of the scaled transverse coherence length $k\sigma_y$. It is seen that the width of the spectral degree of coherence decreases when the width of the spectral density $k\sigma_y$ increases.

### 3.6.3 The far-field spectral degree of polarization

As our last example, we consider a source in which the two components of the electric field have an identical spectral density, but are uncorrelated, i.e.,

$$\begin{aligned} S_x^{(0)}(\boldsymbol{\rho}') &= S_y^{(0)}(\boldsymbol{\rho}'), \\ \mu_{xy}^{(0)}(\boldsymbol{\rho}') &= \mu_{yx}^{(0)}(\boldsymbol{\rho}') = 0. \end{aligned} \tag{3.63}$$

Also, we assume that both non-zero correlation coefficients have a Gaussian form

$$\mu_{ii}^{(0)}(\boldsymbol{\rho}') = e^{-\rho'^2/2\delta_{ii}^2}, \qquad (i = x, y). \tag{3.64}$$

It follows immediately from Eq. (3.6) that the field everywhere in the source plane is completely unpolarized, i.e. the degree of polarization

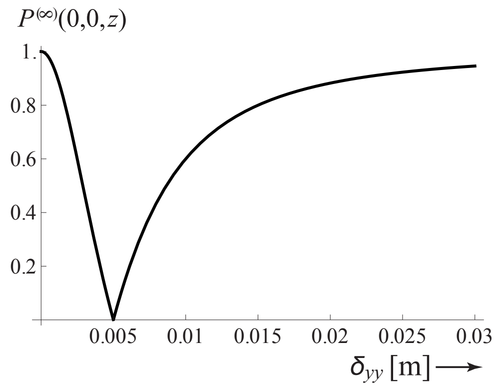


Figure 3.5: The spectral degree of polarization of a beam generated by a quasi-homogeneous source at a far-field axial point. In this example one effective coherence length is taken to be $\delta_{xx} = 0.5$ cm, whereas $\delta_{yy} =$ varies between 0 and 3 cm. The two spectral densities $S_x^{(0)}$ and $S_y^{(0)}$ are assumed to be equal.

$P^{(0)}(\boldsymbol{\rho}') = 0$. However, in the far zone that is generally not the case (see also [James, 1994]). We have from Eq. (3.64) that

$$\tilde{\mu}_{ii}^{(0)}(0) = \frac{1}{2\pi}\delta_{ii}^2. \tag{3.65}$$

Under these circumstances, the expression for the far-zone degree of polarization of the beam on the axis, Eq. (3.43), reduces to a function of the two effective correlation lengths only, namely

$$P^{(\infty)}(0,0,z) = \frac{\left|\delta_{xx}^2 - \delta_{yy}^2\right|}{\delta_{xx}^2 + \delta_{yy}^2}. \tag{3.66}$$

An example of the behavior of $P^{(\infty)}(0,0,z)$ is shown in Fig. 3.5. It is seen that the far-field degree of polarization varies strongly with the correlation length $\delta_{yy}$, and can take on all possible values between zero and unity.

## 3.7 Conclusions

We have studied the far-zone properties of electromagnetic beams that are generated by planar, secondary quasi-homogeneous sources. Two reciprocity relations were derived. The first one relates the spectral density in the far zone to the Fourier transforms of the correlation coefficients in the source plane. The second one relates the spectral degree of coherence in the far zone to the Fourier transforms of both the spectral densities and of the correlation coefficients of the source field. We applied these two relations to demonstrate how the spectral density, the coherence properties and the state of polarization can all change on propagation. While this manuscript was being finalized, a paper [Rodríguez-Herrera and Tyo, 2012] appeared in which some related results were reported.

# APPENDIX A: Derivation of Eq. (3.20)

For a beam-like field generated by a planar, secondary source, we have, according to the first Rayleigh diffraction formula [Mandel and Wolf, 1995, Sec. 3.2.5]

$$E_i(\mathbf{r}) = \frac{-1}{2\pi} \int_{z=0} E_i^{(0)}(\boldsymbol{\rho}') \frac{\partial}{\partial z} \left[ \frac{e^{\mathrm{i}kR}}{R} \right] \mathrm{d}^2\rho', \tag{A-1}$$

where $R = |(\boldsymbol{\rho}', 0) - \mathbf{r}|$. If $\mathbf{r}$ represents a point in the far zone, we have, to a good approximation, that

$$R \approx r - \boldsymbol{\rho}' \cdot \mathbf{s}_\perp. \tag{A-2}$$

Hence,

$$e^{\mathrm{i}kR} \approx e^{\mathrm{i}kr} e^{-\mathrm{i}k\boldsymbol{\rho}' \cdot \mathbf{s}_\perp}. \tag{A-3}$$

It then follows that

$$\frac{\partial}{\partial z} \left[ \frac{e^{\mathrm{i}kR}}{R} \right] = \frac{\partial r}{\partial z} \frac{\partial}{\partial r} \left[ \frac{e^{\mathrm{i}kR}}{R} \right], \tag{A-4}$$

$$\approx \frac{\mathrm{i}k}{r} \cos\theta \, e^{\mathrm{i}kr} e^{-\mathrm{i}k\boldsymbol{\rho}' \cdot \mathbf{s}_\perp}, \tag{A-5}$$

where we have made use of the facts that in the far zone $r \gg \lambda$, together with $z = r\cos\theta$. On making use of Eq. (A-5) in Eq. (A-1) we find that

$$E_i^{(\infty)}(\mathbf{r}) = \frac{-\mathrm{i}k}{2\pi} \cos\theta \, \frac{e^{\mathrm{i}kr}}{r} \int_{z=0} E_i^{(0)}(\boldsymbol{\rho}') \, e^{-\mathrm{i}k\boldsymbol{\rho}' \cdot \mathbf{s}_\perp} \, \mathrm{d}^2\rho', \tag{A-6}$$

$$= -2\pi \mathrm{i}k \cos\theta \, \frac{e^{\mathrm{i}kr}}{r} \tilde{E}_i^{(0)}(k\mathbf{s}_\perp), \tag{A-7}$$

where we used the definition of the Fourier transform, Eq. (3.18). On substituting from Eq. (A-7) into Eqs. (3.1) and (3.16) we obtain the result

$$\begin{aligned} W_{ij}^{(\infty)}(r_1\mathbf{s}_1, r_2\mathbf{s}_2) &= \langle E_i^{(\infty)*}(r_1\mathbf{s}_1) E_j^{(\infty)}(r_2\mathbf{s}_2)\rangle, && \text{(A-8)} \\ &= (2\pi k)^2 \cos\theta_1 \cos\theta_2 \\ &\quad \langle \tilde{E}_i^{(0)*}(k\mathbf{s}_{1_\perp}) \tilde{E}_j^{(0)}(k\mathbf{s}_{2_\perp})\rangle \frac{e^{\mathrm{i}k(r_2-r_1)}}{r_1 r_2}, && \text{(A-9)} \\ &= (2\pi k)^2 \cos\theta_1 \cos\theta_2 \\ &\quad \tilde{W}_{ij}^{(0)}(-k\mathbf{s}_{1_\perp}, k\mathbf{s}_{2_\perp}) \frac{e^{\mathrm{i}k(r_2-r_1)}}{r_1 r_2}, && \text{(A-10)} \end{aligned}$$

which is Eq. (3.20).

# Chapter 4

# Correlation Singularities of Partially Coherent Electromagnetic Beams

This chapter is based on the following publication:

- S. B. Raghunathan, H. F. Schouten, and T. D. Visser, "*Correlation singularities of partially coherent electromagnetic beams*", Optics Letters **37**, pp. 4179-4181 (2012).

**Abstract**
We demonstrate that coherence vortices, singularities of the correlation function, generally occur in partially coherent electromagnetic beams. In successive cross-sections of Gaussian Schell-model beams, their locus is found to be a closed string. These coherence singularities have implications for both interference experiments and correlation of intensity fluctuations measurements performed with such beams.

## 4.1 Introduction

The subject of singular optics [Nye, 1999; Soskin and Vasnetsov, 2001] is the structure of wave fields in the vicinity of optical vortices and polarization singularities. Most studies deal with monochromatic, and hence fully coherent, light.[1] Many wave fields that are encountered in practice, however, are partially coherent. Examples are the fields generated by multi-mode lasers and fields that have traveled through a random medium such as the atmosphere. The statistical properties of these fields are described by correlation functions, such as the *spectral degree of coherence* [Mandel and Wolf, 1995; Gbur and Visser, 2010]. A few years ago it was pointed out that these correlation functions can also exhibit singular behavior [Schouten *et al.*, 2003a]. Such correlation singularities, or "coherence vortices," occur at pairs of points at which the fields are completely uncorrelated. Coherence vortices have since been found in

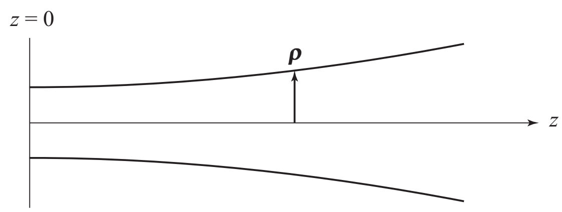


Figure 4.1: Illustrating the notation. The vector $\boldsymbol{\rho} = (x, y)$ indicates a transverse position.

optical beams [Gbur and Visser, 2003b], focused fields [Fischer and Visser, 2004], and in fields produced by Mie scattering [Marasinghe *et al.*, 2010]. These studies are all limited to scalar fields. Although the concept of a spectral degree of coherence has been generalized to electromagnetic beams [Wolf, 2007], the possible existence of *electromagnetic* coherence singularities in practical physical systems has not yet been examined. In this Chapter we show that these singularities occur quite generally in a wide class of electromagnetic beams, namely those of the Gaussian Schell-model type. We describe their evolution in successive cross-sections of these beams, and their physical implications.

[1] This qualification applies, strictly speaking, only to scalar fields.

## 4.2 Cross-spectral density of a random electromagnetic field

The state of coherence and polarization of a random beam that propagates along the $z$-axis is characterized by the *electric cross-spectral density matrix*, which is defined as [Wolf, 2007]

$$\mathbf{W}(\mathbf{r}_1, \mathbf{r}_2, \omega) = \begin{pmatrix} W_{xx}(\mathbf{r}_1, \mathbf{r}_2, \omega) & W_{xy}(\mathbf{r}_1, \mathbf{r}_2, \omega) \\ W_{yx}(\mathbf{r}_1, \mathbf{r}_2, \omega) & W_{yy}(\mathbf{r}_1, \mathbf{r}_2, \omega) \end{pmatrix}, \tag{4.1}$$

where

$$W_{ij}(\mathbf{r}_1, \mathbf{r}_2, \omega) = \langle E_i^*(\mathbf{r}_1, \omega) E_j(\mathbf{r}_2, \omega)\rangle, \quad (i, j = x, y). \tag{4.2}$$

Here $E_i(\mathbf{r}, \omega)$ is a Cartesian component of the electric field at a point $\mathbf{r}$ at frequency $\omega$, of a typical realization of the statistical ensemble representing the beam. The spectral degree of coherence $\eta(\mathbf{r}_1, \mathbf{r}_2, \omega)$ of the field is defined as

$$\eta(\mathbf{r}_1, \mathbf{r}_2, \omega) = \frac{\mathrm{Tr}\, \mathbf{W}(\mathbf{r}_1, \mathbf{r}_2, \omega)}{[\mathrm{Tr}\, \mathbf{W}(\mathbf{r}_1, \mathbf{r}_1, \omega)\, \mathrm{Tr}\, \mathbf{W}(\mathbf{r}_2, \mathbf{r}_2, \omega)]^{1/2}}, \tag{4.3}$$

where Tr denotes the trace. A correlation singularity occurs at pairs of points for which

$$\eta(\mathbf{r}_1, \mathbf{r}_2, \omega) = 0. \tag{4.4}$$

(From here on the $\omega$-dependence of the various quantities is suppressed.) The physical meaning of correlation singularities is twofold. First, when the fields at two points $\mathbf{r}_1$ and $\mathbf{r}_2$ are combined in Young's experiment, the visibility of the ensuing interference fringes depends on the value of $\eta(\mathbf{r}_1, \mathbf{r}_2)$ [Wolf, 2007, Sec. 9.2]. At a singularity, where $\eta(\mathbf{r}_1, \mathbf{r}_2) = 0$, the fringe visibility will be zero. Second, in Hanbury Brown-Twiss experiments one determines the correlation of intensity fluctuations at two points [Brown and Twiss, 1956]. These correlations depend on the so-called *degree of cross-polarization* [Volkov *et al.*, 2008]. It is easily seen that correlation singularities coincide with a divergence of the degree of cross-polarization. The consequences of this are discussed by [Hassinen *et al.*, 2011]. In view of these effects and because of the practical importance of partially coherent beams, it is therefore of interest to ask whether they contain coherence vortices.

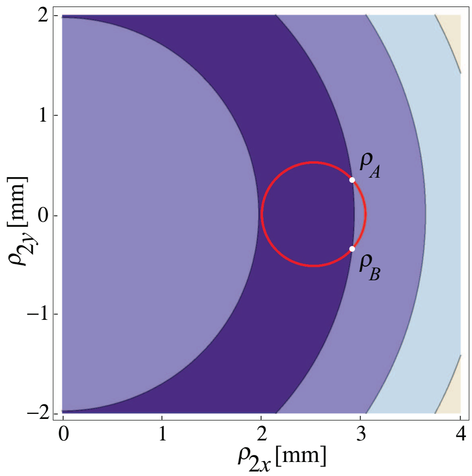


Figure 4.2: The locus of equal modulus of $W_{xx}$ and $W_{yy}$ (red curve), and the contours of $\mathrm{Arg}[W_{xx}] - \mathrm{Arg}[W_{yy}] = \pi \pmod{2\pi}$. Their intersections, $\boldsymbol{\rho}_A$ and $\boldsymbol{\rho}_B$, are correlation singularities. In this example $A_x = 1$, $A_y = 3$, $\lambda = 632.8$ nm, $\sigma = 1$ mm, $\delta_{xx} = 0.2$ mm, $\delta_{yy} = 0.09$ mm, $z = 1.4$ m, and $\boldsymbol{\rho}_1 = (2.5, 0)$ mm.

## 4.3 Correlation singularities

According to Eq. (4.3) coherence vortices occur in a transverse plane $z$ when both

$$|W_{xx}(\boldsymbol{\rho}_1, \boldsymbol{\rho}_2, z)| = |W_{yy}(\boldsymbol{\rho}_1, \boldsymbol{\rho}_2, z)|, \tag{4.5}$$

$$\mathrm{Arg}[W_{xx}(\boldsymbol{\rho}_1, \boldsymbol{\rho}_2, z)] - \mathrm{Arg}[W_{yy}(\boldsymbol{\rho}_1, \boldsymbol{\rho}_2, z)] = \pi \pmod{2\pi}. \tag{4.6}$$

For fixed $\boldsymbol{\rho}_1$ and $z$, the points $\boldsymbol{\rho}_2$ that satisfy condition (4.5) generally form a line. The same holds true for the solutions of Eq. (4.6). We therefore expect the simultaneous solutions, i.e. the coherence vortices, to be isolated points in the two-dimensional $\boldsymbol{\rho}_2$-plane. Note that when the fields at the two points that form an electromagnetic coherence singularity are combined in Young's experiment, the local modulations of $|E_x|^2$ and $|E_y|^2$ on the observation screen have equal magnitude and opposite sign, resulting in zero visibility of the total spectral density.

As we will show by example, such correlation singularities generically occur in Gaussian Schell-model beams. Such beams form a wide class of partially coherent electromagnetic beams for which in the source plane $z = 0$ (see Fig. 4.1) the elements of the cross-spectral density matrix read

$$W_{ij}(\boldsymbol{\rho}_1, \boldsymbol{\rho}_2, z = 0) = \sqrt{S_i(\boldsymbol{\rho}_1) S_j(\boldsymbol{\rho}_2)} \mu_{ij}(\boldsymbol{\rho}_2 - \boldsymbol{\rho}_1), \tag{4.7}$$

with the spectral densities $S_i(\boldsymbol{\rho}) = W_{ii}(\boldsymbol{\rho}, \boldsymbol{\rho})$ and the degree of correlation $\mu_{ij}(\boldsymbol{\rho}_2 - \boldsymbol{\rho}_1)$ both Gaussian functions, i.e.

$$S_i(\boldsymbol{\rho}) = A_i^2 \exp(-\boldsymbol{\rho}^2/2\sigma_i^2), \tag{4.8}$$

$$\mu_{ij}(\boldsymbol{\rho}_2 - \boldsymbol{\rho}_1) = B_{ij} \exp[-(\boldsymbol{\rho}_2 - \boldsymbol{\rho}_1)^2/2\delta_{ij}^2]. \tag{4.9}$$

The parameters $A_i$, $B_{ij}$, $\sigma_i$ and $\delta_{ij}$ are independent of position, but may depend on the frequency $\omega$. In addition, they have to satisfy certain contraints to ensure that the field is beam-like [Wolf, 2007]. As the beam propagates to a plane $z > 0$, and if we take $\sigma_x = \sigma_y = \sigma$, the matrix elements become [Wolf, 2007] [2]

$$W_{ij}(\boldsymbol{\rho}_1, \boldsymbol{\rho}_2, z) = \frac{A_i A_j B_{ij}}{\Delta_{ij}^2(z)} \exp\left[-\frac{(\boldsymbol{\rho}_1 + \boldsymbol{\rho}_2)^2}{8\sigma^2 \Delta_{ij}^2(z)}\right] \times \exp\left[-\frac{(\boldsymbol{\rho}_2 - \boldsymbol{\rho}_1)^2}{2\Omega_{ij}^2 \Delta_{ij}^2(z)}\right] \exp\left[\frac{\mathrm{i}k(\boldsymbol{\rho}_2^2 - \boldsymbol{\rho}_1^2)}{2R_{ij}(z)}\right], \tag{4.10}$$

where

$$\Delta_{ij}^2(z) = 1 + (z/k\sigma\Omega_{ij})^2, \tag{4.11}$$

$$\frac{1}{\Omega_{ij}^2} = \frac{1}{4\sigma^2} + \frac{1}{\delta_{ij}^2}, \tag{4.12}$$

$$R_{ij}(z) = [1 + (k\sigma\Omega_{ij}/z)^2]z. \tag{4.13}$$

We note that the matrix elements of Eq. (4.7) are real-valued and positive.

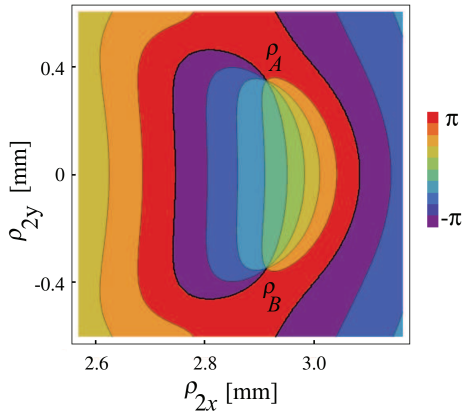


Figure 4.3: Color-coded phase plot of the degree of coherence $\eta(\boldsymbol{\rho}_1, \boldsymbol{\rho}_2, z)$ in the plane $z = 1.4$ m. The singularities at $\boldsymbol{\rho}_A$ and $\boldsymbol{\rho}_B$ have opposite topological charge.

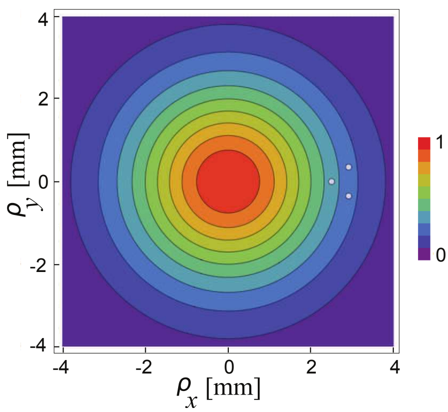


Figure 4.4: Normalized spectral density of the beam in the cross-section $z = 1.4$ m. The points $\boldsymbol{\rho}_1$, $\boldsymbol{\rho}_A$, and $\boldsymbol{\rho}_B$ are indicated by the three white dots.

Therefore, according to Eq. (4.6), there are no correlation singularities in the source plane. However, as we will now show, such singularities are created on propagation. In a cross-section of the beam we choose the point $\boldsymbol{\rho}_1$, and calculate for which points $\boldsymbol{\rho}_2$ both Eqs. (4.5) and (4.6) are satisfied. An example is shown in Fig. 4.2, in which the intersections of the curves, labeled $\rho_A$ and $\rho_B$, indicate two simultaneous solutions.That these points are indeed coherence vortices is also evidenced by Fig. 4.3. At the two singular points all phase contours coincide. It is seen that $\eta(\boldsymbol{\rho}_1, \boldsymbol{\rho}_A, z)$ and $\eta(\boldsymbol{\rho}_1, \boldsymbol{\rho}_B, z)$ have opposite *topological charge*, namely $+1$ and $-1$, respectively [Nye, 1999]. That the singularities formed by the pairs $(\boldsymbol{\rho}_1, \boldsymbol{\rho}_A, z)$ and $(\boldsymbol{\rho}_1, \boldsymbol{\rho}_B, z)$ lie well within the region of appreciable intensity is shown in Fig. 4.4 in which the normalized spectral density of the beam is plotted, together with the three points $\boldsymbol{\rho}_1$, $\boldsymbol{\rho}_A$, and $\boldsymbol{\rho}_B$. It is to be noted that for scalar Gaussian Schell-model beams [Mandel and Wolf, 1995, Eq. 5.6-91], such singularities do not exist.

When the cross-sectional plane $z$ is taken close to the source plane and is then gradually moved away, there first are no coherence singularities, until the pair $(\boldsymbol{\rho}_1, \boldsymbol{\rho}_A, z)$ and $(\boldsymbol{\rho}_1, \boldsymbol{\rho}_B, z)$ is created. This observation explains the opposite topological charge of the two coherence singularities, because, just as for "ordinary" phase singularities, topological charge is conserved in the creation process [Diehl and Visser, 2004]. When the plane $z$ is taken further away from the source, the opposite takes place: the points $\boldsymbol{\rho}_A$ and $\boldsymbol{\rho}_B$ move closer together until they eventually annihilate. This is connected to the fact that as $z \to \infty$ condition (4.6) can no longer be satisfied.

The evolution of the pair of singularities $(\boldsymbol{\rho}_1, \boldsymbol{\rho}_A, z)$ and $(\boldsymbol{\rho}_1, \boldsymbol{\rho}_B, z)$ along the direction of propagation is shown in Fig. 4.5. The surface corresponding to Eq. (4.5) is depicted in green ("equal amplitude"), whereas the surfaces corresponding to Eq. (4.6) are depicted in red ("opposite phase"). It is seen that the singularities, i.e. the intersection of these surfaces, form a closed "string" or loop in the direction of the beam, with one half of the string formed by $\boldsymbol{\rho}_A$ and the other by $\boldsymbol{\rho}_B$, having opposite topological charge. It follows from Eqs. (4.6) and (4.13) that the location of correlation singularities depends crucially on the parameters $\delta_{xx}$

[2] The one but last minus sign of Eq. 4.10 on p. 184 should be a plus sign as derived in the Appendix of this chapter.

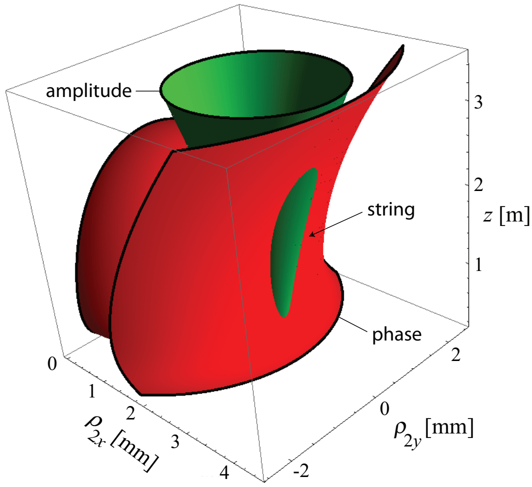


Figure 4.5: The intersection of a surface of equal amplitude (green) and a surface of opposite phase (red) constitutes a string of correlation singularities.

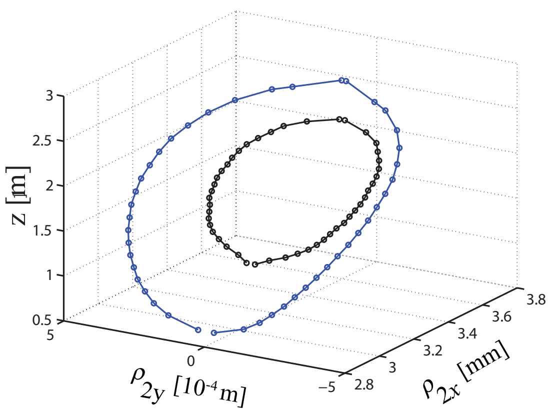


Figure 4.6: Two strings of correlation singularities in a partially coherent beam. The larger string (blue) is for $\delta_{yy} = 0.09$ mm, the shorter string (black) is for the case $\delta_{yy} = 0.12$ mm.

and $\delta_{yy}$, the transverse coherence length of the electric field components $E_x$ and $E_y$, respectively. Indeed, if we increase $\delta_{yy}$ from 0.09 mm (as in all previous examples), to 0.12 mm, the string of singularities becomes markedly shorter, as is shown in Fig. 4.6. For a value near $\delta_{yy} = 0.13$ mm the string disappears.

## 4.4 Conclusion

In conclusion, we have demonstrated that a new type of correlation singularities, namely an electromagnetic coherence vortex, generically occurs in partially coherent beams of the Gaussian Schell-model type. In consecutive cross-sections the singularities form a closed loop. At the end points of the loop the singularities are created or annihilated pairwise. The presence of these singularities have profound consequences for interference experiments performed with partially coherent beams.

## Appendix - The cross-spectral density matrix in the far-zone

In this Appendix we derive an expression for the cross-spectral density matrix in the far-zone. This matrix is given by the formula

$$\mathbf{W}(\boldsymbol{\rho}_1, \boldsymbol{\rho}_2, z) = \iint_{z=0} \mathbf{W}^{(0)}(\boldsymbol{\rho}_1', \boldsymbol{\rho}_2', z) G^*(\boldsymbol{\rho}_1 - \boldsymbol{\rho}_1', z) \times G(\boldsymbol{\rho}_2 - \boldsymbol{\rho}_2', z)\, \mathrm{d}^2\rho_1 \mathrm{d}^2\rho_2. \tag{A-1}$$

Here the paraxial Green's function reads,

$$G(\boldsymbol{\rho}_1 - \boldsymbol{\rho}_1', z) = \frac{-\mathrm{i}k}{2\pi z} e^{\mathrm{i}k(\boldsymbol{\rho}_1 - \boldsymbol{\rho}_1')^2/2z}. \tag{A-2}$$

The cross-spectral density matrix in the source plane is defined as

$$\mathbf{W}_{ij}^{(0)}(\boldsymbol{\rho}_1', \boldsymbol{\rho}_2') = \sqrt{S_i^{(0)}(\boldsymbol{\rho}_1')}\sqrt{S_j^{(0)}(\boldsymbol{\rho}_2')}\, \mu_{ij}^{(0)}(\boldsymbol{\rho}_2' - \boldsymbol{\rho}_1'), \tag{A-3}$$

Here $S_i^{(0)}$ and $S_j^{(0)}$ are the spectral densities of the electric field components $E_i$ and $E_j$ at the points $\boldsymbol{\rho}_1'$ and $\boldsymbol{\rho}_2'$ respectively. $\mu_{ij}^{(0)}$ is the correlation coefficient between the electric field components $E_i$ and $E_j$ at the points $\boldsymbol{\rho}_1'$ and $\boldsymbol{\rho}_2'$. They are defined as

$$S_i^{(0)}(\boldsymbol{\rho}_1') = A_i^2 e^{-\boldsymbol{\rho}_1'^2/2\sigma_i^2}, \tag{A-4}$$

$$S_j^{(0)}(\boldsymbol{\rho}_2') = A_j^2 e^{-\boldsymbol{\rho}_2'^2/2\sigma_j^2}, \tag{A-5}$$

$$\mu_{ij}^{(0)}(\boldsymbol{\rho}_2' - \boldsymbol{\rho}_2') = B_{ij} e^{(\boldsymbol{\rho}_2' - \boldsymbol{\rho}_1')^2/2\delta_{ij}^2}. \tag{A-6}$$

where $A_i$, $B_{ij}$, $\sigma_i$ and $\delta_{ij}$ are constants which are independent of position, but may depend on the frequency. Since $\mu_{xx}^{(0)}(0) = \mu_{yy}^{(0)}(0) = 1$, it follows that

$$B_{ij} = 1 \text{ when } i \ = \ j. \tag{A-7}$$

Since $W$ is a Hermitian positive definite matrix,

$$|B_{ij}| \leq 1 \text{ when } i \ \neq \ j, \tag{A-8}$$

$$B_{ij} = B_{ij}^*, \tag{A-9}$$

$$\delta_{ij} = \delta_{ji}. \tag{A-10}$$

Next, we assume that $\sigma_x = \sigma_y = \sigma$, and thus

$$\mathbf{W}_{ij}^{(0)}(\boldsymbol{\rho}_1', \boldsymbol{\rho}_2') = A_i\, A_j\, B_{ij}\, e^{-\boldsymbol{\rho}_1'^2/4\sigma^2} e^{-\boldsymbol{\rho}_2'^2/4\sigma^2} e^{(\boldsymbol{\rho}_2' - \boldsymbol{\rho}_1')^2/2\delta_{ij}^2}. \tag{A-11}$$

Hence,

$$\begin{aligned} \mathbf{W}(\boldsymbol{\rho}_1, \boldsymbol{\rho}_2, z) = \left(\frac{k}{2\pi z}\right)^2 A_i\, A_j\, B_{ij} \iint e^{-(\boldsymbol{\rho}_1'^2 + \boldsymbol{\rho}_2'^2)/4\sigma^2}\ e^{(\boldsymbol{\rho}_2' - \boldsymbol{\rho}_1')^2/2\delta_{ij}^2} \\ \times\, e^{-\mathrm{i}k(\boldsymbol{\rho}_1 - \boldsymbol{\rho}_1')^2/2z} e^{ik(\boldsymbol{\rho}_2 - \boldsymbol{\rho}_2')^2/2z}\, \mathrm{d}^2\rho_1 \mathrm{d}^2\rho_2. \end{aligned} \tag{A-12}$$

Next we make the change of variables,

$$\begin{aligned} \mathbf{R}^{(-)} &= \boldsymbol{\rho}_2' - \boldsymbol{\rho}_1', \\ \mathbf{R}^{(+)} &= \boldsymbol{\rho}_2' + \boldsymbol{\rho}_1'. \end{aligned} \tag{A-13}$$

The inverse transformations read

$$\begin{aligned} \boldsymbol{\rho}_1' &= \tfrac{\mathbf{R}^{(+)} - \mathbf{R}^{(-)}}{2}, \\ \boldsymbol{\rho}_2' &= \tfrac{\mathbf{R}^{(+)} + \mathbf{R}^{(-)}}{2}. \end{aligned} \tag{A-14}$$

The Jacobian of this transformation is the modulus of the determinant of the $4 \times 4$ matrix

$$\begin{aligned}
\mathbb{J} &= \begin{vmatrix} \partial\rho'_{1x}/\partial R_x^{(+)} & \partial\rho'_{1x}/\partial R_y^{(+)} & \partial\rho'_{1x}/\partial R_x^{(-)} & \partial\rho'_{1x}/\partial R_y^{(-)} \\ \partial\rho'_{1y}/\partial R_x^{(+)} & \partial\rho'_{1y}/\partial R_y^{(+)} & \partial\rho'_{1y}/\partial R_x^{(-)} & \partial\rho'_{1y}/\partial R_y^{(-)} \\ \partial\rho'_{2x}/\partial R_x^{(+)} & \partial\rho'_{2x}/\partial R_y^{(+)} & \partial\rho'_{2x}/\partial R_x^{(-)} & \partial\rho'_{2x}/\partial R_y^{(-)} \\ \partial\rho'_{2y}/\partial R_x^{(+)} & \partial\rho'_{2y}/\partial R_y^{(+)} & \partial\rho'_{2y}/\partial R_x^{(-)} & \partial\rho'_{2y}/\partial R_y^{(-)} \end{vmatrix}, \\
&= \begin{vmatrix} 1/2 & 0 & -1/2 & 0 \\ 0 & 1/2 & 0 & -1/2 \\ 1/2 & 0 & 1/2 & 0 \\ 0 & 1/2 & 0 & 1/2 \end{vmatrix}, \\
&= 1/4.
\end{aligned} \tag{A-15}$$

Since

$$\begin{aligned}
\boldsymbol{\rho}_1'^2 &= \tfrac{1}{4}\left[\mathbf{R}^{(+)2} + \mathbf{R}^{(-)2} - 2\mathbf{R}^{(+)}\cdot\mathbf{R}^{(-)}\right], \\
\boldsymbol{\rho}_2'^2 &= \tfrac{1}{4}\left[\mathbf{R}^{(+)2} + \mathbf{R}^{(-)2} + 2\mathbf{R}^{(+)}\cdot\mathbf{R}^{(-)}\right],
\end{aligned} \tag{A-16}$$

it follows that

$$e^{-(\boldsymbol{\rho}_1'^2+\boldsymbol{\rho}_2'^2)/4\sigma^2} = e^{-[\mathbf{R}^{(+)2}+\mathbf{R}^{(-)2}]/8\sigma^2}, \tag{A-17}$$

$$e^{-(\boldsymbol{\rho}_2'-\boldsymbol{\rho}_1')^2/2\delta_{ij}^2} = e^{-\mathbf{R}^{(-)2}/2\delta_{ij}^2}, \tag{A-18}$$

$$\begin{aligned}
e^{-\mathrm{i}k(\boldsymbol{\rho}_1-\boldsymbol{\rho}_1')^2/2z} &= e^{-\mathrm{i}k\boldsymbol{\rho}_1^2/2z}\, e^{-\mathrm{i}k[\mathbf{R}^{(+)^2}+\mathbf{R}^{(-)^2}-2\mathbf{R}^{(+)}\cdot\mathbf{R}^{(-)}]/8z} \\
&\quad \times e^{\mathrm{i}k[\mathbf{R}^{(+)}-\mathbf{R}^{(-)}]\cdot\boldsymbol{\rho}_1/2z},
\end{aligned} \tag{A-19}$$

$$\begin{aligned}
e^{\mathrm{i}k(\boldsymbol{\rho}_2-\boldsymbol{\rho}_2')^2/2z} &= e^{\mathrm{i}k\boldsymbol{\rho}_2^2/2z}\, e^{\mathrm{i}k[\mathbf{R}^{(+)^2}+\mathbf{R}^{(-)^2}+2\mathbf{R}^{(+)}\cdot\mathbf{R}^{(-)}]/8z} \\
&\quad \times e^{-\mathrm{i}k[\mathbf{R}^{(+)}+\mathbf{R}^{(-)}]\cdot\boldsymbol{\rho}_2/2z}.
\end{aligned} \tag{A-20}$$

Let us define,

$$\beta = \left(\frac{k}{2\pi z}\right)^2 \frac{A_i A_j B_{ij}}{4}, \tag{A-21}$$

Using Eqs. (A-17)–(A-21), we obtain

$$\begin{aligned} W_{ij}(\boldsymbol{\rho}_1, \boldsymbol{\rho}_2, z) = {} & \beta e^{\mathrm{i}k(\boldsymbol{\rho}_2^2 - \boldsymbol{\rho}_1^2)/2z} \iint \; e^{-R^{(-)^2}/2\delta_{ij}^2} \, e^{-(\mathbf{R}^{(+)2} + \mathbf{R}^{(-)2})/8\sigma^2} \\ & \times e^{-\mathrm{i}k\boldsymbol{\rho}_1^2/2z} e^{-\mathrm{i}k[\mathbf{R}^{(+)^2} + \mathbf{R}^{(-)^2} - 2\mathbf{R}^{(+)}\cdot\mathbf{R}^{(-)}]/8z} \\ & \times e^{\mathrm{i}k[\mathbf{R}^{(+)} - \mathbf{R}^{(-)}]\cdot\boldsymbol{\rho}_1/2z} \\ & \times e^{\mathrm{i}k\boldsymbol{\rho}_2^2/2z} \, e^{\mathrm{i}k(\mathbf{R}^{(+)^2} + \mathbf{R}^{(-)^2} + 2\mathbf{R}^{(+)}\cdot\mathbf{R}^{(-)})/8z} \\ & \times e^{-\mathrm{i}k[\mathbf{R}^{(+)} + \mathbf{R}^{(-)}]\cdot\boldsymbol{\rho}_2/2z} \, \mathrm{d}^2 R^{(+)} \mathrm{d}^2 R^{(-)}. \end{aligned} \tag{A-22}$$

Now we define

$$\frac{1}{\Omega_{ij}^2} = \frac{1}{4\sigma^2} + \frac{1}{\delta_{ij}^2}. \tag{A-23}$$

Applying Eq. (A-23) in Eq. (A-22), we obtain

$$\begin{aligned} W_{ij}(\boldsymbol{\rho}_1, \boldsymbol{\rho}_2, z) = {} & \beta \, e^{\mathrm{i}k(\boldsymbol{\rho}_2^2 - \boldsymbol{\rho}_1^2)/2z} \\ & \iint e^{-\mathbf{R}^{(-)^2}/2\Omega_{ij}^2} \, e^{-\mathrm{i}k\mathbf{R}^{(-)}\cdot(\boldsymbol{\rho}_1 + \boldsymbol{\rho}_2)/2z} e^{-\mathbf{R}^{(+)^2}/8\sigma^2} \\ & \times e^{\left\{\left[\mathrm{i}k\mathbf{R}^{(+)}\cdot(\boldsymbol{\rho}_1 - \boldsymbol{\rho}_2)/2z\right] + \left[\mathrm{i}k\mathbf{R}^{(+)}\cdot\mathbf{R}^{(-)}/2z\right]\right\}} \, \mathrm{d}^2 R^{(+)} \mathrm{d}^2 R^{(-)}. \end{aligned} \tag{A-24}$$

Eq. (A-24) can be re-written as

$$\begin{aligned} W_{ij}(\rho_1, \rho_2, z) = {} & \beta \, e^{\mathrm{i}k(\boldsymbol{\rho}_2^2 - \boldsymbol{\rho}_1^2)/2z} \\ & \times \int e^{-\mathbf{R}^{(-)^2}/2\Omega_{ij}^2} \, e^{-\mathrm{i}k\mathbf{R}^{(-)}\cdot(\boldsymbol{\rho}_1 + \boldsymbol{\rho}_2)/2z} \, \mathrm{d}^2 R^{(-)} \\ & \times \int e^{-\mathbf{R}^{(+)^2}/8\sigma^2} \, e^{\mathrm{i}k\mathbf{R}^{(+)}\cdot[\mathbf{R}^{(-)} + (\boldsymbol{\rho}_1 - \boldsymbol{\rho}_2)]/2z} \, \mathrm{d}^2 R^{(+)}. \end{aligned} \tag{A-25}$$

The latter part of Eq. (A-25), is in fact the Fourier transform of a Gaussian function. Thus, the Fourier integral part of Eq. (A-25) reduces to

$$
\begin{aligned}
&\int_{-\infty}^{+\infty} e^{-\mathbf{R}^{(+)^2}/8\sigma^2}\; e^{\mathrm{i}k\mathbf{R}^{(+)}\cdot[\mathbf{R}^{(-)}+(\boldsymbol{\rho}_1-\boldsymbol{\rho}_2)]/2z}\;\mathrm{d}^2R^{(+)} \\
&\quad = \int_{-\infty}^{+\infty} e^{-x^2/8\sigma^2}\; e^{\mathrm{i}kax}\mathrm{d}x \times \int_{-\infty}^{+\infty} e^{-y^2/8\sigma^2}\; e^{\mathrm{i}kby}\mathrm{d}y \\
&\quad = 4\sigma^2 2\pi e^{-2(a^2+b^2)k^2\sigma^2}, \\
&\quad = 8\pi\sigma^2\left\{e^{-(\boldsymbol{\rho}_1-\boldsymbol{\rho}_2)^2k^2\sigma^2/2z^2}\; e^{-\mathbf{R}^{(-)^2}k^2\sigma^2/2z^2}\; e^{-\mathbf{R}^{(-)}\cdot(\boldsymbol{\rho}_1-\boldsymbol{\rho}_2)k^2\sigma^2/z^2}\right\}.
\end{aligned}
\tag{A-26}
$$

Hence

$$
\begin{aligned}
W_{ij}(\boldsymbol{\rho}_1,\boldsymbol{\rho}_2,z,\omega) = \;& \beta e^{\mathrm{i}k(\boldsymbol{\rho}_2^2-\boldsymbol{\rho}_1^2)/2z}\; 8\pi\sigma^2 e^{-(\boldsymbol{\rho}_1-\boldsymbol{\rho}_2)^2k^2\sigma^2/2z^2} \\
&\times \int e^{-\mathbf{R}^{(-)^2}/2\Omega_{ij}^2}\; e^{-\mathrm{i}k\mathbf{R}^{(-)}\cdot(\boldsymbol{\rho}_1+\boldsymbol{\rho}_2)/2z} \\
&\times e^{-\mathbf{R}^{(-)^2}k^2\sigma^2/2z^2}\; e^{-\mathbf{R}^{(-)}\cdot(\boldsymbol{\rho}_1-\boldsymbol{\rho}_2)k^2\sigma^2/z^2}\;\mathrm{d}^2R^{(-)}.
\end{aligned}
\tag{A-27}
$$

Now let us set,

$$
\begin{aligned}
&-\left[\frac{\mathbf{R}^{(-)^2}k^2\sigma^2}{2z^2}+\frac{\mathbf{R}^{(-)^2}}{2\Omega_{ij}^2}+\frac{\mathbf{R}^{(-)}\cdot(\boldsymbol{\rho}_1-\boldsymbol{\rho}_2)k^2\sigma^2}{z^2}\right] = \\
&\qquad\qquad -\alpha\left[\mathbf{R}^{(-)^2}+\mathbf{R}^{(-)}\cdot\hat{\boldsymbol{\beta}}\right],
\end{aligned}
\tag{A-28}
$$

where

$$
\alpha = \frac{k^2\sigma^2}{2z^2}+\frac{1}{2\Omega_{ij}^2},
\tag{A-29}
$$

$$
\hat{\boldsymbol{\beta}} = (\boldsymbol{\rho}_1-\boldsymbol{\rho}_2)\frac{k^2\sigma^2}{\alpha z^2}.
\tag{A-30}
$$

On substituting from Eqs. (A-28) – (A-30) into Eq. (A-27) we obtain

$$
\begin{aligned}
W_{ij}(\boldsymbol{\rho}_1,\boldsymbol{\rho}_2,z,\omega) = \;& 8\pi\sigma^2\beta e^{\mathrm{i}k(\boldsymbol{\rho}_2^2-\boldsymbol{\rho}_1^2)/2z}\; e^{-(\boldsymbol{\rho}_1-\boldsymbol{\rho}_2)^2k^2\sigma^2/2z^2}\; e^{\alpha\hat{\boldsymbol{\beta}}^2/4} \\
&\times \int e^{-\alpha\left[\mathbf{R}^{(-)}+\hat{\boldsymbol{\beta}}/2\right]^2}\; e^{-\mathrm{i}k\mathbf{R}^{(-)}\cdot(\boldsymbol{\rho}_1+\boldsymbol{\rho}_2)/2z}\;\mathrm{d}^2R^{(-)}.
\end{aligned}
\tag{A-31}
$$

Next we apply a change of variables where

$$\mathbf{R} = \mathbf{R}^{(-)} + \frac{\hat{\boldsymbol{\beta}}}{2}. \tag{A-32}$$

The Jacobian of this transformation is unity. Thus, Eq. (A-31) can be re-written as

$$\begin{aligned} W_{ij}(\boldsymbol{\rho}_1, \boldsymbol{\rho}_2, z, \omega) = {} & 8\pi\sigma^2\beta \; e^{\mathrm{i}k(\boldsymbol{\rho}_2^2-\boldsymbol{\rho}_1^2)/2z} \; e^{-(\boldsymbol{\rho}_1-\boldsymbol{\rho}_2)^2 k^2\sigma^2/2z^2} \\ & \times e^{\mathrm{i}k[\boldsymbol{\rho}_2^2-\boldsymbol{\rho}_1^2]k^2\sigma^2/4\alpha z^3} \; e^{\alpha\hat{\boldsymbol{\beta}}^2/4} \\ & \times \int e^{-\alpha\mathbf{R}^2} \; e^{-\mathrm{i}k\mathbf{R}\cdot(\boldsymbol{\rho}_1+\boldsymbol{\rho}_2)/2z} \, \mathrm{d}^2R. \end{aligned} \tag{A-33}$$

From the definition of Fourier transform, we can write

$$\int e^{-\alpha\mathbf{R}^2} \; e^{-\mathrm{i}k\mathbf{R}\cdot(\boldsymbol{\rho}_1+\boldsymbol{\rho}_2)/2z} \, \mathrm{d}^2R = \frac{\pi}{\alpha} e^{-k^2(\boldsymbol{\rho}_1+\boldsymbol{\rho}_2)^2/16\alpha z^2}. \tag{A-34}$$

Applying Eq. (A-34) and using Eqs. (A-21), (A-29), (A-30), (4.11), (4.12) and Eq. (4.13) in Eq. (A-33) and simplifying, we obtain

$$\begin{aligned} W_{ij}(\boldsymbol{\rho}_1, \boldsymbol{\rho}_2, z) = {} & \frac{A_i A_j B_{ij}}{\Delta_{ij}^2(z)} \exp\left[-\frac{(\boldsymbol{\rho}_1+\boldsymbol{\rho}_2)^2}{8\sigma^2\Delta_{ij}^2(z)}\right] \\ & \times \exp\left[-\frac{(\boldsymbol{\rho}_2-\boldsymbol{\rho}_1)^2}{2\Omega_{ij}^2\Delta_{ij}^2(z)}\right] \exp\left[\frac{\mathrm{i}k(\boldsymbol{\rho}_2^2-\boldsymbol{\rho}_1^2)}{2R_{ij}(z)}\right], \end{aligned} \tag{A-35}$$

which is Eq. (4.10).

# Chapter 5

# Topological Reactions of Correlation Functions in Partially Coherent Electromagnetic Beams

This chapter is based on the following publication:

- S. B. Raghunathan, H. F. Schouten, and T. D. Visser, "*Topological reactions of correlation functions in partially coherent electromagnetic beams*", J. Opt. Soc. Am. A **30, pp. 582-588 (2013).**

**Abstract**
It was recently shown that so-called coherence vortices, singularities of the two-point correlation function, generally occur in partially coherent electromagnetic beams. We study the three-dimensional structure of these singularities and show that in successive cross-sections of a beam a rich variety of topological reactions takes place. These reactions involve, apart from vortices, the creation or annihilation of dipoles, saddles, maxima and minima of the phase of the correlation function. Since these reactions happen generically, i.e. under quite general conditions, these observations have implications for interference experiments with partially coherent, electromagnetic beams.

## 5.1 Introduction

It is well known that wave fields exhibit remarkable structures near their zeros of intensity [Nye and Berry, 1974]. These zeros may exist briefly, for example when pulsed fields are interfering with each other, or they may be permanent, when the fields are monochromatic. At such a zero, the amplitude of the field vanishes and its phase is, therefore, undefined or singular. Around these *phase singularities* the phase typically has a vortex-like behavior. Apart from phase singularities, *phase dipoles*, *phase extrema* and *phase saddles* may also occur. These different structures can exist arbitrarily close to one another, and can in fact be created or annihilated in so-called *topological reactions*, see for example [Freund, 2001; Freund, 2000; Freund and Kessler, 2001; Molina-Terriza *et al.*, 2001; Bekshaev *et al.*, 2004; Bezryadina *et al.*, 2006].

The most often-studied phase singularities are those of scalar wave fields, the Airy rings of focal fields being a prime example, see [Born and Wolf, 1999, Sec. 8.8.4] and [Karman *et al.*, 1997]. Singularities of the *Poynting vector* have also been analyzed. These occur in Sommerfeld's diffraction problem [Born and Wolf, 1999, Sec. 11.5], in focused fields [Boivin *et al.*, 1967], and in the transmission of light by subwavelength apertures [Schouten *et al.*, 2003b; Schouten *et al.*, 2004b]. Singularities of individual Cartesian components of the electric field vector have also been described in focal fields [Diehl and Visser, 2004]. Studies of this type (and also of polarization singularities, with which we will not be concerned here) have given rise to the relatively new discipline of *singular optics.* Reviews are presented in [Nye, 1999; Soskin and Vasnetsov, 2001].

In recent years, singular optics has been expanded to include *partially coherent wave fields.* Many fields that are encountered in practice, such as those generated by multi-mode lasers or fields that have traveled through atmospheric turbulence, belong to this category. In such fields the phase is a random quantity and therefore they do not contain "traditional" phase singularities. However, the statistical properties of these fields are described by two-point *correlation functions,* which *do* have a definite phase [Mandel and Wolf, 1995; Wolf, 2007; Gbur and Visser, 2010]. A few years ago it was pointed out that these functions can also exhibit singular behavior [Schouten *et al.*, 2003a]. Such *cor-*

*relation singularities,* or "coherence vortices," occur at pairs of points at which the field is completely uncorrelated. Coherence vortices have since been found in optical beams [Gbur and Visser, 2003b; Bogatyryova *et al.*, 2003; Palacios *et al.*, 2004; Swartzlander Jr and Schmit, 2004; Maleev *et al.*, 2004; Wang *et al.*, 2006b; Swartzlander Jr and Hernandez-Aranda, 2007; Van Dijk and Visser, 2009], focused fields [Fischer and Visser, 2004], in the far-zone of quasi-homogeneous sources [Van Dijk *et al.*, 2009], and in fields produced by Mie scattering [Marasinghe *et al.*, 2010; Marasinghe *et al.*, 2012]. Some of these studies have been carried out in the space-time domain, others in the space-frequency domain. Here we will use the latter approach. This means that the main two-point correlation function we will be dealing with is the *spectral degree of coherence* [Mandel and Wolf, 1995]. Just like their monochromatic counterparts, coherence vortices can also undergo topological reactions. Thus far such reactions have hardly been studied. Notable exceptions are [Wang and Takeda, 2006; Gu and Gbur, 2009; Marasinghe *et al.*, 2011].

In all the coherence studies mentioned above, the analysis was limited to scalar wave fields. Only recently has it has been shown that coherence singularities occur generically in partially coherent *electromagnetic* beams [Raghunathan *et al.*, 2012b]. For the wide class of *electromagnetic Gaussian Schell-model* (GSM) beams [Wolf, 2007] it was demonstrated that, even in the absence of ordinary phase singularities, the spectral degree of coherence typically displays singular behavior. (Notice that scalar GSM beams have no such coherence singularities.)

In this article we demonstrate that electromagnetic GSM beams are intrinsically three-dimensional in nature. We illustrate this by examining the structure of surfaces of equal-phase of the correlation function. In particular, this three-dimensional character implies that different beam cross-sections have different topological features [Freund, 2001]. Thus, an observer moving through successive cross-sectional planes will notice a sequence of *topological reactions.* From the conservation of topological charge and topological index [Nye, 1999; Strogatz, 1994], it is to be expected that the creation or annihilation of coherence vortices involves phase saddles. We find this to be the case, but reactions between phase extrema (maxima and minima), dipoles and phase saddles of the correlation

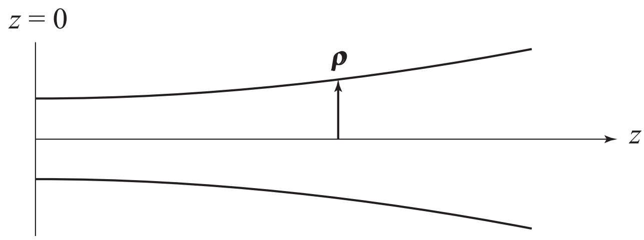


Figure 5.1: Illustrating the notation. A partially coherent, electromagnetic Gaussian-Schell model beam propagates in the $z$-direction. The source plane is taken to be at $z = 0$. The vector $\boldsymbol{\rho} = (x, y)$ indicates a transverse position.

function are also observed. As we will show, a rich variety of topological reactions occurs on propagation of these partially coherent, electromagnetic GSM beams. The observation that different cross-sections of a GSM beam have different coherence properties, has profound implications for their use in scattering [Van Dijk *et al.*, 2010] and interference experiments [Wolf, 2007].

## 5.2 Partially coherent electromagnetic beams

The properties of partially coherent, electromagnetic beams are described in detail in a textbook by Wolf [Wolf, 2007]. Here we summarize some of the main definitions. The state of coherence and polarization of a random beam that propagates along the $z$-axis is characterized by its *electric cross-spectral density matrix*

$$\mathbf{W}(\mathbf{r}_1, \mathbf{r}_2, \omega) = \begin{pmatrix} W_{xx}(\mathbf{r}_1, \mathbf{r}_2, \omega) & W_{xy}(\mathbf{r}_1, \mathbf{r}_2, \omega) \\ W_{yx}(\mathbf{r}_1, \mathbf{r}_2, \omega) & W_{yy}(\mathbf{r}_1, \mathbf{r}_2, \omega) \end{pmatrix}, \tag{5.1}$$

where

$$W_{ij}(\mathbf{r}_1, \mathbf{r}_2, \omega) = \langle E_i^*(\mathbf{r}_1, \omega) E_j(\mathbf{r}_2, \omega) \rangle, \quad (i, j = x, y). \tag{5.2}$$

Here $E_i(\mathbf{r}, \omega)$ is a Cartesian component of the electric field at a point $\mathbf{r}$ at frequency $\omega$, of a typical realization of the statistical ensemble representing the beam, and the angled brackets indicate the ensemble average. The *spectral degree of coherence* $\eta(\mathbf{r}_1, \mathbf{r}_2, \omega)$ of the field is defined as

$$\eta(\mathbf{r}_1, \mathbf{r}_2, \omega) = \frac{\mathrm{Tr}\, \mathbf{W}(\mathbf{r}_1, \mathbf{r}_2, \omega)}{[\mathrm{Tr}\, \mathbf{W}(\mathbf{r}_1, \mathbf{r}_1, \omega)\, \mathrm{Tr}\, \mathbf{W}(\mathbf{r}_2, \mathbf{r}_2, \omega)]^{1/2}}, \tag{5.3}$$

where Tr denotes the trace. A correlation singularity occurs at pairs of points for which $\eta(\mathbf{r}_1, \mathbf{r}_2, \omega) = 0$. (From now on we suppress the $\omega$-dependence of the various quantities.)

The presence of correlation singularities in a wave field has several consequences. First, when the fields at points $\mathbf{r}_1$ and $\mathbf{r}_2$ are combined in Young's experiment, the visibility of the ensuing interference fringes crucially depends on the value of $\eta(\mathbf{r}_1, \mathbf{r}_2)$, see [Wolf, 2007, Sec. 9.2]. At a singularity, where $\eta(\mathbf{r}_1, \mathbf{r}_2) = 0$, the fringe visibility will be zero. This is because the local modulations of $|E_x|^2$ and $|E_y|^2$ on the observation screen have equal magnitude and opposite sign, resulting in a zero visibility of the total spectral density. Second, in experiments of the Hanbury Brown-Twiss type one determines the correlation of intensity fluctuations at two points [Brown and Twiss, 1956]. These higher-order correlations depend on the so-called *degree of cross-polarization* [Volkov *et al.*, 2008]. Correlation singularities coincide with a divergence of the degree of cross-polarization, the consequences of which are discussed in [Hassinen *et al.*, 2011]. Furthermore, it is to be noted that the phase singularities found in monochromatic fields and the coherence singularities of partially coherent fields are not independent of one another. The former can evolve into the latter when the coherence of the field decreases [Gbur *et al.*, 2004; Gbur and Visser, 2006; Visser and Schoonover, 2008; Gbur and Swartzlander, 2008].

Since we are dealing with beams, it is natural to investigate the possible occurence of coherence vortices in a transverse plane $z$ = constant (see Fig. 5.1). We therefore set $\mathbf{r}_1 = (\boldsymbol{\rho}_1, z)$ and $\mathbf{r}_2 = (\boldsymbol{\rho}_2, z)$. According to Eq. (5.3) a coherence vortex exists when both

$$|W_{xx}(\boldsymbol{\rho}_1, \boldsymbol{\rho}_2, z)| = |W_{yy}(\boldsymbol{\rho}_1, \boldsymbol{\rho}_2, z)|, \tag{5.4}$$

and

$$\arg[W_{xx}(\boldsymbol{\rho}_1, \boldsymbol{\rho}_2, z)] - \arg[W_{yy}(\boldsymbol{\rho}_1, \boldsymbol{\rho}_2, z)] = \pi \quad (\mathrm{mod}\ 2\pi), \tag{5.5}$$

where arg denotes the argument or phase of the matrix element.

## 5.3 Electromagnetic Gaussian Schell-model beams

Gaussian Schell-model beams [Wolf, 2007] form a wide class of partially coherent, electromagnetic beams that includes the lowest-order Gaussian laser mode. For such beams the elements of the cross-spectral density matrix in the source plane $z = 0$ read

$$W_{ij}(\boldsymbol{\rho}_1, \boldsymbol{\rho}_2, z = 0) = \sqrt{S_i(\boldsymbol{\rho}_1) S_j(\boldsymbol{\rho}_2)} \mu_{ij}(\boldsymbol{\rho}_2 - \boldsymbol{\rho}_1), \quad (i, j = x, y), \tag{5.6}$$

with the spectral densities of the two individual components of the electric field vector $S_i(\boldsymbol{\rho}) = W_{ii}(\boldsymbol{\rho}, \boldsymbol{\rho})$ and the correlation coefficient $\mu_{ij}(\boldsymbol{\rho}_2 - \boldsymbol{\rho}_1)$ both assumed to be Gaussian functions, i.e.

$$S_i(\boldsymbol{\rho}) = A_i^2 \exp(-\boldsymbol{\rho}^2/2\sigma_i^2), \tag{5.7}$$

$$\mu_{ij}(\boldsymbol{\rho}_2 - \boldsymbol{\rho}_1) = B_{ij} \exp[-(\boldsymbol{\rho}_2 - \boldsymbol{\rho}_1)^2/2\delta_{ij}^2]. \tag{5.8}$$

The parameters $A_i$, $B_{ij}$, $\sigma_i$ and $\delta_{ij}$ are independent of position, but may depend on the frequency $\omega$. In addition, they have to satisfy certain constraints to ensure that the field is beam-like [Wolf, 2007]. As the beam propagates to a plane $z > 0$, and if we take $\sigma_x = \sigma_y = \sigma$, the matrix elements become (see [Wolf, 2007], where the one but last minus sign of Eq. (10) on p. 184 should be a plus sign)

$$\begin{aligned} W_{ij}(\boldsymbol{\rho}_1, \boldsymbol{\rho}_2, z) = {} & \frac{A_i A_j B_{ij}}{\Delta_{ij}^2(z)} \exp\left[-\frac{(\boldsymbol{\rho}_1 + \boldsymbol{\rho}_2)^2}{8\sigma^2 \Delta_{ij}^2(z)}\right] \\ & \times \exp\left[-\frac{(\boldsymbol{\rho}_2 - \boldsymbol{\rho}_1)^2}{2\Omega_{ij}^2 \Delta_{ij}^2(z)}\right] \exp\left[\frac{\mathrm{i}k(\boldsymbol{\rho}_2^2 - \boldsymbol{\rho}_1^2)}{2R_{ij}(z)}\right], \end{aligned} \tag{5.9}$$

where

$$\Delta_{ij}^2(z) = 1 + (z/k\sigma\Omega_{ij})^2, \tag{5.10}$$

$$\frac{1}{\Omega_{ij}^2} = \frac{1}{4\sigma^2} + \frac{1}{\delta_{ij}^2}, \tag{5.11}$$

$$R_{ij}(z) = [1 + (k\sigma\Omega_{ij}/z)^2]z, \tag{5.12}$$

with $k = \omega/c$ the wavenumber associated with frequency $\omega$, $c$ being the speed of light in vacuum.

We note that the diagonal matrix elements as given by Eq. (5.6) are real-valued and positive. Therefore, according to Eq. (5.5), there are no correlation singularities in the source plane. However, as we will illustrate in section 5.4, such singularities can be created as the beam propagates.

## 5.4 The three-dimensional structure of correlation singularities

Let us first analyze the shape of the surfaces of equal phase of the correlation function when there are no coherence singularities present. We choose a fixed point of reference $\boldsymbol{\rho}_1$ and then calculate the phase of $\eta(\boldsymbol{\rho}_1, \boldsymbol{\rho}_2, z)$. An example for $\arg \eta(\boldsymbol{\rho}_1, \boldsymbol{\rho}_2, z) = \pi$ is shown in Fig. 5.2, where two sheets of this constant phase can be seen. (On increasing the field of view, more of these sheets become visible.) If we slightly reduce the value of one of the correlation lengths to $\delta_{yy} = 0.14$ mm, the two initially smooth surfaces get somewhat "dented," as is shown in Fig. 5.3. These dents corresponds to minima of the phase in transverse cross-sections of the beam (i.e., planes for which $z =$ constant), and will be discussed in section 5.5.

On further decreasing $\delta_{yy}$ to 0.12 mm, correlation singularities come into existence. These lines of coherence vortices form a closed string, as shown in Fig. 5.4. For all values of the phase, surfaces of equal phase end on this string. This can either happen from "within" the string, or from "outside" of the string. The former leads to a protrusion of the phase surface, the latter leads to a hole in the surface. As is seen from Fig. 5.5, both cases happen simultaneously: the string (indicated in green) borders both a hole and a protrusion of the phase sheet. Notice that the left-hand sheet is now dented even more.

If we further decrease the value of $\delta_{yy}$, the string of coherence vortices increases in size, and extends to both surfaces of equal phase, as is shown in Fig. 5.6. The protrusion of Fig. 5.5 has grown in size and now connects the two sheets. When the value of $\delta_{yy}$ decreased even more, the string of singularities gradually moves to the left (i.e., to smaller values of $\rho_{2x}$), and only intersects the left-hand phase sheet. The right-hand sheet has returned to its previous smooth state. This is shown in Fig. 5.7.

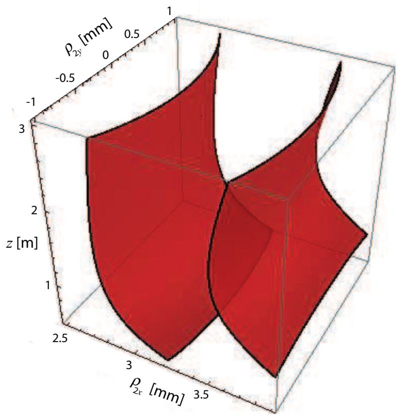


Figure 5.2: Two surfaces for which the phase of $\eta(\boldsymbol{\rho}_1, \boldsymbol{\rho}_2, z)$ equals $\pi$. In this case $\delta_{yy} = 0.18$ mm. The other parameters are $\lambda = 632.8$ nm, $\delta_{xx} = 0.2$ mm, $\sigma = 1$ mm, $A_x = 1$ and $A_y$=3. The reference point $\boldsymbol{\rho}_1 = (2.5, 0)$ mm.

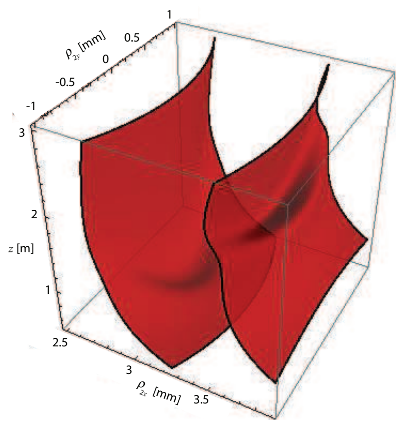


Figure 5.3: Two surfaces for which the phase of $\eta(\boldsymbol{\rho}_1, \boldsymbol{\rho}_2, z)$ equals $\pi$. In this case $\delta_{yy} = 0.14$ mm.

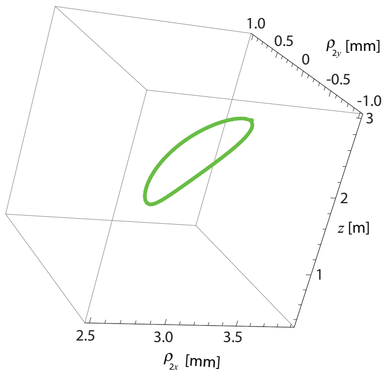


Figure 5.4: A closed string of coherence singularities (green curve).

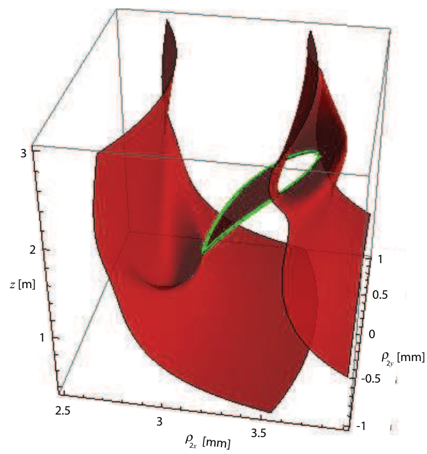


Figure 5.5: Two surfaces for which the phase of $\eta(\boldsymbol{\rho}_1, \boldsymbol{\rho}_2, z)$ equals $\pi$. In this case $\delta_{yy} = 0.12$ mm. A closed string of coherence vortices (green curve) has come into existence. The right-hand phase sheet terminates on the string, creating a hole and a protrusion of the sheet.

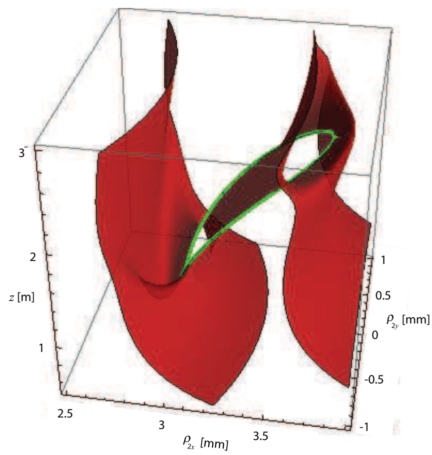


Figure 5.6: A single surface for which the phase of $\eta(\boldsymbol{\rho}_1, \boldsymbol{\rho}_2, z)$ equals $\pi$. In this case $\delta_{yy} = 0.11$ mm. The string of coherence vortices (green curve) has expanded, causing the protrusion of Fig. 5.5 to grow. The two formerly disjointed phase sheets are now connected.

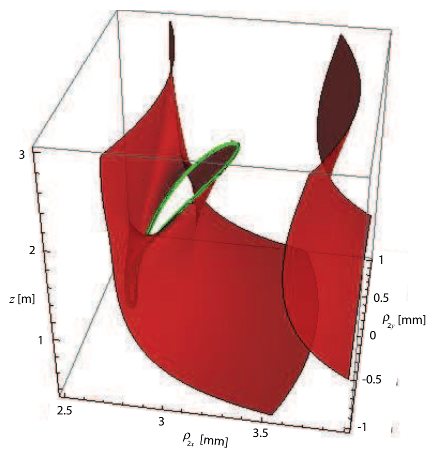


Figure 5.7: Two surfaces for which the phase of $\eta(\boldsymbol{\rho}_1, \boldsymbol{\rho}_2, z)$ equals $\pi$. In this case $\delta_{yy} = 0.06$ mm. The string of coherence vortices (green curve) has moved sideways and now only intersects the left-hand phase sheets. The two phase sheets are again disconnected.

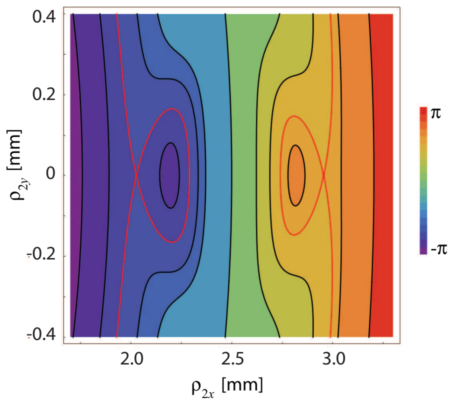


Figure 5.8: Phase contours of $\eta(\boldsymbol{\rho}_1, \boldsymbol{\rho}_2, z)$ in the plane $z = 0.1$ m. A minimum, a maximum and two saddle points (intersections of the red curves) can be seen. In this and in the following examples we have taken $\boldsymbol{\rho}_1 = (2.5, 0)$ mm, $A_x = 1$, $A_y = 3$, $\sigma = 1$ mm, $\delta_{xx} = 0.2$ mm, $\delta_{yy} = 0.12$ mm, and the wavelength $\lambda = 633$ nm.

From the complicated three-dimensional nature of the correlation function as illustrated in Figs. 5.2–5.7 it follows that different transverse cross-sections of the beam will have quite different topological features. Therefore an observer moving from one transverse plane to another, witnesses a series of topological reactions, as will be discussed in the next section.

## 5.5 Topological reactions

As noted above, the phase of monochromatic fields typically has a vortex-like behavior around a phase singularity. This is also true for the phase of the spectral degree of coherence $\eta(\boldsymbol{\rho}_1, \boldsymbol{\rho}_2, z)$ around a correlation singularity. On keeping $\boldsymbol{\rho}_1$ fixed, while traversing in a counter-clockwise manner a closed circuit in the $\boldsymbol{\rho}_2, z$-plane which encompasses a single singularity, the phase of $\eta(\boldsymbol{\rho}_1, \boldsymbol{\rho}_2, z)$ changes by an amount of $2n\pi$. The non-zero integer $n$ is called the *topological charge*. To the singularities (vortices and dipoles) and to the stationary points (extrema and saddles) of the phase of the correlation function we can also assign a *topological index* [Nye, 1998], which

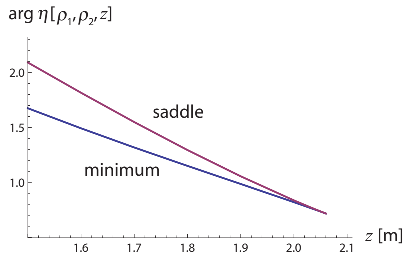


Figure 5.9: Phase of $\eta(\boldsymbol{\rho}_1, \boldsymbol{\rho}_2, z)$ at the minimum and at the phase saddle (visible on the left-hand side in Fig. 5.8), in various cross-sections of the beam.

is defined as the topological charge of the phase singularities of the vector field $\nabla_\perp \arg[\eta(\boldsymbol{\rho}_1, \boldsymbol{\rho}_2, z)]$, where $\nabla_\perp$ denotes differentiation with respect to $\boldsymbol{\rho}_2$. In topological reactions both the charge and index are conserved quantities [Strogatz, 1994]. In Table 5.1 they are listed for different types of points.

Table 5.1: Topological charge and index of singular and stationary points.

| | charge | index |
|---|---|---|
| vortex | $\pm 1$ | 1 |
| saddle | 0 | $-1$ |
| maximum | 0 | 1 |
| minimum | 0 | 1 |
| dipole | 0 | 2 |

In the following examples we first choose a fixed reference point $\boldsymbol{\rho}_1$, and then, keeping all other parameters fixed, we calculate the phase contours of $\eta(\boldsymbol{\rho}_1, \boldsymbol{\rho}_2, z)$ in successive cross-sections of the beam.

A first result is shown in Fig. 5.8 for the plane $z = 0.1$ m. On the left there is a phase minimum together with a phase saddle (the intersection of the red contour line with itself), whereas on the right a phase maximum and another phase saddle can be seen. If the plane of observation is moved away from the source, the minimum and the nearby saddle gradually move

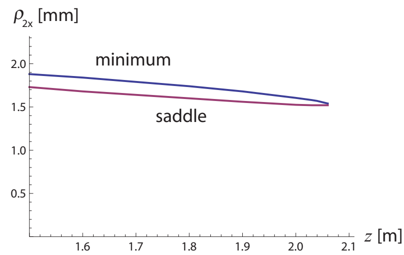


Figure 5.10: The position $\rho_{2x}$ of the minimum (blue curve) and that of the saddle (red curve) in various cross-sections of the beam. Near $z = 2.06$ m the minimum and the saddle point annihilate each other.

together and the phase of $\eta(\boldsymbol{\rho}_1, \boldsymbol{\rho}_2, z)$ at the minimum and at the saddle point converge. This goes on until the minimum and the saddle annihilate each other near $z = 2.06$ m. This process is illustrated in Figs. 5.9 and 5.10.

From here on we will concentrate on the the maximum and its nearby saddle point of Fig. 5.8 which, as we will see, go through a rich series of topological reactions in which both the zero total topological charge and the zero topological index are conserved. As the plane of observation is gradually moved away from the source, the saddle decays into a minimum and two saddle points (near $z = 0.89$ m). The end result of this reaction is shown in Fig. 5.11.

On further moving the cross-sectional plane another reaction occurs: the two phase extrema move closer to each other (along the $\rho_{2x}$-axis) until they form a *dipole* [Hsiung, 1981] with index 2 (near $z = 1.18$ m), as is illustrated in Fig. 5.12. A dipole is formed when the cross-sectionial plane is tangential to the vortex string shown in Fig. 5.4. This dipole immediately decays into two phase vortices with opposite topological charge, which in successive cross-sections gradually move away from each other along the $\rho_{2y}$-direction. The result is depicted in Fig. 5.13. Notice that two vortices occur whenever the cross-sectional plane intersects the vortex string at two points.

According to Eq. (5.12), the factor $R_{ij}(z)$ becomes infinite as $z \to \infty$. This implies that in that limit Eq. (4.6) can no longer be satisfied, since both diagonal elements of the cross-spectral density matrix become real-valued and positive. Therefore the correlation vortices must eventually

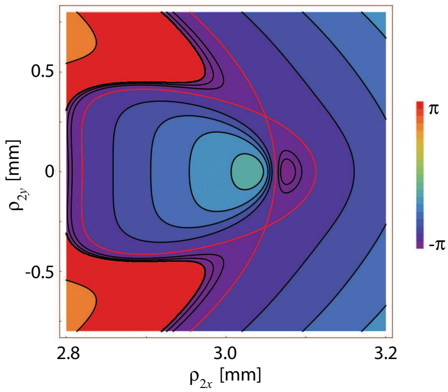


Figure 5.11: Phase contours of $\eta(\boldsymbol{\rho}_1, \boldsymbol{\rho}_2, z)$ in the plane $z = 1.12$ m. The right-hand side phase saddle of Fig. 5.8 has decayed into a minimum and two saddles (intersections of the two red curves).

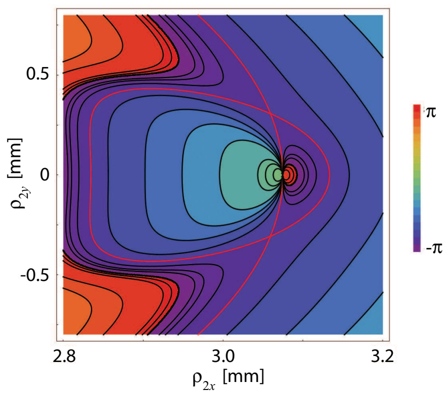


Figure 5.12: Phase contours of $\eta(\boldsymbol{\rho}_1, \boldsymbol{\rho}_2, z)$ in the plane $z = 1.1808$ m, containing a dipole and two saddle points (intersections of the red curves).

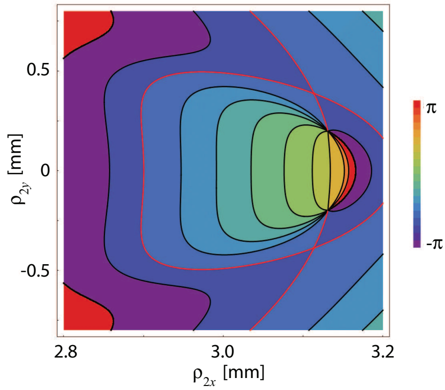


Figure 5.13: Phase contours of $\eta(\boldsymbol{\rho}_1, \boldsymbol{\rho}_2, z)$ in the plane $z = 1.4$ m, containing two vortices ("coherence singularities") and two saddle points (intersections of the red curves).

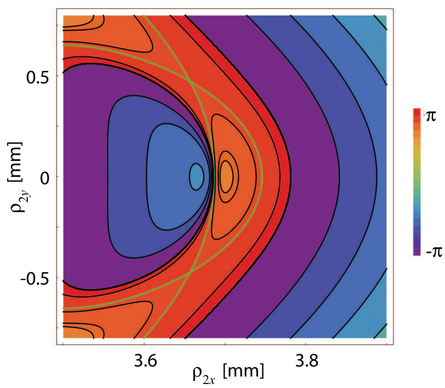


Figure 5.14: Phase contours of $\eta(\boldsymbol{\rho}_1, \boldsymbol{\rho}_2, z)$ in the plane $z = 2.4$ m, containing a maximum, a minimum and two saddle points (intersections of the green curves).

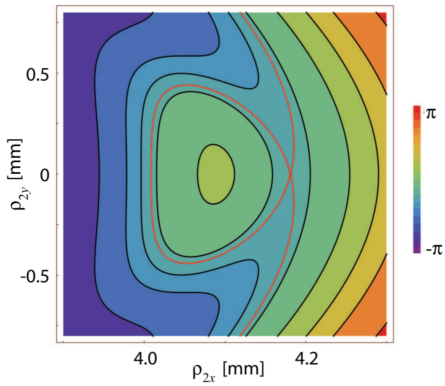


Figure 5.15: Phase contours of $\eta(\boldsymbol{\rho}_1, \boldsymbol{\rho}_2, z)$ in the plane $z = 3.0$ m, containing a maximum and a saddle (intersection of the red curve).

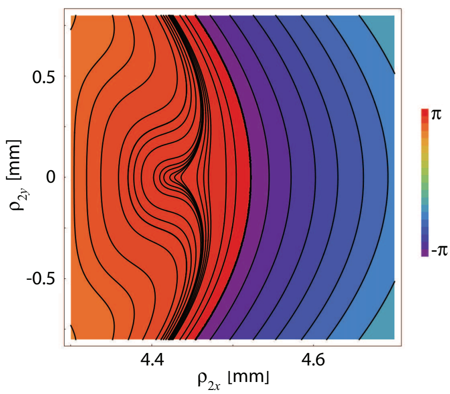


Figure 5.16: Phase contours of $\eta(\boldsymbol{\rho}_1, \boldsymbol{\rho}_2, z)$ in the plane $z = 3.33$ m, right after the final topological reaction. There are no more singularities or stationary points.

disappear. Indeed we find that near $z = 2.35$ m the two vortices briefly form a second dipole, which decays into a maximum and a minimum. These two phase extrema, together with the two remaining saddle points are shown in Fig. 5.14.

The next reaction takes place in the plane $z = 2.81$ m. There the minimum and the two saddle points merge together to form a single saddle point. This is illustrated in Fig. 5.15.

The final reaction occurs at $z = 3.33$ m. The maximum and the saddle annihilate each other, leaving a field without topological features, as is depicted in Fig. 5.16.

## 5.6 Conclusions

We have studied the properties of the correlation function of an electromagnetic, partially coherent beam of the Gaussian Schell-model class. Although the spectral density of such beams has no singular points, the phase of its correlation function does show a rich variety of saddles, extrema, dipoles and vortices. The structure of the correlation function is found to be essentially three-dimensional. This was illustrated by its complex-shaped surfaces of equal phase. On smoothly changing a parameter that characterizes the beam, these surfaces are first slightly deformed and then torn when correlation singularities come into existence. Since different cross-sections of the beam have different topological features, an observer moving from one transverse plane to another, will witnesses a series of complicated topological reactions. In all these reactions the topological charge and the topological index are conserved. We emphasize that all these reactions are generic, i.e., they occur quite generally and not just for special choices of the parameters that characterize the beam. The observation that different cross-sections of partially coherent electromagnetic beams have quite different coherence properties has profound implications for interference and scattering experiments with such beams.

# Chapter 6

# Plasmon switching: Observation of Dynamic Surface Plasmon Steering by Selective Mode Excitation in a Sub-wavelength Slit

This chapter is based on the following publication:

- S. B. Raghunathan, C. H. Gan, T. van Dijk, B. Ea Kim, H. F. Schouten, W. Ubachs, P. Lalanne, and T. D. Visser, "*Plasmon switching: Observation of dynamic surface plasmon steering by selective mode excitation in a sub-wavelength slit*", Optics Express **20**, pp. 15326-15335 (2012).

**Abstract**
We report a plasmon steering method that enables us to dynamically control the direction of surface plasmons generated by a two-mode slit in a thin metal film. By varying the phase between different coherent beams that are incident on the slit, individual waveguide modes are excited. Different linear combinations of the two modes lead to different diffracted fields at the exit of the slit. As a result, the direction in which surface plasmons are launched can be controlled. Experiments confirm that it is

possible to distribute an approximately constant surface plasmon intensity in any desired proportion over the two launching directions. We also find that the anti-symmetric mode generates surface plasmons more efficiently than the fundamental symmetric mode.

## 6.1 Introduction

An electromagnetic field directed at the interface between a metal and a dielectric can cause the free electrons in the metal to oscillate at the same frequency as the field. Under the right conditions such a collective excitation of electrons, known as a surface plasmon (SP), will propagate along the interface, and can be converted back into a freely propagating field when it is scattered by a surface imperfection such as a ridge or a groove [Raether, 1988]. The wavelength of an SP is much smaller than the wavelength of the electromagnetic field by which it is generated. This suggests the possibility of ultra-compact "plasmonic" devices in which information-carrying electromagnetic fields generate SPs that are then processed before being turned back again into a free field [Atwater, 2007]. Following the observation of plasmon-enhanced transmission through subwavelength-size hole arrays [Ebbesen *et al.*, 1998] and single subwavelength apertures [Thio *et al.*, 2001] in metal plates, numerous research efforts to develop nanoscale plasmonic devices were triggered. Plasmonic couplers [Steinberger *et al.*, 2007], waveguides [Maier *et al.*, 2003], interferometers [Gan *et al.*, 2009], lasers [Noginov *et al.*, 2009] and dichroic splitters [Liu *et al.*, 2011] have already been realized. However, for the field of plasmonics to achieve its full potential, it is necessary to control the direction in which SPs are launched. Compact schemes for directional launching of SPs based on geometries such as a nanoslit with a Bragg resonator [Genet and Ebbesen, 2007], an asymmetrically illuminated single nanoslit [Wang *et al.*, 2009] and pairs of nanoslits [Li *et al.*, 2011], and an optimized multi-groove coupler [Baron *et al.*, 2011] have been proposed and implemented, with extinction ratios as high as 50. These schemes all rely on some static, built-in asymmetry that favors a particular direction of SP launching. To address the important aspect of flexible directional launching of SPs, an essential feature for any kind of integrated plasmonic circuitry, we present a generic approach to dynamically switch plasmons between two channels with a constant total intensity and with a nanoscale footprint.

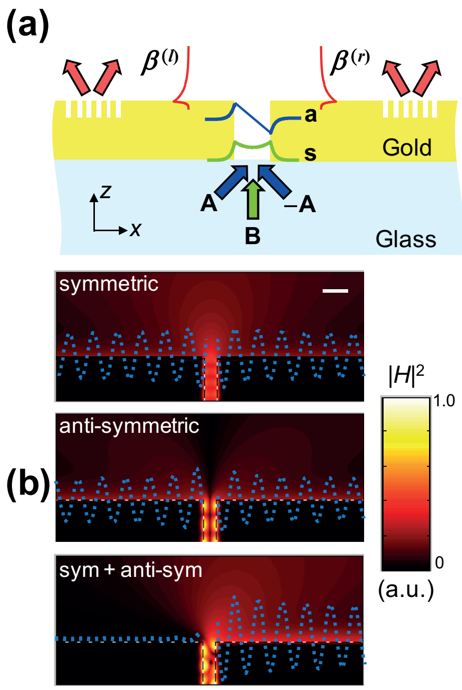


Figure 6.1: Principle of the proposed surface plasmon steering method. (a) A subwavelength slit of width $w$ in a gold film supports only two TM modes for $\lambda/2 \lesssim w \lesssim \lambda$: a symmetric mode (s, green curve) and an anti-symmetric mode (a, blue curve). Three coherent beams, A, -A (with opposite angle of incidence compared to A and $\pi$-phase shifted), and B are incident on the slit from the glass substrate. (b) Illustrating how a coherent superposition of the a and s modes can lead to unidirectional SP launching at a gold-air interface. The first two panels show the intensity of the magnetic field when the slit is illuminated with either the s or the a mode. Superposed dotted blue curves show the total magnetic field scattered on the interface. The length of the white bar in the first panel indicates the illumination wavelength in vacuum ($\lambda = 600$ nm), and the slit width $w$ is $\lambda/2$.

## 6.2 Theory

In its simplest form, our approach is depicted in Fig. 6.1, where a narrow slit in a thin gold film is illuminated from the glass substrate by three coherent beams with Transverse Magnetic (TM) polarization. The slit width is such that for an illumination wavelength $\lambda$ only two TM modes–one symmetric ($TM_0$), the other anti-symmetric ($TM_1$)–are non-evanescent. Beam B is normally incident and therefore only excites the fundamental $TM_0$ mode. In the path of this beam a piezo element is mounted, allowing its phase to be varied. Beams A and $-$A, which have opposite but equal amplitudes, make an angle of $+\theta$ and $-\theta$ with B, respectively. They have the same intensity, but are $\pi-$phase shifted with respect to each other. It follows from symmetry that the combination of these two oblique beams excites only the $TM_1$ mode [Miyata and Takahara, 2012]. At the slit exit, both left and right travelling surface plasmons are generated. Their amplitudes are denoted by $\beta^{(l)}$ and $\beta^{(r)}$, respectively. A series of grooves at 8 $\mu$m from either side of the slit converts the SPs back to freely propagating fields that are detected in the far field.

To illustrate how plasmon beam steering may be achieved with a two-mode nanoslit, Fig. 6.1 shows the interference pattern generated by an appropriate linear combination of the $TM_0$ and $TM_1$ modes in the slit. These modes scatter at the slit exit and a complete extinction of SPs in one launching direction is predicted. The fields are calculated with a frequency-domain, aperiodic Fourier modal method, incorporating perfectly-matched layers (method MM3 in the benchmark article Ref. [Besbes *et al.*, 2007]). The distributions of the magnetic field intensity $|H|^2$ in the near field of the metal-air interface are first shown for the cases where the same slit is illuminated with either the symmetric $TM_0$ or the anti-symmetric $TM_1$ mode. To illustrate the phase relationship between the excited SP fields, the total magnetic field $\mathrm{Re}(H)$ on the gold-air interface is superimposed as a dotted red curve. On each side, the oscillating wave is composed of an SP mode, and a quasi-cylindrical wave that rapidly decays within a few-wavelengths from the slit [Lalanne *et al.*, 2009]. For illumination with either the $TM_0$ or the $TM_1$ mode, the fields on opposite sides of the slit are in phase or $\pi-$phase shifted, respectively. Let us adjust the (complex) amplitude of the $TM_0$ mode such that it excites SPs on the right side of the slit with the same phase and intensity as the $TM_1$ mode. It is apparent that the linear combination of the two modes (Fig. 6.1, lower panel) then gives rise to complete destructive interference on the left side of the slit whereas constructive interference takes place on the right side. In the specific example of Fig. 6.1 it is taken that $\lambda = 600$ nm, $w = \lambda/2$, and the refractive index of gold $n_{\mathrm{Au}} = 0.23 + \mathrm{i}2.98$ (see [Palik, 1998]). The lower panel of Fig. 6.1 clearly shows that the total field at the gold-air interface is almost null to the left of the slit, indicating that not only the SP excitation is zero, but also that the excitation of the accompanying quasi-cylindrical waves is very weak.

As explained, beams A and -A together excite only the $TM_1$ mode, whereas beam B excites only the $TM_0$ mode. At the slit exit, each mode can be scattered into radiation that propagates to the far field, or can be dissipated as absorption loss on the gold surface, or be reflected as a backward propagating mode in the slit. A part of the absorption loss is carried by the SPs launched on both sides of the slit. Let the SP scattering coefficients at the left and right-hand side of the slit for the two-beam system $\{\mathrm{A}, -\mathrm{A}\}$ be $A_a$ and $-A_a$, respectively. For beam B we denote the SP scattering coefficient on each side by $B_s$. To calculate these coefficients, we use the mode orthogonality of translational-invariant lossy waveguides [Lalanne *et al.*, 2009], which yields

$$A_a = \int_{-\infty}^{\infty} [E_z^{(a)}(x,z)\, H^{\mathrm{SP}}(x,z) - H^{(a)}(x,z)\, E_z^{\mathrm{SP}}(x,z)]\, dz, \tag{6.1}$$

and

$$B_s = \int_{-\infty}^{\infty} [E_z^{(s)}(x,z)\, H^{\mathrm{SP}}(x,z) - H^{(s)}(x,z)\, E_z^{\mathrm{SP}}(x,z)]\, dz. \tag{6.2}$$

where the field components $[H^{\mathrm{SP}}(x,z),\, E_z^{\mathrm{SP}}(x,z)]$, corresponding to an SP propagating in the negative $x$-direction with a unit power-flow at $x = 0$, are calculated analytically [Raether, 1988]. Also, $[H^{(a)}(x,z), E_z^{(a)}(x,z)]$ and $[H^{(s)}(x,z),\, E_z^{(s)}(x,z)]$, are the scattered field components of the combined incident field of beams A and $-$A, and of the incident beam B alone, respectively. Note that the integral over $z$ is independent of $x$, provided that $x$ corresponds to an abscissa on the right side of the slit (see details in [Lalanne *et al.*, 2009]).

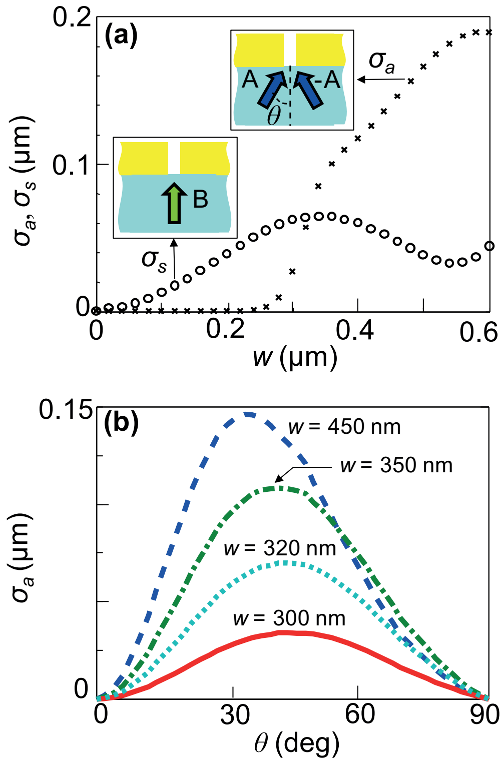


Figure 6.2: The calculated SP cross sections $\sigma_a$ and $\sigma_s$ as defined in Eqs. (6.3) and (6.4) for a unit Poynting vector of each of the incident beams. (a) Variation of $\sigma_a$ and $\sigma_s$ with slit width $w$. The angles of incidence of the plane waves A, -A are taken to be $\theta = \pm 30°$. The two insets indicate the setup for calculating $\sigma_a$ and $\sigma_s$, respectively. (b) Variation of $\sigma_a$ with angle of incidence $\theta$ for slit widths $w = 300, 320, 350$, and 450 nm. The refractive index of gold $n_{\mathrm{Au}} = 0.18 + \mathrm{i}2.99$ for $\lambda = 632.8$ nm, is taken from [PALIK, 1998], and the thickness of the gold film is 200 nm.

We define

$$\sigma_s = 2|B_s|^2, \tag{6.3}$$

which has a dimension of length for our two-dimensional case and can be seen as a SP cross-section [Liu *et al.*, 2008; Verslegers *et al.*, 2010], by analogy with the scattering or extinction cross-sections defined for nanoparticles [Bohren and Huffman, 1983]. The factor 2 takes into account the SPs launched on both sides of the slit. The anti-symmetric case corresponds to a spatially non-uniform illumination of the slit. Usually scattering cross sections are defined for incident fields that do not vary at the scale of the scatterer. However, this Ansatz is not necessary, and in a consistent manner we may define an anti-symmetric SP cross section

$$\sigma_a = 2|A_a|^2, \tag{6.4}$$

where the integral $A_a$ is normalized such that the Poynting-vector modulus of each individual plane wave, A and -A, is one half. On spatial averaging over the fringe pattern formed by the interference of the two incident plane waves, the total energy transported by the two-beam combination is precisely equal to the energy transported by the single plane wave B in the symmetric case. Finally, note that an SP scattering cross-section greater than the geometrical cross section of the slit ($w$) implies that more energy is converted to SPs than is geometrically incident upon it.

Figure 6.2 summarizes the main results obtained for the cross-sections at $\lambda = 632.8$ nm and for a gold-film thickness of 200 nm. In Fig. 6.2(a) the influence of the slit width is shown. The calculation of $\sigma_a$ is performed by assuming that the angle of incidence of the plane waves with amplitude A and -A is $\theta = 30°$. Starting from $w = 0$, the SP cross section of the symmetric case (circles) increases gradually to a maximum value $\sim 60$ nm at $w \approx 300$ nm, and then decreases as the slit width is further increased. The overall behavior is consistent with earlier works on the ability of isolated slits or grooves to launch SPs [Lalanne *et al.*, 2009]. More interesting is the anti-symmetric case (crosses) for which the slit is placed at an anti-node of the interference pattern formed by the two incident plane waves. For very small slit widths, the incident field on the slit is virtually null and the $TM_1$ mode is weakly excited. In addition, since the $TM_1$ mode is below cutoff, the energy transfer towards the upper slit aperture is inefficient, and it is only when this mode becomes propagating (for $w \approx 300$ nm) that a rising behavior is observed. Then $\sigma_a$ rapidly becomes significantly larger than $\sigma_s$. This remarkable result (note that the incident field is null at the slit center for the anti-symmetric case) attests to the great potential of the $TM_1$ mode to deliver large and steady SP flows, a property that is rarely used in plasmonic devices [Schuller and Brongersma, 2009] whose operation mostly rely on the fundamental $TM_0$ mode and on tiny slits or grooves. [Raether, 1988; Atwater, 2007; Ebbesen *et al.*, 1998; Thio *et al.*, 2001; Steinberger *et al.*, 2007; Liu *et al.*, 2011; Genet and Ebbesen, 2007; Wang *et al.*, 2009; Li *et al.*, 2011; Baron *et al.*, 2011]

Figure 6.2(b) shows the influence of the angle $\theta$ on the SP cross section $\sigma_a$. Starting from $\theta = 0$ (a degenerate asymptotic case for which the incident field is null), the general trend is an increase of $\sigma_a$ to a peak value for an intermediate angle of incidence, followed by a monotonic decrease to null for $\theta = 90°$. This behavior depends only weakly on the slit width, although we note that as $w$ increases, the angle for maximum SP excitation is gradually shifted to a less oblique angle of incidence, ranging from $46° > \theta > 36°$ for the range of slit widths considered from 300 nm to 450 nm. For $\theta \approx 20°$ and $w = 450$ nm as used in the experiment hereafter, $\sigma_a = 100$ nm, implying that 22% of the energy directly incident onto the slit is converted into SPs launched on the upper interface.

Turning our attention back to the plasmon switch (Fig. 6.1), it is clear that the SP amplitudes $\beta^{(l)}$ and $\beta^{(r)}$ of the left and right traveling surface plasmons may be represented as a linear combination of the SPs excited by the $TM_0$ and the $TM_1$ mode. It follows that $\beta^{(l)}$ and $\beta^{(r)}$ are given by the expressions

$$\beta^{(l)}(\delta) = B_s\, e^{\mathrm{i}\delta} + A_a, \tag{6.5a}$$

$$\beta^{(r)}(\delta) = B_s\, e^{\mathrm{i}\delta} - A_a, \tag{6.5b}$$

where $\delta$ is a variable phase controlled by the voltage across the piezo element in the normally incident beam B. As will be seen shortly, the independent excitation of the two modes, together with the adjustable phase $\delta$, allows us to control the direction in which the SPs are launched. By using variable grey filters or by varying the angle of incidence, it is possible to carefully tune the intensity of the beams to compensate for the difference between SP cross-sections $\sigma_a$ and $\sigma_s$, and hence set $|B_s| = |A_a|$. In that case we have for the two SP intensities $I^{(l)}(\delta)$ and $I^{(r)}(\delta)$ the formulas

$$I^{(l)}(\delta) = |\beta^{(l)}(\delta)|^2 = 2|B_s|^2(1 + \cos\delta), \tag{6.6a}$$

$$I^{(r)}(\delta) = |\beta^{(r)}(\delta)|^2 = 2|B_s|^2(1 - \cos\delta). \tag{6.6b}$$

We note that a) the total plasmon intensity $I^{(l)}(\delta) + I^{(r)}(\delta) = 4|B_s|^2$ is independent of the phase $\delta$, and b) the ratio $I^{(l)}(\delta)/I^{(r)}(\delta)$ ranges from zero to infinity when $\delta$ is varied. In other words, under precise coherent illumination, a single slit supporting two propagating modes allows one to dynamically distribute a fixed surface plasmon flow between left-going SPs and right-going SPs.

We note that for wider slits, that allow more than two TM modes, one could use the same scheme to obtain plasmon steering. In such a multi-mode slit the combination of beams A and -A only excites odd modes, whereas beam B excites only even modes. Cancellation of the combined odd modes by the combined even modes at one side of the slit can be achieved by balancing the amplitudes of the beams. The SPs are then launched from the other side of the slit. However, in a wider slit the conversion of incident light into SPs will be less efficient as more light is directly transmitted.

## 6.3 Experiment

Figure 6.3 shows the experimental setup with which the proposed steering of the SP intensities was realized. The linearly-polarized output of a 16 mW He-Ne laser operating at $\lambda = 632.8$ nm is first divided into three beams. Each beam is passed through a combination of quarter-wave plates and a linear polarizer such that the field at the sample is TM polarized. To ensure coherent mode excitation, the path difference between the arms was minimized by use of delay lines in arms B and A. Arm B is normally incident, whereas arms A and -A are obliquely incident in air at $+30°$ and $-30°$, respectively. By mounting the last mirror in arm -A on a micrometer linear translator the two oblique arms are made to have a $\pi$ phase difference with respect to each other. The last mirror in Arm B is mounted

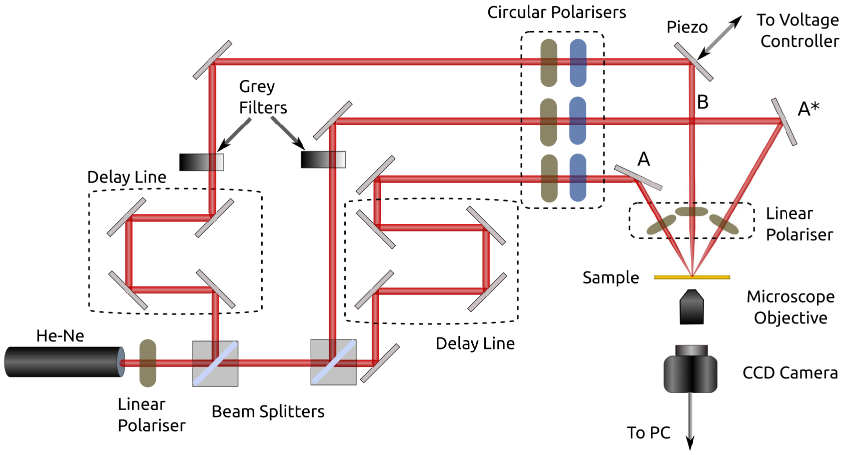


Figure 6.3: Sketch of the experimental setup. The sample is illuminated from the glass-substrate side.

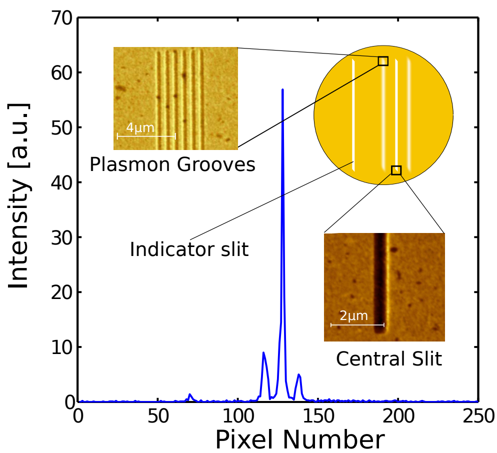


Figure 6.4: Typical line trace of the CCD camera screen, perpendicular to the slits

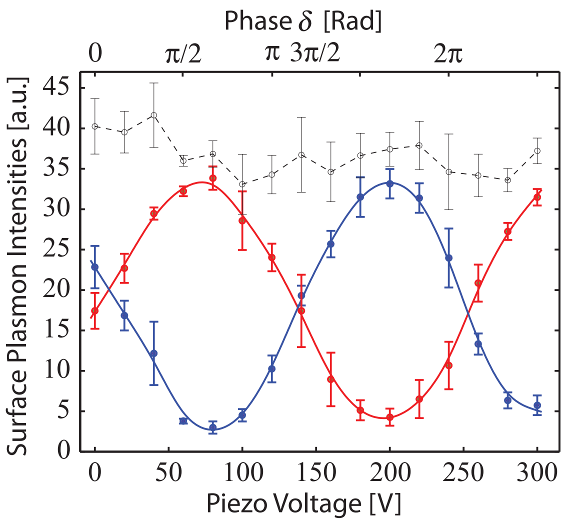


Figure 6.5: Experimental results of the proposed plasmon switching method. The SP intensities $I^{(l)}(\delta)$ (red curve) and $I^{(r)}(\delta)$ (blue curve) are shown as a function of the phase $\delta$ of arm B or, equivalently, as a function of the voltage across the piezo element. The total intensity $I^{(l)}(\delta) + I^{(r)}(\delta)$ is shown as a dotted grey curve. The error bars indicate the standard deviation of ten independent measurements.

on top of a piezo element which is connected to a DC voltage source with a range of $0-300$ V. The voltage across the piezo determines the phase $\delta$ of beam B. In a separate interference experiment with the same laser, the piezo voltage scale was calibrated in terms of phase, yielding that a 120 V ramp corresponds to a $\pi-$phase shift in $\delta$.

Scanning electron microscopy (SEM) images of the fabricated sample are shown in the insets of Fig. 6.4. Subwavelength slits with widths varying between 250 and 650 nm were etched by electron-beam lithography followed by ion-beam etching in a 200 nm thick gold layer evaporated onto a 0.5 mm thick fused-silica substrate. On either side of this "central slit", at a distance of 8 $\mu$m, there is a set of 6 grooves with a 600 nm center-to-center spacing.

Due to their tiny widths, only the central slits are etched all through-out the gold film, whereas the grooves are only partially engraved. To ease the alignment procedure, there is a reference slit located at a distance of around 25 $\mu$m to the left of each central slit. A 450 nm wide slit, which supports both the $TM_0$ and $TM_1$ modes, was used for the experimental results reported hereafter, but similar results have been obtained with other widths. The 8 $\mu$m slit-grooves separation helps suppress the amplitude of the quasi-cylindrical waves so that the grooves serve only to scatter the SPs. This ensures that the line trace pattern of the CCD camera in the far-field is effectively proportional to the intensity of the SPs and is not contaminated with additional direct-wave contributions [LALANNE AND HUGONIN, 2006].

A typical line trace of the CCD camera screen, perpendicular to the slits is shown in Fig. 6.4. The first low peak on the left (near pixel 70) is the signal from the indicator slit. The second and fourth peak are the intensities $I^{(l)}(\delta)$ and $I^{(r)}(\delta)$ from surface plasmons scattered by the left-hand grooves and right-hand grooves, respectively. The highest peak is the intensity transmitted by the central slit. The insets show sample details of the the central slit and the plasmon grooves made by a scanning electron microscope.

Experimental results for the 450 nm wide slit are shown in Fig. 6.5, where the intensities of the left- and right-travelling surface plasmons, $I^{(l)}(\delta)$ and $I^{(r)}(\delta)$ are plotted as a function of the voltage across the piezo element that regulates the phase $\delta$ of the normally incident beam. The agreement with Eqs. (6.6) is very good. It is seen that more than 94% of the surface plasmons are launched to the left when the piezo voltage is 80 V, whereas for a voltage of 200 V about 92% is launched to the right. For intermediate voltage settings, arbitrary ratios of $I^{(l)}(\delta)/I^{(r)}(\delta)$ can be obtained, which makes the device act as a variable beam splitter. The average total intensity $I^{(l)}(\delta) + I^{(r)}(\delta) = 36.6$ (dotted grey line). The attained visibility of 0.82 is limited by several factors, viz. a) the three beams not being spatially fully coherent due to the relatively low coherence length of the He-Ne laser, b) the amplitudes of arms A and -A being different by about $2 - 4\%$, and c) the amplitude $|B_s|$ differing from $|A_a|$ by about $2 - 5\%$. Notice however, that the sum of the two SP intensities is rather constant, with a mean value of 36.6 and a relative standard deviation less than 7% over the entire voltage sweep. Also the peak to minimum distance of 120 V is in excellent agreement with the independently observed $\pi$ change in the phase $\delta$ of arm B. Additionally, by performing far-field measurements of the intensity radiated by the slit, we have observed a "lighthouse effect", i.e. the maximum in the far-field intensity distribution can be continuously shifted from the left to the right and vice versa, as one varies the voltage across the piezo element. This suggests that one may also achieve beam steering in the far-field of a two-mode nanoslit by controlling the linear combination of the two modes. [1]

## 6.4 Conclusion

In conclusion, we have demonstrated that the selective coherent excitation of the two fundamental TM modes in a sub-wavelength slit allows us to launch an approximately constant intensity of surface plasmons either to the left or to the right of the slit; or to distribute them in any desired ratio over these two directions. This gives, for the first time, dynamic control over the directionality of surface plasmons. Our theoretical analysis shows that, although its excitation requires a null illumination at the slit center, the $TM_1$ mode above cutoff offers the potential of higher SP conversion efficiencies compared to narrow sub-wavelength apertures that support only the $TM_0$ mode. Note that the radially polarized $TM_{01}$ mode of subwavelength circular holes [Vassallo, 1991] presents an axial field singularity and is likely, just as the $TM_1$ mode of slits, to efficiently generate SPs.

The present work illustrates how the combination of a static symmetric structure with a versatile illumination scheme may lead to the controlled launching of surface or guided waves at the nanoscale, and as such it may be considered a generic demonstration. Indeed, further work is needed to realize a competitive device. With additional calculations, we have checked for $\lambda = 0.6$ $\mu$m that as high as 40% and 55% of the $TM_0$ and $TM_1$ modes are scattered into SPs at the slit exit aperture. Therefore, the throughput of our experimental system is presently limited by the coupling between the incident beams and the slit modes. This coupling can be further improved by increasing either the refractive index of the substrate, or the cross-section of the slit aperture. Different approaches that preserve the symmetry are possible, for example surrounding the slit

[1] This is demonstrated in Chapter 7.

with an array of optimized phased grooves [Baron *et al.*, 2011; Garcia-Vidal *et al.*, 2003a; Degiron and Ebbesen, 2004], or placing a nano-antenna at the near-field of the slit entrance [Aydin *et al.*, 2009]. This would keep the transverse size of the switching device below the diffraction limit. A drastic miniaturization of our table-top illumination setup can be achieved with micro-optical components and gratings, and thanks to the very fast development of active plasmonics technologies [MacDonald *et al.*, 2008], it would be interesting to investigate architectures for full on-chip integration. Such an ultra-compact plasmonic switch would have potential application in telecommunications and optical sensing.

# Chapter 7

# Beam Steering by Selective Mode Excitation in a Sub-wavelength Slit

This chapter is based on the following publication:

- S. B. Raghunathan, C. H. Gan, T. van Dijk, B. Ea Kim, H. F. Schouten, W. Ubachs, P. Lalanne, and T. D. Visser, "*Beam steering by selective mode excitation in a sub-wavelength slit*", to be submitted (2013).


**Abstract**
We analyse and measure the radiation pattern of a sub-wavelength slit carved out of a thin gold film. The slit width is designed such that only the first two TM-modes are non-evanescent. By controlling the phase difference between three coherent laser beams that are incident on the slit, the two guided modes can be excited individually. It is demonstrated that different superpositions the modes lead to a change in the direction of maximum radiated intensity from $-10°$ to $+10°$. This method can be used to selectively address two for-zone detectors placed under these angles.

## 7.1 Introduction

The study of light transmission through small apertures has a venerable history [Rayleigh, 1897; Bethe, 1944; Bouwkamp, 1954; Born and Wolf, 1999]. The study of these nano-slit systems has been a subject of renewed interest since Ebbesen *et al.* [Ebbesen *et al.*, 1998] demonstrated experimentally that certain arrays of cylindrical cavities cut in metal plates allow light transmission that is orders of magnitude larger than the prediction by standard aperture theory. This extraordinary transmission in nano-metallic structures has been attributed to the coupling of light with surface plasmon polaritons (SPPs)[Ebbesen *et al.*, 1998; Porto *et al.*, 1999; Martin-Moreno *et al.*, 2001] and Fabry-Pérot cavity-like resonant modes [Astilean *et al.*, 2000; Takakura, 2001]. A wide range of optical phenomena, such as beaming, focusing, and wave-guiding [Schouten *et al.*, 2003c] in these systems has been theoretically predicted and experimentally verified [Lezec *et al.*, 2002].

An important aspect of light transmission by nano-apertures is the directionality of the radiated field. A highly directional transmission can be achieved by using a single sub-wavelength slit surrounded by surface corrugations or grooves [Garcia-Vidal *et al.*, 2003b; Wang *et al.*, 2006a]. Other schemes, such as varying the refractive index inside resonant neighbouring subwavelength slits [Vincenti *et al.*, 2009], have also been used. However, these schemes typically depend on a static built-in asymmetry in the device to obtain radiation in a specific direction. Achieving dynamic beam steering in subwavelength apertures opens up the possibilities of fabricating phased-array nano-antennas with a strong and flexible directionality. In this publication, we report a novel method that enables us to selectively address two detectors situated in the far zone of a subwavelength slit.

In a recent publication [Raghunathan *et al.*, 2012a], we demonstrated a set-up that selectively excites two coherent TM-modes in a subwavelength slit. This allowed for the dynamic steering of SPPs in the two launching directions perpendicular to the slit. In this article, we demonstrate experimentally, that by controlling the linear combination of these two modes within the subwavelength slit it is possible to achieve a dynamic steering of the slit's radiation field.

## 7.2 Analysis

Consider three coherence laser beams impinging on a 500 nm wide sub-wavelength slit etched in a 200 nm thick gold film deposited on a quartz plate, see Fig. 7.1. At a wavelength of 632.8 nm, this slit supports two non-evanescent TM-modes, one of which is symmetric and one of which is anti-symmetric. A normally incident beam, B, excites the symmetric $TM_0$-mode. Two obliquely incident beams, A and $-$A, make angles of 20° and $-20°$ with B. Beams A and $-$A are set to same intensity, but are out of phase. Although the two oblique beams individually excite both the symmetric and the anti-symmetric mode, their superposition results in the cancellation of the symmetric mode and excites only the anti-symmetric $TM_1$-mode. The path of beam B contains a piezo element, which is used to vary the relative phase $\delta$ of the two guided modes.

As an approximate model of our device we consider a two-dimensional, perfectly conducting waveguide. In that case we have for the $y$-component of the magnetic field of the two TM-modes the expressions [Pollack and Stump, 2002]

$$\begin{array}{rcll} H_y(x,z) & = & C_1 \exp(\mathrm{i}k_{z0}z), & (\mathrm{TM}_0) \\ H_y(x,z) & = & C_2 \sin(\pi x/w) \exp(\mathrm{i}k_{z1}z). & (\mathrm{TM}_1) \end{array} \tag{6.1}$$

Here $C_1, C_2$ are both constants. The phase $\delta$ is controlled by the voltage across the piezo element. Also, $k_{zi}$ with $i = 0, 1$ denotes the $z$-component of the effective wave vector of the $\mathrm{TM}_i$ mode. The intensity in the far zone equals [Schouten *et al.*, 2004a]

$$I(\theta) \propto \cos^2(\theta) \left| \tilde{H}_y[k \sin(\theta)] \right|^2, \tag{6.2}$$

where $k = \omega/c$, $c$ being the speed of light, denotes the wavenumber associated with frequency $\omega$, and the tilde indicates the Fourier transform. Hence when both waveguide modes are excited

$$\tilde{H}_y(u) = \frac{C_1}{\pi u} \sin(uw/2) - \mathrm{i}\frac{C_2}{\pi u} \cos(uw/2) \frac{u^2}{(\pi/w)^2 - u^2}. \tag{6.3}$$

On making use of Eqs. (6.3) and (6.2) we can calculate the radiation pattern of the slit as a function of the phase $\delta$ caused by the piezo element.

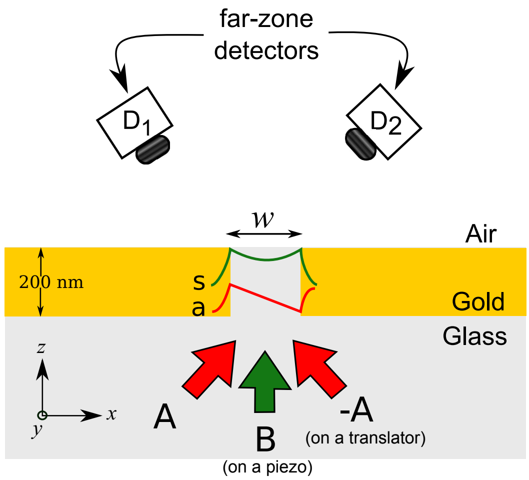


Figure 7.1: A subwavelength slit of width $w = 500$ nm in a gold film supports only two TM modes for $w < \lambda$, a symmetric mode (s, green curve) and an anti-symmetric mode (a, red curve). Three coherent beams, A, -A (with opposite angle of incidence compared to A and $\pi$-phase shifted), and B are incident on the slit from the glass substrate.

Three examples are shown in Fig. 7.2 for three values $\delta$. It is seen that the radiation can be targeted towards either $\theta \approx 15^\circ$ or $\theta \approx -15^\circ$. Also it is possible to distribute the intensity more equally.

## 7.3 Experiment

The experimental setup consists of a 16 mW He-Ne laser operating at 632.8 nm, whose output is divided into three beams. These beams are then passed through three separate linear polarizers, the orientation of which is fixed such that the field at the sample is TM polarized. To ensure a coherent mode excitation, the path difference between the arms was minimized by use of delay lines in arm B and arm A. By mounting the last mirror in arm -A on a micrometer linear translator, connected to a DC voltage source, the phase difference of the two oblique arms is set to be $\pi$. The last mirror in arm B is mounted on top of a piezo element and connected to a DC voltage source with a range of $0 - 300$ V. This

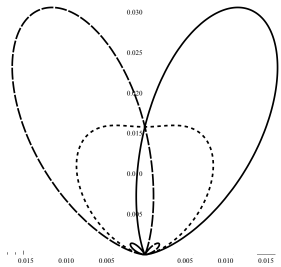


Figure 7.2: The radiation pattern of a sub-wavelength slit for three values of the phase difference $\delta$. For the dashed curve $\delta = -\pi/2$, for the dotted curve $\delta = 0$ and for the solid curve $\delta = \pi/2$.

voltage determines the phase difference $\delta$. A CCD camera was positioned at a distance of 3 mm from the sample to capture the radiation pattern with a field of view from $-40°$ to $+40°$.

A plot of the measured radiation pattern of the individual modes is shown in Fig. 7.3. The blue curve in the figure represents the far-field pattern of the symmetric mode and the red curve represents the far-field pattern of the anti-symmetric mode. Both the radiation patterns are symmetric with respect to the normal, only that for the anti-symmteric mode the lobes on either side of the normal, with the maxima at $+10°$ and $-10°$, are out of phase. The sharp peaks in the radiation patterns correspond to the laser beam being directly transmitted through the sample, and these occur at $0°$, $+20°$ and $-20°$.

The beam B illuminating the slit is set such that at the angles $+10°$ and $-10°$ both the symmetric and the anti-symmetric mode radiation patterns have the same intensity. Therefore maximal constructive and destructive interference will take place in these two directions.

In Figs. 7.4, 7.5 and 7.6 the intensity of the combined radiation pattern of $TM_0$ and $TM_1$ at a distance of 3 mm from the sample, is plotted as a function of the azimuthal angle for three different voltages across the piezo element in beam B. The maximum of the radiation patterns in the figures 3-5 are at $+10°$ and $-10°$, as it depends not on the direct transmission through the sample, but on the superposition between the symmetric and the anti-symmetric mode as shown in the figure. Thus, only the diffracted

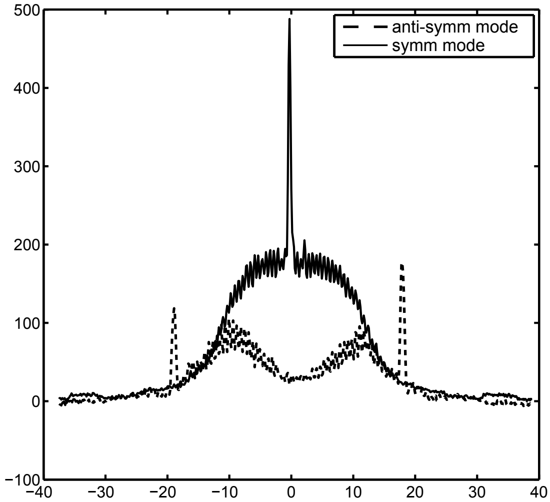


Figure 7.3: Plot of the radiation from a symmetric (blue curve) and an anti-symmetric (red curve) mode.

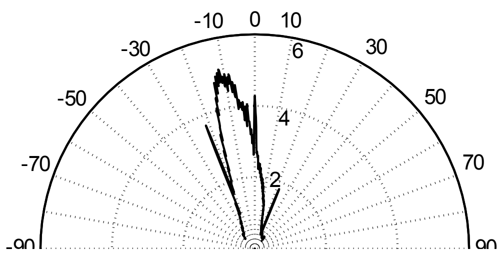


Figure 7.4: (Colour online) Polar plot of light diffracted from the sub-wavelength aperture. The radial scale indicates the intensity (a.u.). The peak of the diffracted light is towards left at an angle of $+10°$.

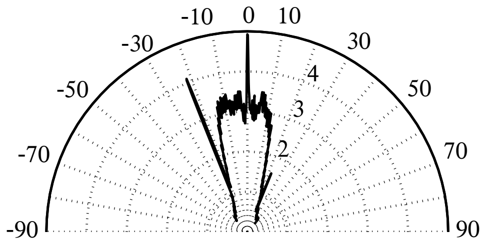


Figure 7.5: (Colour online) Polar plot of light diffracted from the subwavelength aperture. The radial scale indicates the intensity (a.u.). The peak of the diffracted light is at an angle on 0°

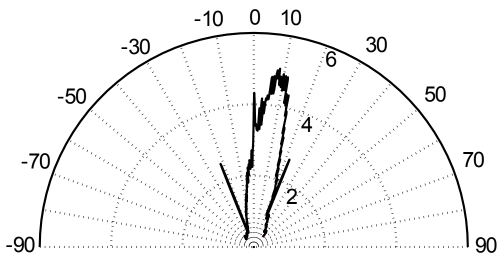


Figure 7.6: (Color online) Polar plot of light diffracted from the subwavelength aperture. The radial scale indicates the intensity (a.u.). The peak of the diffracted light is towards right at an angle of +10°

field will reach detectors placed in the far-field at $\pm 10°$. The effect of the direct transmission can be mitigated by using a thicker and hence more opaque gold film.

## 7.4 Conclusion

In conclusion, we have demonstrated a method to dynamically steer the radiation from a sub-wavelength slit. By controlling the phase difference of the two non-evanascent TM-modes, it is possible to steer the radiation maximum from $-10°$ to $10°$. This gives the possibility of selectively addressing one or two detectors positioned in the far zone of the slit. A simple model provides a good qualitative agreement with the experimental results.

# Bibliography

G. S. Agarwal and E. Wolf, "Higher-order coherence functions in the space-frequency domain", *J. Modern Optics* 40, 8, pp. 1489–1496 (1993).

L. Allen, S. M. Barnett, and M. J. Padgett, *Optical Angular Momentum*, Optics and Optoelectronics. Institute of Physics Publishing, Bristol, UK (2003).

S. Astilean, P. Lalanne, and M. Palamaru, "Light transmission through metallic channels much smaller than the wavelength", *Opt. Commun.* 175, 4, pp. 265–273 (2000).

H. A. Atwater, "The promise of plasmonics", *Scientific American* pp. 56 – 63 (2007).

K. Aydin, A. O. Cakmak, L. Sahin, Z. Li, F. Bilotti, L. Vegni, and E. Ozbay, "Split-ring-resonator-coupled enhanced transmission through a single subwavelength aperture", *Phys. Rev. Lett.* 102, pp. 013904–1 – 013904–4 (2009).

A. Baron, E. Devaux, J. C. Rodier, J. P. Hugonin, E. Rousseau, C. Genet, T. W. Ebbesen, and P. Lalanne, "Compact antenna for efficient and unidirectional launching and decoupling of surface plasmons", *Nano Letters* 11, 10, pp. 4207–4212 (2011).

A. Y. Bekshaev, M. S. Soskin, and M. V. Vasnetsov, "Transformation of higher-order optical vortices upon focusing by an astigmatic lens", *Opt. Commun.* 241, 4, pp. 237–247 (2004).

M. V. Berry, “Singularities in waves and rays”, *Les Houches lecture series session* 35, pp. 453–543 (1981).

M. Besbes, J. P. Hugonin, P. Lalanne, S. van Haver, O. T. A. Janssen, A. M. Nugrowati, M. Xu, S. F. Pereira, H. P. Urbach, A. S. van de Nes, P. Bienstman, G. Granet, A. Moreau, S. Helfert, M. Sukharev, T. Seideman, F. I. Baida, B. Guizal, and D. Van Labeke, “Numerical analysis of a slit-groove diffraction problem”, *J. Eur. Opt. Soc. Rapid Publ* 2, pp. 7022–1 –7022–17 (2007).

H. A. Bethe, “Theory of diffraction by small holes”, *Physical Review* 66 , 7-8, pp. 163–182 (1944).

A. Bezryadina, D. N. Neshev, A. S. Desyatnikov, J. Young, Z. Chen, and Y. S. Kivshar, “Observation of topological transformations of optical vortices in two-dimensional photonic lattices”, *Opt. Express* 14, 18, pp. 8317 (2006).

G. V. Bogatyryova, C. V. Felde, P. V. Polyanskii, S. A. Ponomarenko, M. S. Soskin, and E. Wolf, “Partially coherent vortex beams with a separable phase”, *Opt. Lett.* 28, 11, pp. 878–880 (2003).

C. F. Bohren and D. R. Huffman, “Absorption and scattering of light by small particles”, *J Wiley & Sons, New York* (1983).

A. Boivin, J. Dow, and E. Wolf, “Energy flow in the neighborhood of the focus of a coherent beam”, *J. Opt. Soc. Am.* 57, 10, pp. 1171–1175 (1967).

M. Born and E. Wolf, *Principle of Optics (expanded) 7th Ed*, Cambridge University Press (1999).

C. J. Bouwkamp, “Diffraction theory”, *Phys. Soc. Rep. Progr. Phys.* 17, pp. 35–100 (1954).

M. E. Brezinski, *Optical Coherence Tomography: Principles and Applications*, Elsevier Science (2006).

H. R. Hanbury Brown and R. Q. Twiss, “Correlation between photons in two coherent beams of light”, *Nature* 177, pp. 27 – 29 (1956).

W. H. Carter and E. Wolf, “Coherence and radiometry with quasi-homogeneous planar”, *J. Opt. Soc. Amer.* 67, pp. 785–796 (1977).

W. H. Carter and E. Wolf, “An inverse problem with quasi-homogeneous sources”, *J. Opt. Soc. Amer. A* 2, pp. 1994–2000 (1985).

P. H van Cittert, “Die Wahrscheinliche Schwingungsverteilung in einer von einer Lichtquelle direkt oder mittels einer Linse beleuchteten Ebene”, *Physica* 1, 16, pp. 201 – 210 (1934).

E. Collett and E. Wolf, “Beams generated by Gaussian quasi-homogeneous sources”, *Opt. Commun.* 32, pp. 27–31 (1980).

A. Degiron and T. Ebbesen, “Analysis of the transmission process through single apertures surrounded by periodic corrugations”, *Opt. Express* 12, 16, pp. 3694–3700 (2004).

D. W. Diehl and T. D. Visser, “Phase singularities of the longitudinal field components in the focal region of a high-aperture optical system”, *J. Opt. Soc. Am. A* 21, 11, pp. 2103–2108 (2004).

T. van Dijk, D. G. Fischer, T. D. Visser, and E. Wolf, “Effects of spatial coherence on the angular distribution of radiant intensity generated by scattering on a sphere”, *Phys. Rev. Lett.* 104, 17, 173902 (2010).

T. van Dijk, G. Gbur, and T. D. Visser, “Shaping the focal intensity distribution using spatial coherence”, *J. Opt. Soc. Am. A* 25, 3, pp. 575–581 (2008).

T. van Dijk and T. D. Visser, “Evolution of singularities in a partially coherent vortex beam”, *J. Opt. Soc. Am. A* 26, 4, pp. 741–744 (2009).

T. W. Ebbesen, H. J. Lezec, H. F. Ghaemi, T. Thio, and P. A. Wolff, “Extraordinary optical transmission through sub-wavelength hole arrays”, *Nature* 391, pp. 667 – 669 (1998).

D. G. Fischer and T. D. Visser, “Spatial correlation properties of focused partially coherent light”, *J. Opt. Soc. Am. A* 21, 11, pp. 2097–2102 (2004).

J. T. Foley and E. Wolf, “Radiometry with quasihomogeneous sources”, *J. Mod. Opt.* 42, pp. 787–798 (1995).

I. Freund, “Optical vortex trajectories”, *Opt. Commun.* 181, 1, pp. 19–33 (2000).

I. Freund, “Critical foliations”, *Opt. Lett.* 26, 8, pp. 545–547 (2001).

I. Freund and D. A. Kessler, “Critical point trajectory bundles in singular wave fields”, *Opt. Commun.* 187, 1, pp. 71–90 (2001).

A. T. Friberg, T. D. Visser, W. Wang, and E. Wolf, “Focal shifts of converging diffracted waves of any state of spatial coherence”, *Opt. Commun* 196, 1-6, pp. 1 – 7 (2001).

K. T. Gahagan and G. A. Swartzlander, “Simultaneous trapping of low-index and high-index microparticles observed with an optical-vortex trap”, *J. Opt. Soc. Am. B* 16, 4, pp. 533–537 (1999).

Q. Gan, Y. Gao, and F. J. Bartoli, “Vertical plasmonic Mach-Zehnder interferometer for sensitive optical sensing”, *Opt. Express* 17, 23, pp. 20747–20755 (2009).

F. J. Garcia-Vidal, H. J. Lezec, T. W. Ebbesen, and L. Martin-Moreno, “Multiple paths to enhance optical transmission through a single subwavelength slit”, *Phys. Rev. Lett.* 90, pp. 213901–1 – 213901–4 (2003a).

F. J. Garcia-Vidal, L. Martin-Moreno, H. J. Lezec, and T. W. Ebbesen, “Focusing light with a single subwavelength aperture flanked by surface corrugations”, *Appl. Phys. Lett.* 83, 22, pp. 4500–4502 (2003b).

G. Gbur and G. A. Swartzlander, “Complete transverse representation of a correlation singularity of a partially coherent field”, *J. Opt. Soc. A. B* 25, 9, pp. 1422–1429 (2008).

G. Gbur and T. D. Visser, "Can spatial coherence effects produce a local minimum of intensity at focus?", *Opt. Lett.* 28, 18, pp. 1627–1629 (2003a).

G. Gbur and T. D. Visser, "Coherence vortices in partially coherent beams", *Opt. Commun.* 222, 1, pp. 117 – 125 (2003b).

G. Gbur and T. D. Visser, "Phase singularities and coherence vortices in linear optical systems", *Opt. Commun.* 259, 2, pp. 428–435 (2006).

G. Gbur and T. D. Visser, "The structure of partially coherent fields", *Progress in Optics* 55 (E. Wolf, ed.), pp. 285–341 (2010).

G. Gbur, T. D. Visser, and E. Wolf, "'Hidden'singularities in partially coherent wavefields", *J. Opt. A: Pure Appl. Opt.* 6, 5, pp. S239 (2004).

G. Gbur and E. Wolf, "Spreading of partially coherent beams in random media", *J. Opt. Soc. Am. A* 19, 8, pp. 1592–1598 (2002).

C. Genet and T. W. Ebbesen, "Light in tiny holes", *Nature* 445, pp. 39 – 46 (2007).

Y. Gu and G. Gbur, "Topological reactions of optical correlation vortices", *Opt. Commun.* 282, 5, pp. 709–716 (2009).

T. Hassinen, J. Tervo, T. Setälä, and A. T. Friberg, "Hanbury Brown–Twiss effect with electromagnetic waves", *Opt. Express* 19, 16, pp. 15188–15195 (2011).

J. O. Hirschfelder, A. C. Christoph, and W. E. Palke, "Quantum mechanical streamlines. i. square potential barrier", *The Journal of Chemical Physics* 61, pp. 5435 (1974a).

J. O. Hirschfelder, C. J. Goebel, and L. W. Bruch, "Quantized vortices around wavefunction nodes. ii", *The Journal of Chemical Physics* 61, pp. 5456 (1974b).

C. C. Hsiung, *A first course in differential geometry*, Series in Undergraduate Texts. International Press (1981).

D. F. V. James, "Change of polarization of light-beams on propagation in free space", *J. Opt. Soc. Am. A* 11, pp. 1641–1643 (1994).

P. B. Johnson and R. W. Christy, "Optical constants of the noble metals", *Phys. Rev. B* 6, pp. 4370–4379 (1972).

G. P. Karman, M. W. Beijersbergen, A. Van Duijl, and J. P. Woerdman, "Creation and annihilation of phase singularities in a focal field", *Opt. Lett.* 22, 19, pp. 1503–1505 (1997).

K. Kim and E. Wolf, "Propagation law for Walther's first generalized radiance function and its short wavelength limit with quasi-homogeneous sources", *J. Opt. Soc. Amer. A* 4, pp. 1233–1236 (1987).

O. Korotkova, M. Salem, and E. Wolf, "The far-zone behavior of the degree of polarization of electromagnetic beams propagating through atmospheric turbulence", *Opt. Commun.* 233, pp. 225–230 (2004).

O. Korotkova, T. D. Visser, and E. Wolf, "Polarization properties of stochastic electromagnetic beams", *Opt. Commun.* 281, pp. 515–520 (2008).

P. Lalanne and J. P. Hugonin, "Interaction between optical nano-objects at metallo-dielectric interfaces", *Nature Physics* 2, 8, pp. 551–556 (2006).

P. Lalanne, J. P. Hugonin, H. T. Liu, and B. Wang, "A microscopic view of the electromagnetic properties of sub-metallic surfaces", *Surface Science Reports* 64, 10, pp. 453 – 469 (2009).

H. J. Lezec, A. Degiron, E. Devaux, R. A. Linke, L. Martin-Moreno, F. J. Garcia-Vidal, and T. W. Ebbesen, "Beaming light from a subwavelength aperture", *Science* 297, 5582, pp. 820–822 (2002).

X. Li, Q. Tan, B. Bai, and G. Jin, "Experimental demonstration of tunable directional excitation of surface plasmon polaritons with a subwavelength metallic double slit", *Applied Physics Letters* 98, 25, pp. 251109 (2011).

H. Liu, P. Lalanne, X. Yang, and J. P. Hugonin, "Surface plasmon generation by subwavelength isolated objects", *IEEE Journal of Selected Topics in Quantum Electronics* 14, 6, pp. 1522–1529 (2008).

J. S. Q. Liu, R. A. Pala, F. Afshinmanesh, W. Cai, and M. L. Brongersma, "A submicron plasmonic dichroic splitter", *Nat. Commun.* 2, pp. 525 (2011).

B Lu, B. Zhang, and B. Cai, "Focusing of a Gaussian Schell-model beam through a circular lens", *J. Mod. Optics* 42, pp. 289–298(10) (1995).

K. F. MacDonald, Z. L. Sámson, M. I. Stockman, and N. I. Zheludev, "Ultrafast active plasmonics", *Nature Photonics* 3, 1, pp. 55–58 (2008).

S. A. Maier, P. G. Kik, H. A. Atwater, S. Meltzer, E. Harel, B. E. Koel, and A. A. G. Requicha, "Local detection of electromagnetic energy transport below the diffraction limit in metal nanoparticle plasmon waveguides", *Nat. Mater.* 2, pp. 229 – 232 (2003).

I. D. Maleev, D. M. Palacios, A. S. Marathay, and G. A. Swartzlander, "Spatial correlation vortices in partially coherent light: theory", *J. Opt. Soc. Am. B* 21, 11, pp. 1895–1900 (2004).

L. Mandel and E. Wolf, *Selected papers on coherence and fluctuations of light, 1850-1966*, SPIE milestone series. SPIE Optical Engineering Press (1970).

L. Mandel and E. Wolf, *Optical Coherence and Quantum Optics*, Cambridge University Press (1995).

M. L. Marasinghe, D. M. Paganin, and M. Premaratne, "Coherence-vortex lattice formed via Mie scattering of partially coherent light by several dielectric nanospheres", *Opt. Lett.* 36, 6, pp. 936–938 (2011).

M. L. Marasinghe, M. Premaratne, and D. M. Paganin, "Coherence vortices in Mie scattering of statistically stationary partially coherentfields", *Opt. Express* 18, 7, pp. 6628–6641 (2010).

M. L. Marasinghe, M. Premaratne, D. M. Paganin, and M. A. Alonso, "Coherence vortices in Mie scattered nonparaxial partially coherent beams", *Opt. Express* 20, 3, pp. 2858–2875 (2012).

L. Martin-Moreno, F. J. Garcia-Vidal, H. J. Lezec, K. M. Pellerin, T. Thio, J. B. Pendry, and T. W. Ebbesen, "Theory of extraordinary optical transmission through subwavelength hole arrays", *Phys. Rev. Lett.* 86, 6, pp. 1114–1117 (2001).

M. Miyata and J. Takahara, "Excitation control of long-range surface plasmons by two incident beams", *Opt. Express* 20, 9, pp. 9493–9500 (2012).

B. L. Moiseiwitsch, *Integral equations*, Longman Group Limited (1977).

G. Molina-Terriza, J. Recolons, J. P. Torres, L. Torner, and E. M. Wright, "Observation of the dynamical inversion of the topological charge of an optical vortex", *Phys. Rev. Lett.* 87, 2, pp. 23902 (2001).

M. A. Noginov, G. Zhu, A. M. Belgrave, R. Bakker, V. M. Shalaev, E. E. Narimanov, S. Stout, E. Herz, T. Suteewong, and U. Wiesner, "Demonstration of a spaser-based nanolaser", *Nature* 460, pp. 1110–1112 (2009).

L. Novotny and B. Hecht, *Principles of nano-optics*, Cambridge University Press (2006).

J. Nye, *Fine Structure of Light: Caustics and Wave Dislocations,*, Inst. Phys. Publ. (1999).

J. F. Nye, "Unfolding of higher-order wave dislocations", *J. Opt. Soc. Am. A* 15, 5, pp. 1132–1138 (1998).

J. F. Nye and M. V. Berry, "Dislocations in wave trains", *Proceedings of the Royal Society of London. A. Mathematical and Physical Sciences* 336, 1605, pp. 165–190 (1974).

D. M. Palacios, I. D. Maleev, A. S. Marathay, and G. A. Swartzlander Jr, "Spatial correlation singularity of a vortex field", *Phys. Rev. Lett.* 92, 14, pp. 143905 (2004).

E. D. Palik, *Handbook of Optical Constants of Solids*, Academic Press, San Diego (1998).

G. L. Pollack and D. R. Stump, *Electromagnetism*, Addison Wesley (2002).

J. A. Porto, F. J. Garcia-Vidal, and J. B. Pendry, "Transmission resonances on metallic gratings with very narrow slits", *Phys. Rev. Lett.* 83, 14, pp. 2845–2848 (1999).

J. Pu, M. Dong, and T. Wang, "Generation of adjustable partially coherent bottle beams by use of an axicon-lens system", *Appl. Opt.* 45, pp. 7553 (2006).

H. Raether, *Surface plasmons on smooth and rough surfaces and on gratings*, Springer (1988).

S. B. Raghunathan, T. van Dijk, E. J. G. Peterman, and T. D. Visser, "Experimental demonstration of an intensity minimum at the focus of a laser beam created by spatial coherence: Application to optical trapping of dielectric particles", *Opt. Lett.* 35, pp. 4166–4168 (2010).

S. B. Raghunathan, C. H. Gan, T. van Dijk, B. E. Kim, H. F. Schouten, W. Ubachs, P. Lalanne, and T. D. Visser, "Plasmon switching: Observation of dynamic surface plasmon steering by selective mode excitation in a sub-wavelength slit", *Opt. Express* 20, pp. 15326–15335 (2012a).

S. B. Raghunathan, H. F. Schouten, and T. D. Visser, "Correlation singularities in partially coherent electromagnetic beams", *Opt. Lett.* 37, 20, pp. 4179–4181 (2012b).

L. Rao and J. Pu, "Spatial correlation properties of focused partially coherent vortex beams", *J. Opt. Soc. Am. A* 24, 8, pp. 2242–2247 (2007).

L. Rayleigh, “On the passage of waves through apertures in plane screens, and allied problems”, *The London, Edinburgh, and Dublin Philosophical Magazine and Journal of Science* 43, 263, pp. 259–272 (1897).

O. G. Rodríguez-Herrera and J. S. Tyo, “Generalized van cittert–zernike theorem for the cross-spectral density matrix of quasi-homogeneous planar electromagnetic sources”, *Jnl. of the Optical Society of America A* 29, pp. 1939–1947 (2012).

H. F. Schouten, G. Gbur, T. D. Visser, and E. Wolf, “Phase singularities of the coherence functions in Young’s interference pattern”, *Opt. Lett.* 28, 12, pp. 968–970 (2003a).

H. F. Schouten, T. D. Visser, G. Gbur, D. Lenstra, and H. Blok, “Creation and annihilation of phase singularities near a sub-wavelength slit”, *Opt. Express* 11, 4, pp. 371–380 (2003b).

H. F. Schouten, T. D. Visser, G. Gbur, D. Lenstra, and H. Blok, “Connection between phase singularities and the radiation pattern of a slit in a metal plate”, *Phys. Rev. Lett.* 93, pp. 173901 (2004a).

H. F. Schouten, T. D. Visser, and D. Lenstra, “Optical vortices near sub-wavelength structures”, *Journal of Optics B: Quantum and Semiclassical Optics* 6, 5, pp. S404 (2004b).

H. F. Schouten, T. D. Visser, D. Lenstra, and H. Blok, “Light transmission through a subwavelength slit: Waveguiding and optical vortices”, *Phys. Rev. E* 67, 3, 036608 (2003c).

J. A. Schuller and M. L. Brongersma, “General properties of dielectric optical antennas”, *Opt. Express* 17, 26, pp. 24084–24095 (2009).

M. S. Soskin, V. N. Gorshkov, M. V. Vasnetsov, J. T. Malos, and N. R. Heckenberg, “Topological charge and angular momentum of light beams carrying optical vortices”, *Physical Review A* 56, 5, pp. 4064 (1997).

M. S. Soskin and M. V. Vasnetsov, “Singular Optics”, volume 42 of *Progress in Optics*, pp. 219 – 276, Elsevier (2001).

J. J. Stamnes, *Waves in Focal Regions*, Adam Hilger (1986).

B. Steinberger, A. Hohenau, H. Ditlbacher, F. R. Aussenegg, A. Leitner, and J. R. Krenn, “Dielectric stripes on gold as surface plasmon waveguides: Bends and directional couplers”, *Applied Physics Letters* 91, 8, 081111 (2007).

S. H. Strogatz, *Nonlinear Dynamics and Chaos: With Applications to Physics, Biology, Chemistry, and Engineering*, Perseus Pub. (1994).

G. A. Swartzlander Jr and R. I. Hernandez-Aranda, “Optical Rankine vortex and anomalous circulation of light”, *Phys. Rev. Lett.* 99, 16, pp. 163901 (2007).

G. A. Swartzlander Jr and J. Schmit, “Temporal correlation vortices and topological dispersion”, *Phys. Rev. Lett.* 93, 9, pp. 93901 (2004).

D. G. Fischer T. D. Visser and E. Wolf, “Scattering of light from quasi-homogeneous sources by quasi-homogeneous media”, *Jnl. of the Optical Society of America A* 23, pp. 1631–1638 (2006).

Y. Takakura, “Optical resonance in a narrow slit in a thick metallic screen”, *Phys. Rev. Lett.* 86, 24, pp. 5601–5603 (2001).

T. Thio, K. M. Pellerin, R. A. Linke, H. J. Lezec, and T. W. Ebbesen, “Enhanced light transmission through a single subwavelength aperture”, *Opt. Lett.* 26, 24, pp. 1972–1974 (2001).

T. Van Dijk, H. F. Schouten, and T. D. Visser, “Coherence singularities in the field generated by partially coherent sources”, *Phys. Rev. A* 79, 3, 033805 (2009).

C. Vassallo, *Optical waveguide concepts*, Elsevier (1991).

E. Verdet, “Étude sur la constitution de la lumière non polarisée et de la lumière partiellement polarisée”, *Ann. Sci. Ecole. Norm. Supér* 2, pp. 291–316 (1865).

L. Verslegers, Z. Yu, P. B. Catrysse, and S. Fan, "Temporal coupled-mode theory for resonant apertures", *J. Opt. Soc. Am. B* 27, 10, pp. 1947–1956 (2010).

M. A. Vincenti, A. D'Orazio, M. Buncick, N. Akozbek, M. J. Bloemer, and M. Scalora, "Beam steering from resonant subwavelength slits filled with a nonlinear material", *J. Opt. Soc. Am. B* 26, 2, pp. 301–307 (2009).

T. D. Visser, G. Gbur, and E. Wolf, "Effect of the state of coherence on the three-dimensional spectral intensity distribution near focus", *Opt. Commun* 213, 1-3, pp. 13 – 19 (2002).

T. D. Visser and R. W. Schoonover, "A cascade of singular field patterns in Young's interference experiment", *Opt. Commun.* 281, 1, pp. 1–6 (2008).

S. N. Volkov, D. F. V. James, T. Shirai, and E. Wolf, "Intensity fluctuations and the degree of cross-polarization in stochastic electromagnetic beams", *J. of Optics A* 10, pp. 055001 (2008).

C. Wang, C. Du, Y. Lv, and X. Luo, "Surface electromagnetic wave excitation and diffraction by subwavelength slit with periodically patterned metallic grooves", *Opt. Express* 14, 12, pp. 5671–5681 (2006a).

L. Wang and B. Lu, "Propagation and focal shift of $J_0$-correlated Schell-model beams", *Optik* 117, 4, pp. 167 – 172 (2006).

W. Wang, Z. Duan, S. G. Hanson, Y. Miyamoto, and M. Takeda, "Experimental study of coherence vortices: Local properties of phase singularities in a spatial coherence function", *Phys. Rev. Lett.* 96, 7, pp. 73902 (2006b).

W. Wang, A. T. Friberg, and E. Wolf, "Focusing of partially coherent light in systems of large Fresnel numbers", *J. Opt. Soc. Am. A* 14, 2, pp. 491–496 (1997).

W. Wang and M. Takeda, "Coherence current, coherence vortex, and the conservation law of coherence", *Phys. Rev. Lett.* 96, pp. 223904 (2006).

Y. Wang, X. Zhang, H. Tang, K. Yang, Y. Wang, Y. Song, T. H. Wei, and C. H. Wang, “A tunable unidirectional surface plasmon polaritons source”, *Opt. Express* 17, 22, pp. 20457–20464 (2009).

E. Wolf, “Optics in terms of observable quantities”, *Il Nuovo Cimento* 12, pp. 884–888 (1954).

E. Wolf, “A macroscopic theory of interference and diffraction of light from finite sources. ii. fields with a spectral range of arbitrary width”, *Proceedings of the Royal Society of London. Series A, Mathematical and Physical Sciences* 230, 1181, pp. 246–265 (1955).

E. Wolf, “New theory of partial coherence in the space-frequency domain. part i: spectra and cross spectra of steady-state sources”, *J. Opt. Soc. Am.* 72, 3, pp. 343–351 (1982).

E. Wolf, “New theory of partial coherence in the space-frequency domain. part ii: Steady-state fields and higher-order correlations”, *J. Opt. Soc. Am. A* 3, 1, pp. 76–85 (1986).

E. Wolf, *Selected works of Emil Wolf: with commentary*, World Scientific Pub. (2001).

E. Wolf, *Introduction to the Theory of Coherence and Polarization of Light*, Cambridge University Press (2007).

E. Wolf and W. H. Carter, “Fields generated by homogeneous and by quasi-homogeneous planar secondary sources”, *Opt. Commun.* 50, pp. 131–136 (1984).

E. Wolf and D. F. V. James, “Correlation-induced spectral changes”, *Rep. Prog. Physics* 59, pp. 771–818 (1996).

E. Wolf and Y. Li, “Conditions for the validity of the Debye integral representation of focused fields”, *Opt. Commun* 39, 4, pp. 205 – 210 (1981).

F. Zernike, “The concept of degree of coherence and its application to optical problems”, *Physica* 5, 8, pp. 785 – 795 (1938).

# List of publications

- **S. B. Raghunathan**, and N. V. Budko, "*Effective permittivity of finite inhomogeneous objects*", Phys. Rev. B 81, 054206 (2010).
- **S. B. Raghunathan**, T. van Dijk, E. J. G. Peterman, and T. D. Visser, "*Experimental demonstration of an intensity minimum at the focus of a laser beam created by spatial coherence: Application to optical trapping of dielectric particles*", Opt. Lett. 35 pp. 4166 – 4168 (2011).
- **S. B. Raghunathan**, T. van Dijk, H. F. Schouten, W. Ubachs, T. D. Visser, P. Lalanne, J. P. Hugonin and C. H. Gan , "*Plasmon Switching: Observation of dynamic surface plasmon steering by selective mode excitation in a sub-wavelength slit*", Optics Express 20, pp. 15326-15335 (2012).
- **S. B. Raghunathan**, H. F. Schouten, and T. D. Visser, "*Correlation singularities of partially coherent electromagnetic beams*", Opt. Lett. 37, pp. 4179–4181 (2012).
- **S. B. Raghunathan**, T. D. Visser, and E. Wolf "*Far-zone properties of electromagnetic beams generated by quasi-homogeneous sources*", Opt. Commun. 295, pp. 11-16 (2013).
- **S. B. Raghunathan**, H. F. Schouten, and T. D. Visser, "*Topological reactions of correlation functions in partially coherent electromagnetic beams*", J. Opt. Soc. Am. A. 30, pp. 582-588 (2013).
- **S. B. Raghunathan**, H. F. Schouten, and T. D. Visser, "*Observation of dynamic beam steering in a subwavelength slit by selective mode excitation*", in preparation (2013).

# Samenvatting

De Nederlandstalige titel van dit proefschrift luidt: *Studies in Optica – Coherentie en Oppervlakte Plasmonen.* De verschillende hoofdstukken zijn gebaseerd op reeds verschenen of voor publikatie geaccepteerde artikelen. Alleen het laatste hoofdstuk moet nog worden ingediend. Hoofdstuk 1 bevat een korte toelichting van verschillende concepten die we later zullen gebruiken. Het gaat om begrippen uit de coherentie theorie, de singuliere optica en de plasmonica. Hoofdstuk 2 beschrijft een experimentele studie naar partieel coherente laserbundels. In eerdere theoretische artikelen is voorspeld dat het focuseren van Bessel-gecorreleerd licht tot een intensiteitsverdeling leidt die bij het brandpunt een minimum heeft. Deze voorspelling is niet alleen geverifieerd, maar we laten tevens zien hoe door het variëren van een iris de intensiteit bij het focus traploos van een minimum in het gebruikelijke maximum is te veranderen. Een mogelijke toepassing hiervan is het selectief manipuleren van deeltjes met een hogere dan wel een lagere brekingsindex dan het omringende medium. Hoofdstuk 3 is een theoretische analyse van een grote klasse van partieel coherente bronnen, namelijk die van het quasi-homogene type. Verschillende zogenaamde reciprociteitsrelaties, die de velden in het bronvlak aan die in het verre veld relateren, worden afgeleid. Met deze resultaten kunnen we makkelijk bestuderen hoe het spectrum, de polarisatie en de coherentie van licht verandert bij voortplanting. Hoofdstuk 4 behandelt een onderwerp uit de singuliere optica. Dat golfvelden fase singulariteiten kunnen bevatten is wel-bekend. Dat dit ook geldt voor correlatiefuncties is echter een meer recent inzicht. We laten met numerieke voorbeelden zien dat zogenaamde coherentie vortices algemeen voorkomen in partieel coherente elektromagnetische bundels. In Hoofdstuk 5 bekijken we de elektromagnetische bundels uit het vorige hoofdstuk in meer detail. Het blijkt dat de coherentie eigenschappen in verschillende dwarsdoorsnedes in het algemeen sterk van elkaar verschillen. Dat betekent dat een waarnemer die een opeenvolging van zulke doorsnedes bekijkt, een hele reeks topologische reacties zal zien. In deze reacties worden vortices, zadelpunten en andere structuren gecreëerd en geannihileerd. Hoofdstuk 6 beschrijft een experiment waarin een speciaal soort oppervlaktegolven, zogenaamde oppervlakte plasmonen, centraal staan. Door de ultra-korte lengteschalen waardoor deze golven worden gekarakteriseerd, houden ze een grote belofte in voor opto-elektronische toepassingen. Tot nu toe is het echter niet goed mogelijk om plasmonen dynamisch van richting te laten veranderen. We laten zien hoe met behulp van selectieve excitatie van geleide golven in een nano-spleet een plasmon-schakelaar te realiseren valt. De gemeten data stemmen goed overeen met de voorspellingen van een simpel model. In Hoofdstuk 7 wordt dezelfde techniek van selectieve excitatie van geleide golven gebruikt voor een ander doel, namelijk het beïnvloeden van het stralingspatroon van een sub-golflengte spleet in een metalen film. We tonen aan dat het hierdoor mogelijk is om het uitgezonden licht naar één van twee detectoren te sturen, of om het licht over beide detectoren te verdelen.

# Acknowledgments

In the course of completing my dissertation, I had to go through a transition from a student to a researcher. This would not have been possible without my promoter and supervisor Prof. dr. Taco Visser. Graduate students do not always get the opportunity to work 'with' a professor, and it has been a great pleasure working with you. I would like to thank you for your patience in first understanding my train of thought and later helping me improve my scientific writing skills. It has been a tremendous learning experience for me, and I admire your composure during the last four years despite having to work in a turbulent work atmosphere. I would like to thank Dr. Neil Budko for getting me introduced to Taco and for all the motivating discussion. I would also like to thank Prof. dr. W. M. G. Ubachs and Prof. dr. ir. E. J. G. Peterman for their help and support during my work at the LaserLaB, VU. I would also like to thank Dr. Edcel Salumbides for his help with the experiments. I would like to extend my gratitude to Jacques Bouma for his help in setting up different experiment at the LaserLaB.

The workplace both at Delft and in Amsterdam has never been only about work, thanks to my office mates. Thomas has been a great colleague and a friend. He has been ever so patient in listening to my rambling and helping me out with my experiments. I would like to thank Wilco for the endless discussions we have had about beer, North Korea, Asperger's syndrome, NS and sometimes about Higgs boson. You have been a wonderful office mate and a friend. I would like to thank Xiaoyan for all the spirited discussions. I wish you success with your study and research.

I would like to thank my previous house mates Dushyant, Aarabi, Sandeep and Christiane for the great time we had at AVS. Many thanks to Sid, Laia, Prem, Sruti, Joe, Mariam, Rajeev, Shiva, Nestor, Fabian, Mireia, Maarten and Anoop for keeping the life outside work alive and partying. I would also like to thank the 'Marcushof' group, Giorgio, Mattia and Ashu for all the light hearted moments. A special thanks to Venkat and Venkatesh for all their help, support and much needed company during tough times.

A good traveler has no fixed plans. I would first like to thank Kesvan, Ayyappa, Madhavan and Venkatasubramaniam for an awesome eurotrip. When the weather gets cold the tough go to the north pole. Many thanks to the great group of 'cold' travelers Gunjan, Brhamesh, Sumit, Bhuvana, Amit, JK and Ajith who have helped me live up to this. I hope we plan warmer trips someday! Gunjan: Special thanks to you for all the support you provided in difficult times and for having confidence in me, more than I had in myself. This means a lot to me.

Lastly, I would like to thank my parents and my brother for the years of unconditional love and support they have provided. More importantly, thank you for standing by me when I needed help. Special thanks to my dad for kindling my curiosity in physics and my mom for helping me out in everything else.

Shreyas Raghunathan
April 2013.

# Biography

Shreyas Bhargav Raghunathan was born in Kolar Gold Fields, Karnataka, on 10 May 1985. He received his Bachelor's degree in Electronics and communication from Anna University in 2006. He joined as a Masters student at Delft University of Technology the same year and graduated with a degree in Electrical Engineering in 2008. He decided to continue as a PhD candidate in the Laboratory of Electromagnetic Research at Delft University of Technology.